Application des polymères conducteurs en bioélectronique

Dion Khodagholy Araghy

Conducting Polymer Devices for Bioelectronics

Dion Khodagholy

July 2012

Abstract

The emergence of organic electronics – a technology that relies on carbon-based semiconductors to deliver devices with unique properties – represents one of the most dramatic developments of the past two decades. A rapidly emerging new direction in the field involves the interface with biology. The "soft" nature of organics offers better mechanical compatibility with tissue than traditional electronic materials, while their natural compatibility with mechanically flexible substrates suits the non-planar form factors often required for implants. More importantly, their ability to conduct ions in addition to electrons and holes opens up a new communication channel with biology. The coupling of electronics with living tissue holds the key to a variety of important life-enhancing technologies. One example is bioelectronic implants that record neural signals and/or electrically stimulate neurons. These devices offer unique opportunities to understand and treat conditions such as hearing and vision loss, epilepsy, brain degenerative diseases, and spinal cord injury.

The engineering aspect of the work includes the development of a photolithographic process to integrate the conducting polymer poly(3,4-ethylenedioxythiophene: poly(styrene sulfonate) (PEDOT:PSS) with parylene C supports to make an active device. The technology is used to fabricate electrocorticography (ECoG) probes, high-speed transistors and wearable biosensors. The experimental work explores the fundamentals of communication at the interface between conducting polymers and the brain. It is shown that conducting polymers outperform conventional metallic electrodes for brain signals recording.

Organic electrochemical transistors (OECTs) represent a step beyond conducting polymer electrodes. They consist of a conducting polymer channel in contact with an electrolyte. When a gate electrode excites an ionic current in the electrolyte, ions enter the polymer film and change its conductivity. Since a small amount of ions can effectively "block" the transistor channel, these devices offer significant amplification in ion-to-electron transduction.

Using the developed technology a high-speed and high-density OECTs array is presented. The dense architecture of the array improves the resolution of the recording from neural networks and the transistor's temporal response are 100 μs, significantly faster than the action potential. The experimental transistor responses are fit and modeled in order to optimize the gain of the transistor. Using the model, an OECT with two orders of magnitude higher normalized transconductance per channel width is fabricated as compared to Silicon-based field effect transistors. Furthermore, the OECTs are integrated to a highly conformable ECoG probe. This is the first time that a transistor is used to record brain activities *in vivo*. It shows a far superior signal-to-noise-ratio (SNR) compared to electrodes. The high SNR of the OECT recordings enables the observation of activities from the surface of the brain that only a perpetrating probe can record.

Finally, the application of OECTs for biosensing is explored. The bulk of the currently available biosensors often require complex liquid handling, and thus suffer from problems associated with leakage and contamination. The use of an organic electrochemical transistor for detection of lactate by integration of a room temperature ionic liquid in a gel-format, as a solid-state electrolyte is demonstrated.

Acknowledgements

I am grateful for all the support and guidance I have received over the last 3 years at Centre Microelectroique de Provence (CMP). First and foremost, I have a lifetime debt to my advisor, George Malliaras, who gave me the opportunity to join his young department, BioElectronics Laboratory (BEL), and explore my interests from scratch, which made it very fascinating. I would frequently find myself in his office seeking advice. His great and encouraging personality always inspired me and made it truly 3 years of pleasure to work for him. I am especially thankful to Christophe Bernard, who was like a second advisor to me. I am grateful for his help in carrying out research at Timone hospital, and his support to organize surgical implantations and write papers. At Timone hospital, I am thankful to Thomas doublet and Pascale Quilichini who made the *in vivo* experiments appear seamless. I am also thankful to the members of the BEL department, who helped make this research possible and taught me a great deal, in particular, Roisin Owens. Her knowledge in biology, her patience, and lab space were invaluable. Through collaborations, I have had the opportunity to interact with world-class researchers without whom some of this work could not have been done. I am grateful to Manfred Lindau for the opportunity to visit his labs at Cornell Univeristy, spend time with his group, and learn about electrophysiology.

Without funding, however, I would not have had this opportunity. I gratefully acknowledge funding from Ecole Nationale Supérieure des Mines de Saint-Etienne for the graduate student fellowship, the ANR through the project MUSIC, and through additional grants from région PACA, Marie CURIE, as well as the Partner university funding (PUF) providing financial support to conduct research at Cornell University. Throughout my time at BEL, it was my friends and family that helped build such a memorable and enjoyable experience. Though there are too many to list here, I must name a few. Without the atmosphere we established, I'm not sure I would have ever come into the lab. I'm further thankful to Moshe Garfunkel, Jonathan Rivnay, Michele Sessolo and Leslie Jimison. Moshe has become one of my preferred

collaborators and one of my best friends. I could not have done this work without him. Michele and Jon taught the scientific culture and how to peruse a high-risk research. I very much enjoy working with them and they kept me sane. Leslie's stamina and management skills were always a perfect example on how to conduct a productive research.

Finally, through all this I have had the unwavering support of my loved ones: my mom and dad, Minelli my sister and Nareh my girlfriend. Thank you for putting up with me. Thank you for making me smile, laugh and relax.

Contents

Chapter 1

1 Introduction

Research on organic electronics dates back to the 1960s, to studies of the electronic properties of organic crystals. [1] At the end of the 1970s, Heeger, MacDiarmid, and Shirakawa demonstrated that polyacetylene can become highly conducting when doped with iodine, [2] a discovery for which they won the Nobel Prize for Chemistry in 2000. The discovery that plastic can be made electrically conductive created a great deal of enthusiasm, and a variety of applications including lightweight cables and 'smart' windows were proposed. In 1989, the discovery by the group led by Richard Friend in Cambridge that poly(p-phenylene vinylene) (PPV) can yield efficient electroluminescent devices propelled conjugated polymers into the modern era. [3] Since then, tremendous developments have taken place in the field. Conjugated polymer-based light-emitting diodes (LEDs) were commercialized in small-format displays by Philips a few years ago. More recently, conjugated polymers were commercialized in large-area, low-cost solar cells by Konarka and are on their way to applications in transistors for display backplanes by Plastic Logic.

This chapter will review the basic principles of sensors based on conjugated polymers used for biological applications. Conjugated polymers share a common structural feature: the bonding along the polymer backbone consists of alternating single and double carbon–carbon bonds (called conjugation). A key requirement for a polymer to become semiconducting is that there should be an overlap of molecular orbitals to allow the formation of delocalized molecular wave functions. When the carbon atoms form double bonds, it is through their sp2 hybrid orbitals, thus producing three σ bonds within a plane and leaving out of plane π orbitals. The π orbitals of neighboring carbon atoms can overlap, giving rise to electron delocalization along the polymer chain. There is thus a delocalization of the π-electron system along the backbone, which promotes facile charge transport within the polymer chain (intrachain hopping, which is necessary for macroscopic conduction, will depend on the details of chain packing in the film). The filled π orbitals

constitute the valence states, while the empty ones form the conduction states (Figure 1). It is important to note that the σ bonds are substantially stronger than the π bonds and are able to hold the polymer intact even in the presence of electrons, holes, and excitons (bound electron–hole pairs).

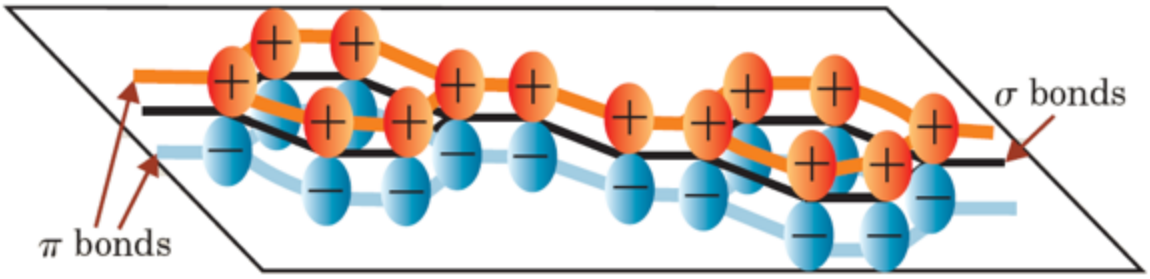

Figure 1: Bonding in conjugated polymers.

Conjugated polymers can be doped to become significantly conducting, in which case they are referred to as conducting polymers. The addition of electron acceptors results in p-type doping, while the addition of electron donors results in n-type doping. A major difference compared traditional electronic materials such as silicon is that the dopants do not substitute carbon atoms along the polymer chain, but are rather accommodated between polymer chains. A second difference is that free charges cause a deformation of the polymer chain, and the combination of the charge and the deformation is called a polaron. Two polarons can combine and stabilize each other, forming a bipolaron. Polaron and bipolaron states are located within the forbidden energy gap, causing new absorption features.

Conjugated polymers are of interest due to their facile, low-temperature processing (flexible side chains are added to the conjugated backbone to enhance solubility and to optimize packing within films). They are usually deposited in films from solution using techniques such as spin coating, screen-printing, and even spray painting. Annealing with a solvent or a modest temperature is often used to control the morphology and yield highquality films. A second technique for producing films of interest for sensors is direct electrochemical growth on a conducting substrate. Good quality films can also be produced, though the fact that they are adhered to the substrate limits our ability to analyze and purify them. It also limits the device configurations that can be achieved (such as applications that require the film to be deposited on an insulator). Solution processing translates to lower fabrication costs, a major advantage for sensors. An additional feature of polymers is the tunability of their chemical and electronic properties, achieved via chemical synthesis: properties such as electron affinity, ionization potential, and band gap can be manipulated by changing the backbone or side chains and appropriate groups can be introduced that endow the sensors with sensitivity toward particular analytes. This

tunability translates into potential gains in sensitivity and selectivity of sensors. Polymers show relatively open structures, allowing molecules to diffuse into films and interact not only with the surface, but also with the whole bulk. This is an advantage over inorganic crystals, which usually require high temperatures to function effectively as gas sensors. Finally, the absence of broken bonds at conjugated polymer surfaces translates into a well-defined interface with the medium in which the analyte is present (gas or liquid).

This chapter will first provide a brief background on the transduction mechanisms involved in polymer based chemical and biological sensors therefore the sensing process occur in liquid (the analyte is in a liquid solution). Mechanical pressure transducers, light and radiation sensors, and so on are beyond the scope of this work.

In the ideal case, a sensor consists of two components: a recognition element and a transducer. The recognition element interacts with the analyte in a specific manner, while the transducer translates the interaction into a measurable signal. The analyte can be in the liquid phase. Its interaction with the recognition element can be either physical (e.g., the analyte is absorbed on the recognition element) or chemical (the analyte participates in a chemical reaction with the recognition element). We classified sensors according to their transduction mechanism such as electrical, optical, mechanical, etc.).

1.1.1 Electrical sensors

Soon after the discovery of conducting polymers, it was found that their electrical properties can be sensitive to a multitude of factors in their environment, including the presence of various gases and the pH. For example, their conductivity can be affected by the presence of gas molecules that cause charge trapping, or by the addition or loss of ions that act as dopants. Such events can be probed by measurements of charge density, mobility, conductivity, work function, and impedance, among others. Figure 2 shows the most frequently used configurations in electrical sensors. Conducting polymers (i.e., doped conjugated polymers) are usually employed in electrochemical sensors and chemiresistors, while the pristine form (which is semiconducting) is used in field effect transistors.

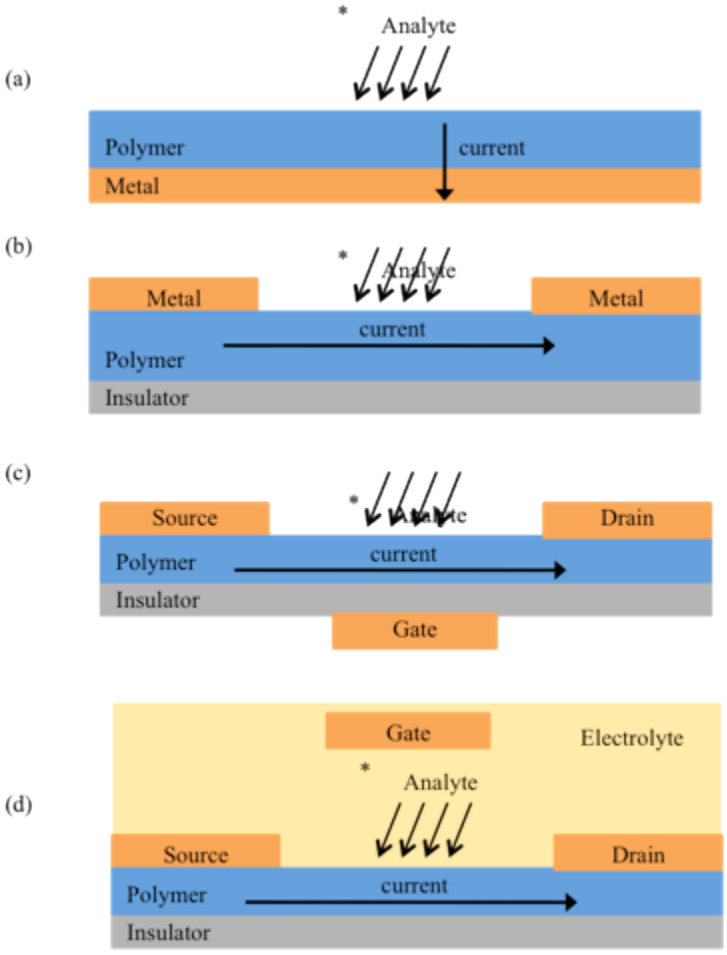

Figure 2: Different configurations for electrical sensors: (a) electrochemical sensor, (b) chemiresistor, (c) organic field effect transistor, and, (d) organic electrochemical transistor .

Polymer Metal Insulator Electrolyte

In electrochemical sensors (which include amperometric and potentiometric sensors), the polymer, usually in a conducting state (heavily doped), is coated on the working electrode of a typical electrochemical setup that also includes reference and counter electrodes. In amperometric sensors, one measures the current caused by redox reactions between the analyte and the conducting polymer. As a result of these reactions, the surface of the conducting polymer itself is reduced or oxidized and charge is transferred to/from the underlying metal electrode. The tunability of the electronic properties of conducting polymers comes in handy in electrochemical detection, as one can, for example, tailor the energy levels of a polymer, thereby controlling its propensity to participate in redox reactions.

Amperometric sensors have been developed intensively for biological sensing. As we discuss below, conducting polymers with immobilized or entrapped enzymes (which provide selectivity) have been used to facilitate the transfer of electrons between an analyte and a metal electrode. In this configuration, the conducting polymer is often assumed to mediate transfer of the electrons between the enzyme and the metal electrode, though the exact mechanism remains unknown. [4] Amperometric sensor devices have very simple architectures and can be mass produced cheaply and easily. [5]

Judicious design of these sensors is important to ensure facile interpretation of signals. For example, it is customary to make the reference electrode much larger than the working electrode. This is because the impedance associated with the reference electrode can then be considered negligible when compared with that of the working electrode.

In potentiometric sensors, the analyte induces changes in the chemical potential of the conducting polymer, which is detected as a change in the potential difference between the working and the reference electrode. Unlike amperometric sensors, the size of the signal does not depend on the area of the working electrode; therefore, potentiometric sensors are more amenable to miniaturization.

Chemiresistors, also known as conductometric sensors, detect changes in current flow through a polymer film in response to analyte interactions. These are the simplest electrical sensors, and the sensor configuration consists of a conducting polymer film with two metal electrodes on either side (Figure 2b). These sensors are inexpensive and easy to fabricate, and therefore very popular. Adsorption of polar chemicals on the surface of the sensor can cause reversible changes in DC conductivity at ambient temperatures. [6,7] These changes may arise from doping or dedoping of the polymer through redox reactions with the analyte. [8–17] Analytes can also change the conformation of the polymer backbone. [18,19] Therefore, despite

the simplicity of the measurement, it is not always easy to determine the reason for the observed changes in the response of the sensor upon exposure to analyte. Spectroscopy techniques and geometrical variation of the device can be used to shed light on the mechanism of interaction between the analyte and the polymer. [18]

As the interaction of the analyte with the polymer can occur throughout the bulk of the film (B), at the surface (S), at the interface with the insulating substrate (I), or at the contacts (C), a model such as the one shown in Figure 3 is often employed in order to analyze the results. [18,20,21] It should be noted that in addition to conductance, capacitance and inductance can also be measured to interrogate the device and gain additional insights into the mechanism of polymer–analyte interaction. [22,23]

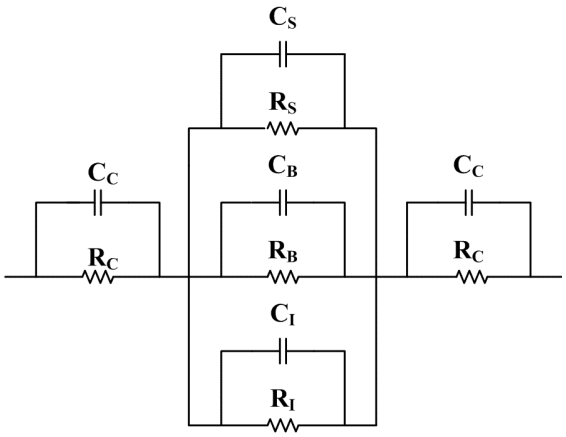

Figure 3: Equivalent circuit of a chemiresistor from Janata, J. Crit. Rev. Anal. Chem. 2002, 32 (2), 109–120

Organic thin-film transistors (OTFTs) can be classified into two types: organic field-effect transistors (OFETs) and organic electrochemical transistors (OECTs). OFETs consist of a semiconducting channel (a conjugated polymer in this case), which is separated from a gate electrode by an insulator (gate dielectric) (Figure 2c). [24] Source and drain electrodes allow electrical contact to the channel. With no voltage applied at the gate, the current that flows in the channel is small and the transistor is said to be in the OFF state. The charge density in the conjugated polymer film, however, can be dramatically increased through the application of a gate voltage (field-effect doping), resulting in a large current in the channel (ON state). For sufficiently large gate voltages, the current that flows in the polymer channel is independent of the voltage applied across the source–drain electrodes and is given by

$$I_{DS}^{Sat} = \frac{WC_i}{2L}\mu_{FET}(V_{GS} - V_T)^2 \qquad (1.1)$$

Where W and L are the width and length of the channel, respectively, C_i is the capacitance per unit area of the gate dielectric, μ_{FET} is the field-effect mobility, V_{GS} is the applied gate voltage, and V_T is the threshold voltage.

OFETs have been used in sensors in two configurations: The first configuration, called the ion-sensitive OFET (IS-OFET), substitutes the gate electrode for an electrolyte and has been used frequently in biosensing. As the name implies, these devices are sensitive to the ion concentration at the electrolyte/gate dielectric interface. Analytes that cause a change in that concentration can therefore be detected, as they indirectly cause a change in the gate voltage, and, according to equation 1.1 , change the current that flows through the channel. The second configuration involves direct contact of the semiconducting polymer channel with the analyte and has been used predominantly in gas sensing. Sensing in this configuration occurs by the absorption of the analyte onto the polymer layer and subsequent diffusion into grain boundaries, leading to interactions with the whole channel of the transistor. As in the case of chemiresistors, this interaction may involve swelling of the polymer, [25] charge trapping/detrapping processes, and/or raising or lowering energy barriers between grain boundaries. Other possible mechanisms may include a partial charge transfer from the analyte, [26,27] or a change in electron hopping rate caused by the gas vapor, [28] which can arise from disturbances in the local potential caused by dipolar molecules. In this configuration, OFETs bear a lot of similarities to chemiresistors, although OFETs should be considered as multiparameter sensors due to the existence of a gate electrode. An interaction with an analyte can be quantified not only by means of changes in conductance, but also by transconductance, mobility, threshold voltage, leakage current, and other parameters. OFETs can be easily integrated into electronic circuits and their selectivity can be tuned through a proper choice of the organic sensing layer. [29] Despite the fact that chemiresistors are simpler and easier to fabricate compared to OFETs, the latter are more sensitive due to the inherent signal amplification they offer. It should be noted that the majority of OFETs used for sensing applications utilize small molecules rather than polymers; therefore, they will not be discussed here.

OECTs, or conducting polymer transistors, represent the second class of polymer OTFTs. Originally invented by Wrighton in the 1980s, [30] OECTs consist of a conducting polymer channel in contact with an electrolyte (Figure 2d). A gate electrode is immersed in the electrolyte, while source and drain electrodes permit electrical contact to the channel. Given that the polymer channel is doped, an OECT is normally in the ON state (high channel current). The application of a gate voltage can cause ions from the electrolyte to enter the polymer film and dedope it, decreasing its conductivity and bringing the transistor to the OFF state. Therefore, OECTs provide a means to convert ionic currents in the electrolyte to electronic currents in the polymer channel. [31] OECTs have been used both in gas-phase and in liquid-

phase sensing, but are particularly interesting for biosensing applications, as they provide a direct link between the worlds of biology and electronics. Their sensing mechanism relies on changes in the ionic current that are induced by an analyte, as discussed in the examples given later in this chapter.

1.1.2 Optical sensors

Conjugated polymers have been used in optical sensors predominantly as recognition elements, though examples of their use as part of the transducer are becoming increasingly more common. The division between these two roles for optical sensors is clearer than in the case of electrical sensors; hence, we use it as the basis of our discussion herein: in the most usual configuration, the analyte interacts with a conjugated polymer film and causes a change in the optical properties of this film. An external system of light source/photodetector measures the change. According to this example, the polymer film is the recognition element, and the external illumination/detection system is the transducer.

Changes in the redox state of a conjugated polymer lead to strong modifications of the electronic band structure, which translates to changes that can be measured with optical transducers. For example, the formation of polarons and bipolarons during absorption of gases results in changes in the absorption spectrum of a conjugated polymer. [32] Binding of analytes can also result in changes in the conformation of the polymer, which can correspondingly alter its optical properties. In colorimetric sensors, the conducting polymer interacts with the analyte in a manner that changes its absorbance. In the case of fluorescence sensors, changes in intensity, wavelength, or lifetime of emission are detected. As excitons in conjugated polymers are highly mobile and sample a large part of the polymer chain during their lifetime, there is significant amplification: a single quencher can quench the whole polymer chain, which is the equivalent of a very large number of individual chromophores. Two experimental configurations are particularly suited for optical sensing; in the first one the optical transmission of a film is measured, [33] while in the second one the polymer is used as a cladding of an optical fiber (Figure 4). [34,35]

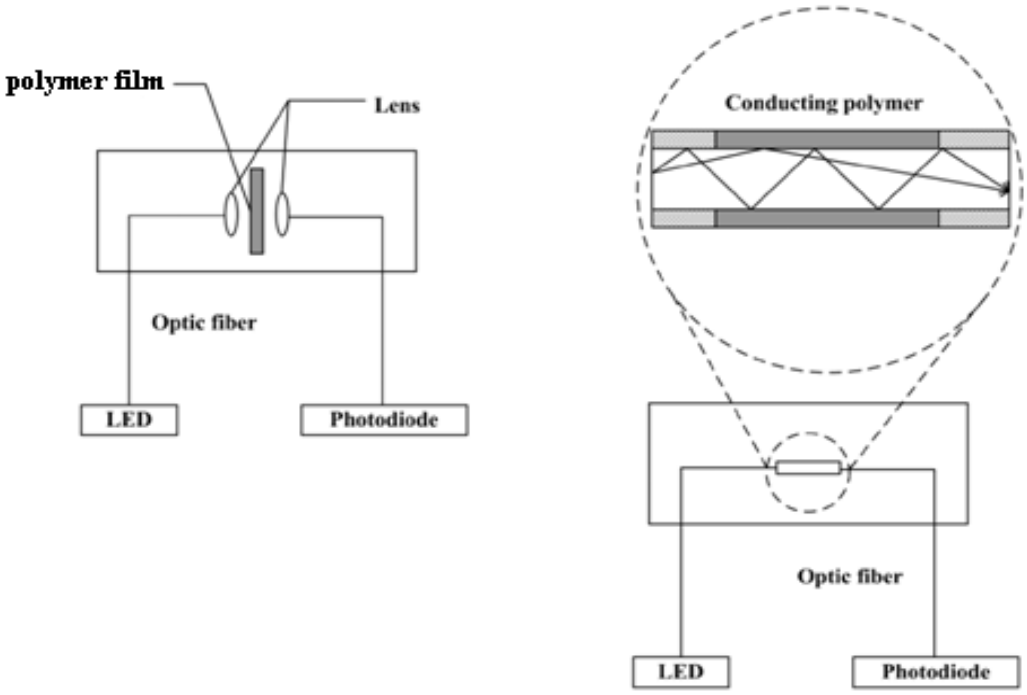

Figure 4: Optical sensors configurations: a) transmission of light through a polymer film, b) polymer used as cladding of optical fiber from Bai, H.; Shi, G. Q. Sensors 2007, 7 (3), 267–307.

Polymers have also been used in the transducers of optical sensors: organic light-emitting diodes (OLEDs) have been used as alternatives to traditional light excitation sources such as filament or arc lamps, lasers, and inorganic LEDs. OLEDs consist of organic semiconductor layer(s) sandwiched between metal electrodes. Under the application of an applied bias, electrons and holes injected from opposite electrodes recombine in the organic stack, producing light emission. [24] The main advantages of OLEDs are facile miniaturization and potentially low cost. The first use of OLEDs as excitation sources in chemical sensors was by Kopelman and co-workers in 2002. [36] The majority of OLEDs used for sensing applications utilize small molecules rather than polymers; therefore, they will not be discussed here. There are, however, some examples on the use of polymer based OLEDs (often called PLEDs) in sensing applications. [37,38] Organic photodetectors, which have a similar structure to OLEDs but perform the reverse operation (convert light into current), have also been used as transducers in optical sensors. The combination of OLEDs and photodetectors promises to deliver low-cost transducers that are particularly suited for remote monitoring and point-of-care diagnostics.

1.1.3 Mechanical sensors

Conjugated polymers have been used in piezoelectric sensors in two configurations: in quartz crystal microbalance (QCM) sensors and in surface acoustic wave (SAW) sensors. The polymer in this case acts only as an active layer, which tunes the surface properties of piezoelectric crystals and improves both the detection limit (by adsorbing more analyte molecules) and selectivity (by introducing special interactions with analytes).

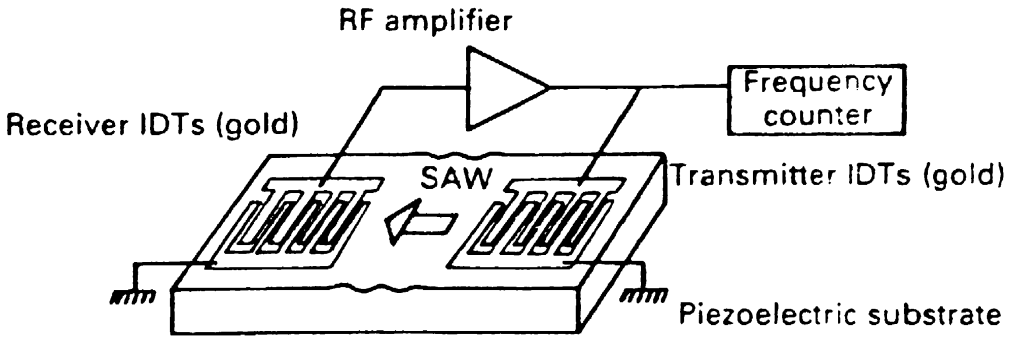

Figure 5: Schematic of a SAW device from Chang, S. M.; Muramatsu, H.; et al. Mater. Sci. Eng., C 2000, 12 (1–2), 111–123

The sensing principle of SAW sensors is based on bulk acoustic waves as introduced by King in 1959. [39] The very first studies relating to the use of SAW devices as gas sensors were reported in 1979 by Wohltjen and Dessy. [40] The standard design for a SAW device is shown schematically in Figure 5. These devices contain metallic electrodes, which are usually made of gold in an interdigitated (IDT) format on a quartz surface. One side of the sensor provides a reference signal, while the other side is usually coated with a material sensitive to analytes (such as a conjugated polymer). An input radio frequency voltage is applied across the transmitter, which induces deformation in the piezoelectric substrate. When a gas is absorbed on the surface of the polymer, it causes a shift in the SAW device resonant frequency. A phase or frequency shift is recorded between the input and output voltages to determine the gas concentration. [41–43] The resonant frequency of a quartz crystal changes with its mass load; [44] thus, measuring the resonance frequency shift can define the concentration of absorbed analyte.45–50 These sensors have very low detection limits (<1 ppm) since piezoelectric crystals are very sensitive to mass uptake. [51–53] For the same reason, however, the selectivity of piezoelectric crystal sensors is poor.

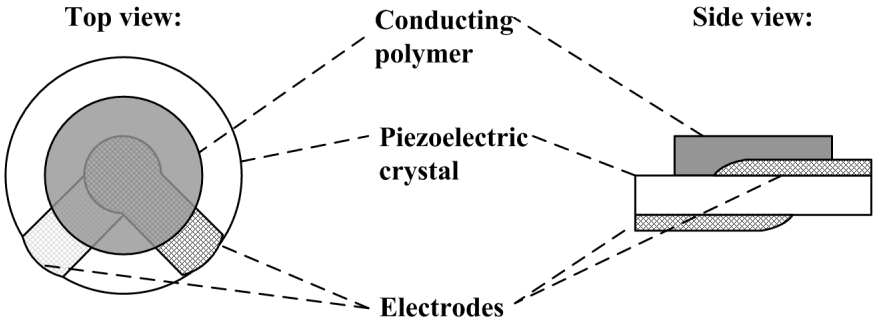

Figure 6: Schematic of a QCM sensor from Bai, H.; Shi, G. Q. Sensors 2007, 7 (3), 267–307.

A typical schematic diagram of a QCM is shown in Figure 6. It consists of a polymer-coated quartz crystal and a pair of electrodes. QCM sensors are widely used for the characterization of thin layers, fluids, and gases due to their high mass sensitivity and durability. The sensing principle relies on the fact that changes in the mass of the polymer due to analyte absorption change the weight and, therefore, the frequency of oscillation of the QCM. [48]

1.2 Liquid-Phase Sensing

When considering polymer based sensors in the liquid phase, it becomes apparent that the majority of the development has occurred in the realm of biosensors. We will consider here two main categories for liquid-phase sensors: electrical and optical. These different sensor types are discussed in the following sections.

1.2.1 Electrical Sensors in Liquid Sensing

To put the development of polymer based sensors into perspective, it makes sense to follow the evolution of glucose sensors. The very urgent need of diabetics to measure blood glucose levels represents a world market worth approximately $5 billion, [49] and has driven a tremendous amount of research in the glucose sensing arena. The majority of commercially available glucose sensors are electrochemical sensors based on a technology described by Clark and Lyons in 1962, who demonstrated the first example of an electrode based method for detection of O2. [50] The basic sensing principle (using electrochemistry) in commercially available systems has not changed significantly in the past four or five decades, apart from a trend toward miniaturization. [49] A number of technological advances allowed the development of a portable glucose sensor called ExacTech in 1988 using inexpensive, disposable enzyme electrodes. [51] The first advance occurred in 1984 when a UK group reported the use of the organic semiconductor ferrocene as a more efficient means of mediating electron transfer in glucose sensors. [52] In a similar vein, molecular wires consisting of polymers capable of charge transfer were used to connect the redox center of the enzyme directly to the electrode, thereby increasing the sensitivity of the sensor (e.g., the osmium containing three-dimensional redox hydro- gel, (poly[1-vinyl imidazole osmium (4,4'-dimethyl- bipyridine)(2)Cl])(+/2+)) described by Vijayakumar et al. [53]

A second major advance followed the use in the late 1970s and early 1980s of chemically modified electrodes (see Reference [54] for a review), constituting the first attempts at using conducting polymer electrodes for so called redox polymer mediated electrocatalysis. From there, it was a relatively short step to combining conducting polymer electrodes with enzymes for biosensors, thus moving away from the system proposed by Clark and Lyons. The third major advance was in the method of immobilization of the enzyme, which was first improved by entrapment within electrochemically deposited PPy to function as an amperometric glucose sensor, [55] combining a controlled method of localization of the enzyme to defined areas on the electrode with a method of electrical communication from the redox center of the enzyme for

detection of electrons. The use of cross linked redox polymers in combination with polyethylene glycol for covalent binding of redox enzymes was carried out by Gregg and Heller as an alternative to the entrapment of enzymes within electropolymerized polymer and suggested to require less enzyme and use conditions more compatible with enzyme function. [56]

In addition to being used for glucose detection, electrical sensors have been developed for pH, ions, heavy metals, small molecules, nucleotides, and enzymes/proteins. Proof of concept has also been demonstrated utilizing antibodies and whole cells as recognition elements. We discuss some characteristic examples below, by order of application as opposed to chronologically.

1.2.1.1 Electrochemical sensors

Most electrochemical sensors using conducting polymers utilize the conducting polymer simply as a coating over a metal electrode. We focus here on examples where the electrical properties of the conducting polymers are put into play, rather than just a passive use of the polymer coating for immobilization or other reasons.

Huang and MacDiarmid showed the effect of pH on conducting polymers – in particular PANI. [57] They showed that the pH influenced the redox processes of PANI in aqueous electrolytes. This principle was subsequently used to develop a variety of pH sensors, such as that proposed by Hailin and co-workers, who showed a simple PPy pH sensor fabricated on paper, which utilizes the change in resistance of PPy upon exposure to different pH values. [58] One example of a heavy metal sensor was produced by Rahman et al., who used polyterthiophene and reacted it with ethylenediaminetetraacetic acid (EDTA) in the presence of a catalyst. The conducting polymer was polymerized on a glossy carbon electrode. The EDTA was then used for complexation with Pb2+, Cu2+, and Hg2+ ions for detection of these heavy metals in aqueous samples, as measured by square wave voltammetry. This sensor was suggested for use in water or urine samples. [59]

Kumar et al. showed detection of NADH and NAD using poly(p-aminobenzene sulfonic acid) (PBSA) films doped with flavins. Amperometric responses were measured to detect NADH/NAD in the micromolar range. [60] The positively charged flavins were electropolymerized in the presence of the negatively charged PABS and the composite material was then deposited on a glassy carbon electrode as shown in Figure 7a. The flavins were reported to act as dopants in the electropolymerization process of p-aminobenzene sulfonic acid. This device was then used for the detection of NADH and NAD+, showing electrocatalytic oxidation of NADH and reduction of NAD+ in a

reversible manner. Figure 7b shows a cyclic voltammetry plot of different concentrations of NADH and a plot of current versus NADH concentration.

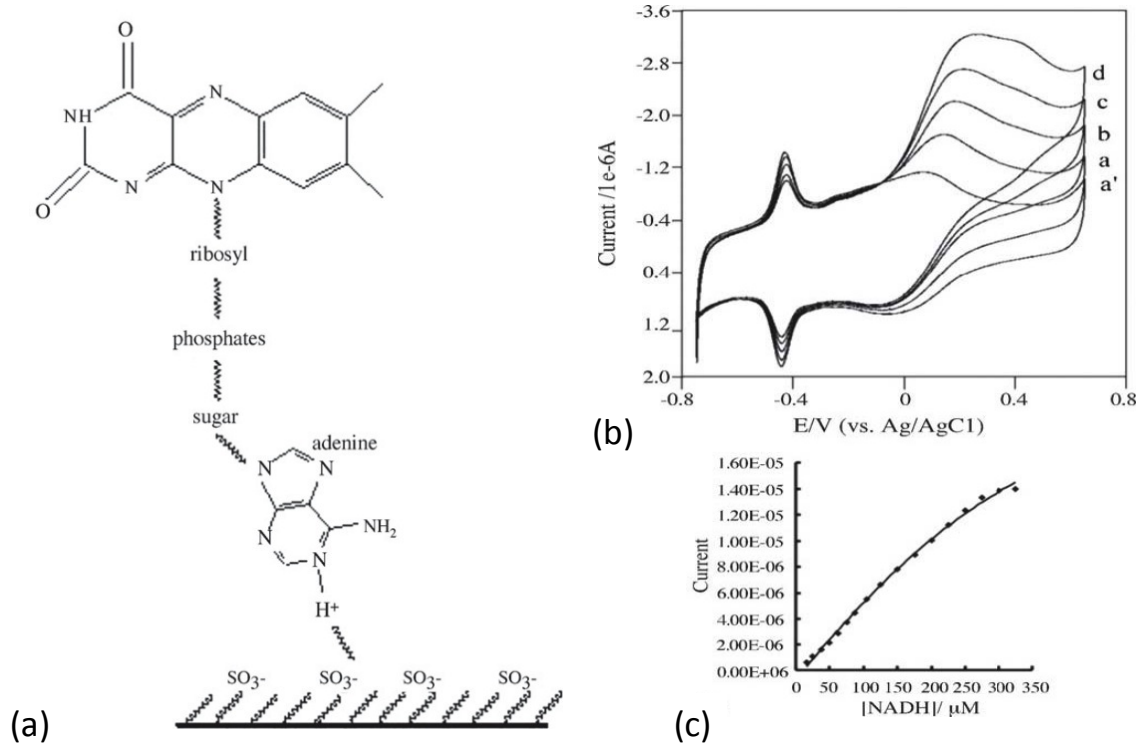

Figure 7: Immobilization scheme (a), cyclic voltammogram at different concentrations of NADH (b), and a plot of current vs. NADH concentration at -0.4 V(c) from Kumar, S. A.; Chen, S. M. Sens. Actuators, B 2007, 123 (2), 964–977.

The use of conducting polymers in DNA-based sensors has been attempted; however, a major limitation lies within the fact that DNA hybridization does not imply any electron transfer. The same is true of antibody–antigen interactions. However, research has been carried out using conducting polymers as transducers, with DNA probes/antigens grafted or entrapped in the polymer. The binding of the complementary probe/antibody causes a change in the redox properties of the polymer, which can be detected by cyclic voltammetry, for example. A variety of techniques have been used for immobilization of DNA, including adsorption, entrapment, and affinity binding (e.g., avidin–biotin complexation). [61] For a review on electrical conjugated polymer DNA sensors, see Reference [62]. Perhaps the first example of conjugated polymer use in DNA sensing was by Korri-Youssoufi et al. in 1997, who entrapped single-stranded oligonucleotides within PPy on a Pt electrode. Cyclic voltammograms showed changes in the redox potential of

the polymer film upon binding of complementary oligonucleotides. Detection sensitivity was found to increase with oligonucleotide length. [63]

Rodriguez and Alocilja reported the fabrication of a single-stranded DNA biosensor for the detection of Escherichia coli DNA using a Pt electrode with electropolymerized PPy and entrapped DNA (based on the method of Korri-Youssoufi et al. [63]). By cyclic voltammetry, they showed a difference of approximately 20 μA between complementary and noncomplementary DNA strands upon addition of 1μg of DNA. [64] Mouffouk and Higgins reported the synthesis of a COOH-functionalized EDOT monomer, whose copolymerization with EDOT on a Pt disk electrode generated a PEDOT coating with pendant carboxyl groups. This was then covalently linked to nucleic acids (using standard chemical immobilization techniques). By cyclic voltammetry, a shift in the polymer p-doping peak was seen upon hybridization, but not on exposure to a noncomplementary oligonucleotide, although it should be noted that the nucleic acids were present in excess (i.e., this shows proof of principle but not detection limits). [65] A further example of a DNA sensor, this time for the detection of sequences specific to the hepatitis C virus (HCV), was demonstrated by Josowicz and co-authors, using oligonucleotides on the surfaces of microelectrodes. As in other examples, the polymer (in this case a modified PPy) was electropolymerized and then functionalized with the oligonucleotide. The authors show extremely low detection limits (1.82×10^{-21} M) and note the effects of changing the spacer arm that tethers the DNA to the polymer backbone in terms of kinetics and sensitivity. They also go on to show how the microelectrode can be integrated into an AFM-SECM (atomic force microscopy–scanning electrochemical microscopy) tip for highly localized DNA detection. [66] Figure 8 shows detection of an 18-base oligonucleotide of HCV with a decrease in signal demonstrated upon binding of complementary DNA (but not of noncomplementary DNA).

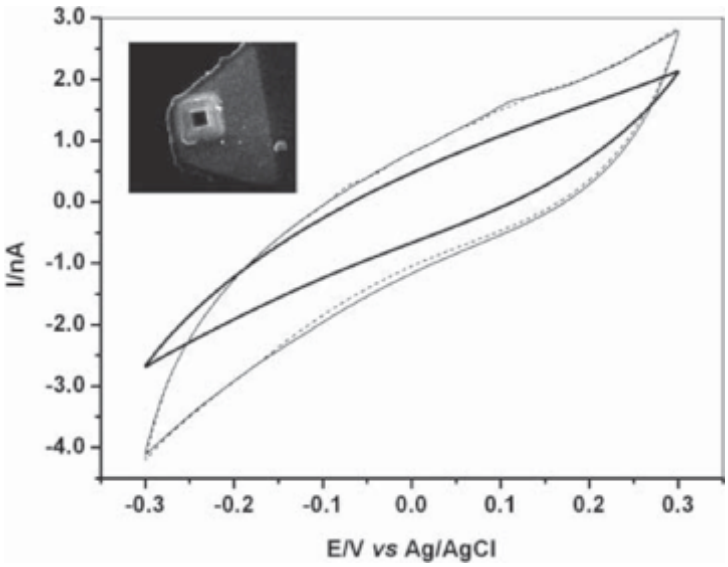

Figure 8: Cyclic voltammograms, show the detection of 18-mer DNA hybridization: (light solid line) PPy/pTPTC3-PO3H2-Mg2+/HCV-1 DNA probe; (dashed line) after exposure to 1.0×10^{-9} mol/L non-complementary DNA; (dark solid line) same electrode after hybridization with target HCV-1 DNA (18-mer, 1.0×10^{-9} mol/L) for 10 min from Riccardi, C. D. S.; Kranz, C.; et al. Anal. Chem. 2008, 80 (1), 237–245

As mentioned previously, glucose oxidase has been heavily studied for use in biosensing. The Higson group has published a suite of papers based on the use of microelectrodes combined with redox enzymes including glucose oxidase, alcohol dehydrogenase, and acetylcholinesterase. The basic principle is that sonochemical ablation of insulating polymer (polydiamino-benzene) layers at electrode surfaces exposes localized areas, which can act as localized microelectrodes and collectively as amicroelectrode array. Upon subsequent electropolymerization of the conducting polymer (in this case PANI) in the presence of redox enzyme, mushroom-shaped microelectrodes form in the cavities, and can then be interrogated by either impedimetric or amperometric methods. [67] The sensor scheme is shown in Figure 9.

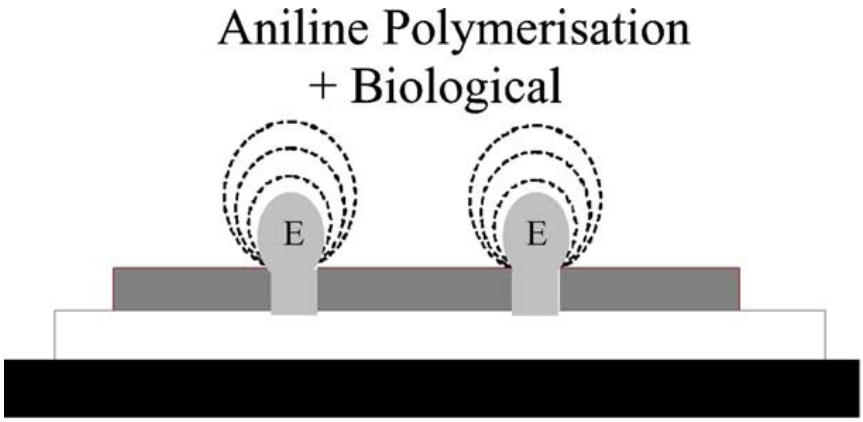

Figure 9: Schematic of microelectrode arrays from Barton, A. C.; Collyer, S. D.; et al. Biosens. Bioelectron. 2004, 20 (2), 328–337.

One major advantage of this method is the population of microelectrodes on the sensor surface (up to 2×10^5 cm^{-2}). The principle was shown to good effect with alcohol dehydrogenase entrapped in electropolymerized PANI to detect ethanol concentration in the millimolar range, reportedly due to the effect of interaction of the carbonyl enzymatic product and the PANI. The same group reported an extremely sensitive detection of certain organophosphate pesticides using a similar device, but this time with acetylcholinesterase immobilized. The organophosphates act as inhibitors of the enzyme, and the authors speculate that there is an amplification effect that allows detection of organophosphates down to 10^{-17} M. [68]

Malhotra and co-workers have shown the detection of cholesterol using two enzymes (cholesterol esterase and cholesterol oxidase), which work in succession to produce cholesterol ester, immobilized on a PANI-coated ITO electrode. This device relies on amperometric detection, which does not appear to have any amplification, and the range of detection is limited. [69] The same group recently described immobilization of cholesterol oxidase onto Langmuir–Blodgett films of poly[2- methoxy-5-(2'-ethyl-hexyloxy)-1,4-phenylene vinylene] (MEH-PPV), and while they show that the sensor is robust (up to 55 °C), the linear range of detection of cholesterol is reported between 1.29 and 12.29 mM. [70]

Pham and co-workers have recently published several papers using quinones as mediators for redox enzymes such as pyruvate oxidase (PyOD) and also for DNA sensing. They use a polymer called poly(JUG) (poly(5-hydroxy-1,4-naphthoquinone)), which contains a quinone, and copolymerize it with a modified JUG known as JUGA containing a carboxylic acid site (5- hydroxy-3-thioacetic acid-1,4-naphthoquinone) for attachment of the recognition element (PyOD, oligonucleotide, etc.). The resulting copolymer is known as

poly(JUG-co-JUGA). The quinone integrated into the polymer acts as an electron mediator allowing efficient recycling of the enzyme and permitting an extremely low working potential, thus avoiding side-oxidation products. [71] The report demonstrates a very selective detection of oxidation of pyruvate by PyOD (as per the scheme shown in Figure 10) with no signal obtained upon addition of urea, uric acid, glycine, or ascorbic acid – components commonly found in biological fluids. The same group has developed a similar sensor for DNA sensing. [72]

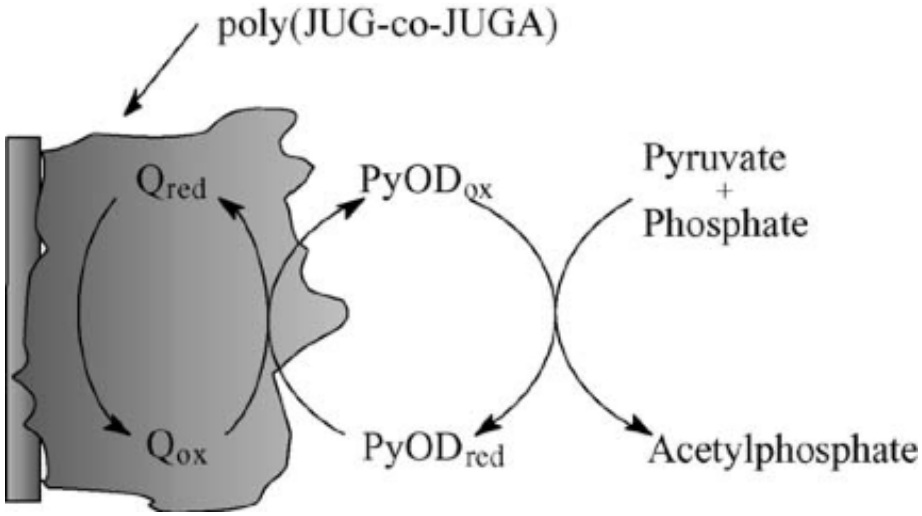

Figure 10: Schematic of the catalytic cycle for the PyOD/poly(JUG-*co*-JUGA)-modified electrode in anaerobic conditions (Q refere to chrage) from Dang, L. A.; Haccoun, J.; et al. Electrochim. Acta 2006, 51 (19), 3934–3943.

Mouffouk et al. have shown the electropolymerization of abiotin-functionalized polyterthiophene which undergoes large changes upon binding of avidin to the biotin, which they hypothesize is due to blocking of ion motion by the bound protein. [73] To synthesize the biotin-functionalized polyterthiophene, the authors electrocopolymerized a biotin-functionalized terthiophene with a terthiophene. This copolymer was necessary as it was not possible to electropolymerize a redox active film of the biotin-functionalized terthiophene alone. The authors report a detection limit of 5×10^{-14} M avidin and show that addition of excess bovine serum albumin causes only small changes in electrochemical properties, thereby ruling out nonspecific adsorption as the cause of changes upon binding of avidin. They also note that a water-compatible polymer (in development) would obviate the need for switching from aqueous buffer for measurements and nonaqueous electrolyte for electrochemical measurements.

Nishizawa et al. coated a microarray electrode with PPy and a penicillinase membrane. When the enzyme reaction occurred, conductivity changes were

detected by the increase in the current between two arrays at a constant applied voltage. [74] A variety of other enzymes have been used in conducting polymer electrode sensors, and these have been reviewed usefully, by type of transducer, by Lange et al. [75] Two other excellent reviews of conducting polymers for sensor applications that review protein applications include those by McQuade et al. [76] and Guimard et al. The first immunosensors with conducting polymers were reported in the 1990s, fabricated by trapping antibodies in PPy membranes on electrode surfaces. The antibody-modified electrodes were then pulsed to cycle the conducting polymer from reduced form to oxidized form and back. During this process, a sample containing the complementary antigen to the antibody was introduced and an electrochemical signal could be detected that was concentration dependent and was additionally suggested to be reversible. [77] Reversibility of antigen– antibody interactions is extremely interesting for sensing applications, as it implies that sensors can be reused, making it a very desirable quality. It was later postulated by Gooding et al. that the reversibility of the antibody–antigen reaction was as a consequence of the pulsing of the electrochemical potential on the timescale of 200ms, thereby modulating the immunoreactions. [78] The theory is that antigen–antibody interactions consist of two phases: an initial phase involving coulombic and van der Waals forces and a second phase involving hydrogen bonding and hydrophobic forces. It is the second phase that essentially determines the irreversibility of the reaction. The authors provide evidence that the pulsing time is too short for the second phase of binding to occur, thus allowing the reaction to be reversible. They further note that although the binding constant for the reaction is lower, this did not compromise the selectivity of the sensor.

Detection of Listeria monocytogenes has also been reported using screen-printed carbon electrodes onto which PANI was electropolymerized and then functionalized thereafter with avidin. [79] Biotinylated polyclonal anti-InlB (an L. monocytogenes surface protein) was then incorporated into the electrode via biotin–avidin binding. Impedance changes in the polymer layer were then measured upon addition of different concentrations of InlB protein. As a control, a nonspecific antibody was immobilized on another electrode and InlB added, but little or no response was seen (as shown in Figure 11). The authors derive a lower limit of detection of 4.1 pg ml^{-1}.

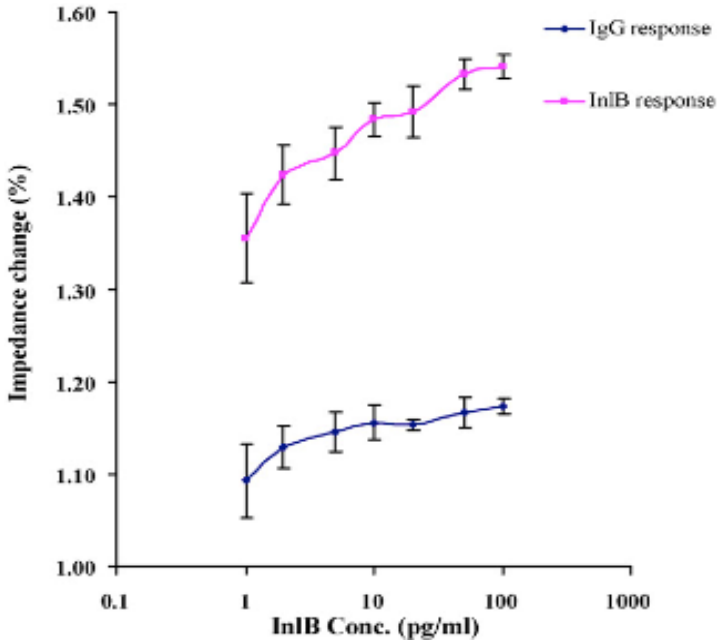

Figure 11: Calibration curves showing the impedance change for increasing InlB antigen concentrations, for both sample and control sensors from Tully, E.; Higson, S. P.; et al. Biosens. Bioelectron. 2008, 23 (6), 906–912.

Dadarwal et al. published a report using conducting polymer electrodes for detection of Salmonella infecting bacteriophage. [80] This is not a diagnostic but rather a screening method to search for bacteriophage to be used for indicating the presence of Salmonella species. This study used a chemical polymerization method to cover polycarbonate membranes with PPy and subsequently deposit Salmonella cells on the membrane, and fix them there by applying vacuum to pull the cells into the membrane pores. Upon addition of bacteriophage, the Salmonella cells are lysed, resulting in a change in the electrochemistry of the polymer, as measured by cyclic voltammetry.

1.2.1.2 Transistors

IS-OFETs for monitoring potassium ion concentrations are also developed for medical applications. [81] Rai et al. have developed an IS-OFET, first, as a pH sensor and, second, by functionalizing with the K+-ion channel valinomycin (as shown in Figure 12), as a potassium sensor. Regioregular P3HT was used in combination with a tantalum oxide dielectric (the tantalum oxide also served as an ion-specific membrane for the pH sensor). The device was then encapsulated with a polyvinyl alcohol film, leaving windows for exposure to ions. The dynamic range for the pH sensor was between pH 6.5 and 9.5, while the detection range for potassium ions was between 1 and 25mM. The authors suggest that these sensors can provide reliable estimation of pH and potassium ion concentration at low operating voltages.

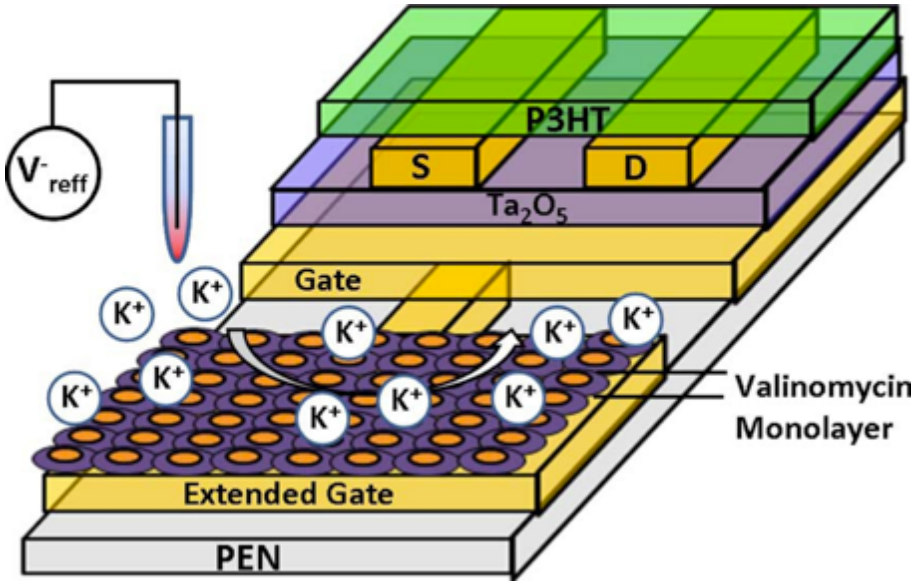

Figure 12: Schematic of an ISFET for potassium ion sensing from Rai, P.; Jung, S.; et al. IEEE Sens. J. 2009, 9 (12), 1987–1995.

In one example of DNA sensing on OTFTs, Yan et al. showed the use of an OTFT fabricated on a silicon substrate. [82] The conjugated polymer used was a regioregular polythiophene (P3HT), which was deemed to have high field-effect mobility. DNA was immobilized on the substrates by simple adsorption, followed by hybridization of complementary molecules, and this was visualized by fluorescence microscopy (the target DNA was labeled with a fluorescent label). The DNA was immobilized directly on the electrodes (Au) followed by addition of the P3HT. The authors state that by immobilizing the DNA on the Au electrodes, rather than on the conjugated polymer, as was

done by another group who immobilized DNA onto pentacene, [83] the device achieves greater stability. The immobilization of DNA on the OTFT electrodes was found to change the channel current and the field-effect mobility of the device. The authors suggest that this device has great promise for cost-effective, field-deployable sensors. The performance of this sensor is shown in Figure 13. The concentration of DNA immobilized on the device was 2 μM, and the same concentration was used for hybridization. The time of immobilization was varied from 4 to 48 h, while the hybridization time was 2 h.

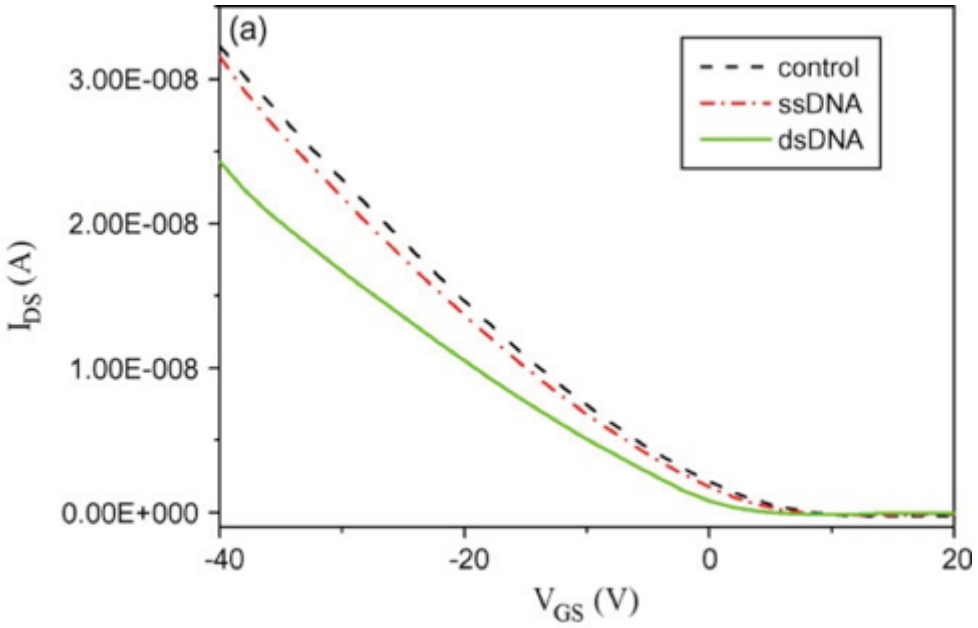

Figure 13: Transfer characteristics of three OTFTS used for DNA sensing from Yan, F.; Mok, S. M.; et al. Biosens. Bioelectron. 2009, 24 (5), 1241–1245.

Bartic et al. [84] have demonstrated an IS-OFET based on a P3HT channel and a tantalum oxide gate dielectric (thus a hybrid organic/inorganic device), onto which glucose oxidase was immobilized. When exposed to glucose solutions, the drain current reflected the glucose concentration. This response was understood in terms of the pH change that takes place when the immobilized glucose oxidase converts glucose to gluconic acid and thereby increases the proton concentration near the tantalum oxide surface.

The first demonstration of the OECT for glucose sensing was by Zhu et al. using a commercially available PEDOT:PSS formulation. [85] This work was subsequently refined and the technique was used to measure glucose in the micromolar range, appropriate for detection of glucose in human saliva. [86] In this sensor, the enzyme was added in solution rather than being

immobilized on the sensor surface. A further modification of the device involved the incorporation of ferrocene as a mediator. [87] In this report, the channel, source, drain, and gate electrodes are fabricated from PEDOT:PSS, providing a simple architecture for enzymatic sensing that can be fabricated using a one-layer patterning process. Detection of glucose with and without the ferrocene mediator is shown in Figure 14. Finally, it has also been demonstrated by Yang et al. that it is possible to achieve multianalyte sensing by integration of OECTs with a surface-directed microfluidic system. [88] Simultaneous detection of lactate and glucose in the millimolar range was demonstrated.

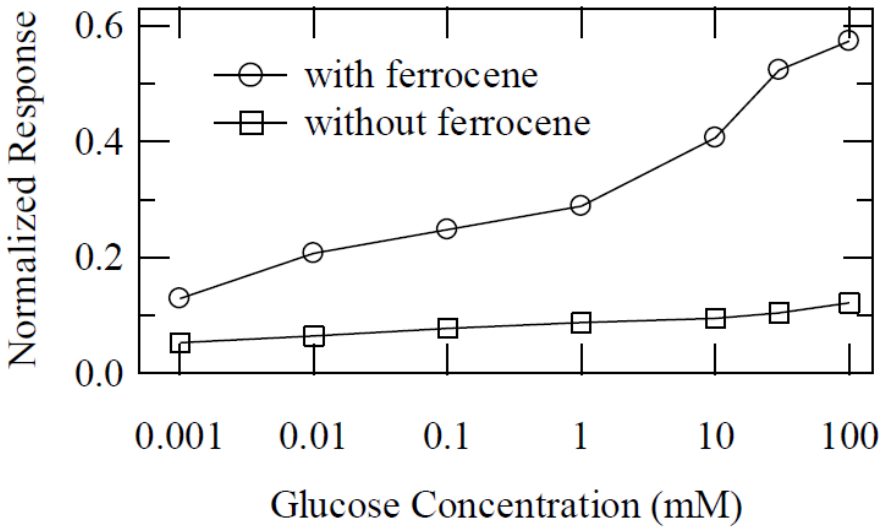

Figure 14: Normalized response to glucose concentration for an OECTs preloaded with a mixture with (open circles) and without (open squares) ferrocene mediator from Shim, N. Y.; Bernards, D. A.; et al. Sensors 2009, 9 (12), 9896–9902.

The preceding OECT sensors were based on addition of the enzyme in solution, and it was shown that addition of free-floating enzyme can result in quantitative measurement of metabolites down to the micromolar range. Other OTFT-based sensors for glucose have immobilized the enzyme within a conducting polymer film, for example, by using spin-coating techniques or by entrapping the enzyme during electrochemical polymerization. The entire sensor was then encapsulated in a cellulose acetate membrane to prevent escape of the enzyme-conducting polymer matrix. The device showed a linear increase in the drain current upon increase in glucose concentration in the millimolar range, with a response time of seconds. [89]

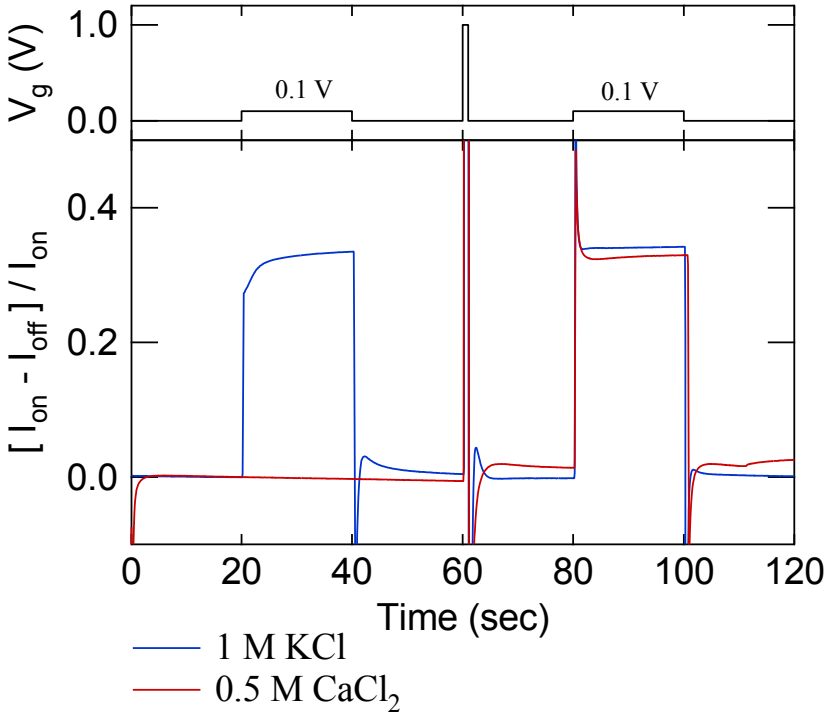

Figure 15: A voltage applied at the gate electrode (V_g) of an OECT causes K^+ ions to go through the gramicidin channels and change the drain current (I_d). No response is observed for Ca^{2+}, as gramicidin is not permeable to divalent ions. When a 1V pulse at the gate destroys the membrane, it can be seen that the transistor itself cannot discriminate mono-from divalent ions from Bernards, D. A.; et al. APL, 2006, (89), 053505.

Beyond glucose oxidase sensing, ion channels embedded in lipid bilayers have also been integrated with OECTs. [90] In this study, gramicidin, a bacterial peptide that forms dimers to span lipid bilayers, was used as a model ion channel, as it is accepted as a good model for ion channel function. It was shown that the ionic currents through the gramicidin channels can be detected as a modulation in the drain current (Figure 15). Due to the transistor geometry, a small number of cations can dedope portions of the organic film; therefore, these devices offer significant amplification in ion-to-electron conversion using a simple detection scheme. The devices used for this demonstration utilized suspended lipid bilayer membranes, which are not stable over time. However, recent progress in covalent tethering has yielded lipid membranes that are stable for periods of a few months. [91] Such membranes might help yield ion channel-based sensors that are stable enough for applications in the field.

1.2.1.3 Electronic tongues

Several examples exist in the literature of artificial taste sensors or so called 'electronic tongues' based on either amperometric or conductometric methods. These sensors are based on arrays of nonspecific detectors whose overall response to a given chemical forms a 'fingerprint', and thus, a chemical compound may be 'recognized' by its characteristic fingerprint. The electronic tongue idea can be generalized and used with other types of sensors (e.g., transistors); hence, it merits special mention. Riul et al. report films made of layers of conducting polymer films and other materials deposited onto gold electrodes. Then, using impedance spectroscopy, they show that unique signatures could be detected for six types of red wine. The sensor was also able to distinguish samples according to variety, vintage, and producer when combined with an artificial neural network for data treatment. [92] The use of ultrathin films of conducting polymers mixed with different materials, whose response to distinct tastes varies in such a way that a high resolving power is rendered to the tongue, combined with artificial neural networks to treat the data obtained from a set of sensing units, allows high accuracy in the sample recognition process. The electronic tongue process is depicted in Figure 16.

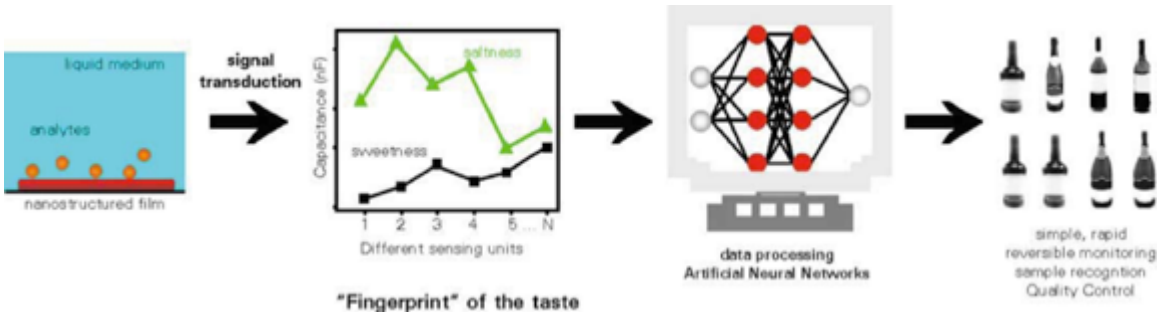

Figure 16: the procedure for identifying wines with an electronic tongue from Riul, A.; de Sousa, H. C.;et al. Sens. Actuators, B 2004, 98 (1), 77–82.

A second electronic tongue study was published by De Saja and co-workers, this time to detect prohibited adulterants in wine using a similar approach. They used two families of sensors: one based on phthalocyanine-based carbon paste electrodes and the second on PPy doped with a range of counterions. [94] The electrochemical response of the electrodes is reported to depend on the ions and electroactive molecules present in the solution. The authors state that due to the different nature of the electrodes the response to electroactive molecules/ions present is very different, and thus, an array of these different electrodes provides greater specificity to the system.

1.2.2 Optical Sensors in Liquid Sensing

As mentioned in the introduction, the principal use of conjugated polymers in optical sensors has been as recognition elements, though examples of their use as part of the transducer are becoming available. Water-soluble conjugated polymers are of particular interest for use in optical sensor applications. These polymers typically have charged functional groups on the conjugated polymer backbone and therefore combine the semiconducting behavior of conjugated polymers with the charge-mediated behavior of polyelectrolytes. These molecules were first developed in the 1980s and have gone on to be used in a variety of applications such as PLEDs and optoelectronic devices. [95] An illustration of a conjugated polyelectrolyte (CPE) is shown in Figure 17.

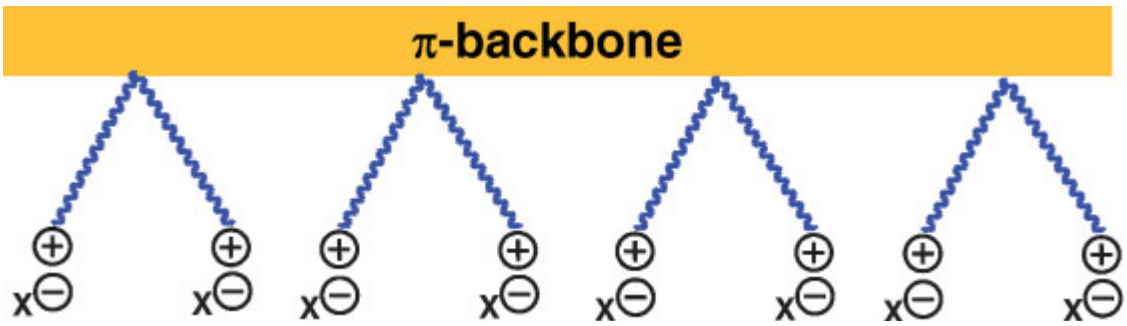

Figure 17: Generalized structural components of a cationic conjugated polyelectrolyte. Negative ionis represent the dopant and positive charges represents the charges of the conjugated back-bone

Due to the unique electronic structure of conjugated polymers, excitations can be efficiently transferred over long distances in ways not possible for assemblies of weakly interacting chromophores. Several types of water-soluble conjugated polymers have been explored including PPVs, polythiophenes, polyphenylethylenes, and polyfluorenes. The latter represents a material type of this category that has been widely used in biological and chemical sensing applications, mostly due to the ease with which they can be molecularly tuned to suit the application. In addition, they have high fluorescence quantum yields (20–40% in solution). One drawback of these polymers is their tendency to aggregate in solution, which affects their fluorescence; however, this is a feature that may be addressed in the future with synthesis. In summary, these molecules show tremendous potential for a wide variety of sensing applications, although issues of aggregation, nonspecific interactions, and quantum yield must still be addressed. It must also be noted that, although these molecules amplify

optical signals, they cannot be considered as sensors in themselves as they ultimately require an additional signal transduction mechanism for measuring and quantifying the signal.

1.3 Conclusion

In this have attempted to highlight examples of sensors based on conjugated polymers, in the liquid phase. It covered electrical, optical sensors and, a small number of mechanical sensors. The reviewed examples not only to highlight the breadth of this field, but also to illustrate that the field is by no means saturated and that the field has evolved since its conception and indeed continues to evolve. Conjugated polymer sensors are becoming ever more sensitive, with lower detection limits and wider dynamic ranges, while improvements are also being made to the specificity and speed of detection.

Conjugated polymers are uniquely appropriate for the development of sensors for a variety of reasons, including (1) facile, low-temperature processing resulting in low-cost, disposable sensors; (2) tunability of their chemical and electronic properties, achieved via chemical synthesis, translating into potential gains in sensitivity and selectivity of sensors; and (3) the well-defined interface between the conjugated polymer and the medium in which the analyte is present is beneficial because of the absence of broken bonds. In addition, as illustrated by key examples, the possibility of doping of conjugated polymers not only is beneficial in terms of addition of recognition elements, but also allows an additional level of tuning and specificity.

The breadth of analytes used in conjugated polymer sensors is dizzyingly large, covering everything from explosives (TNT) to viruses (HCV) and the examples highlighted here represent only the tip of iceberg. Sensors were considered in terms of their detection limits as well as the sensing parameter used to achieve detection. The work described here represents an enormous amount of progress in the application of conjugated polymers to the field of sensing. Due to the truly flexible nature of conjugated polymers, it is expected that research in this area will continue to be novel and exciting.

References

[1] Pope, M.; Swenberg, C. E. Electronic Processes in Organic Crystals and Polymers; Oxford University Press: New York, 1999.

[2] Shirakawa, H.; Louis, E. J.; et al. J. Chem. Soc., Chem. Commun. 1977, 16, 578–658.

[3] Burroughes, J. H.; Bradley, D. D. C.; et al. Nature 1990, 347 (6293), 539–541.

[4] Gerard, M.; Chaubey, A.; et al. Biosens. Bioelectron. 2002, 17 (5), 345–359.

[5] Zhuang, C.; Buttner, W. J.; et al. Electroanalysis 1992, 4 (3), 253–266.

[6] Hanawa, T.; Kuwabata, S.; et al. Synth. Met. 1989, 30 (2), 173–181.

[7] Persaud, K. C. In IEE Colloquium on Molecular Electronics, London, UK, 19 October 1990.

[8] Nguyen, V. C.; Potje-Kamloth, K. Thin Solid Films 1999, 338 (1–2), 142–148.

[9] Van, C. N.; Potje-Kamloth, K. Thin Solid Films 2001, 392 (1), 113–121.Janata, J. Crit. Rev. Anal. Chem. 2002, 32 (2), 109–120.

[10] Janata, J. Crit. Rev. Anal. Chem. 2002, 32 (2), 109–120.

[11] Mello, S. V.; Dynarowicz-Latka, P.; et al. Colloids Surf., A 2002, 198, 45–51.

[12] Xie, D.; Jiang, Y. D.; et al. Colloids Surf., B 2002, 81 (2–3), 158–164.

[13] Bhat, N. V.; Gadre, A. P.; et al. J. Appl. Polym. Sci. 2003, 88 (1), 22–29.

[14] An, K. H.; Jeong, S. Y.; et al. Adv. Mater. 2004, 16 (12), 1005.

[15] Elizalde-Torres, J.; Hu, H. L.; et al. Sens. Actuators, B 2004, 98 (2–3),

218–226.

[16] Li, G. F.; Josowicz, M.; et al. Appl. Phys. Lett. 2004, 85 (7), 1187–1189.

[17] Ram, M. K.; Yavuz, O.; et al. Synth. Met. 2005, 151 (1), 77–84.

[18] Janata, J. Proc. IEEE 2003, 91 (6), 864–869.

[19] Chen, H.; Josowicz, M.; et al. Chem. Mater. 2004, 16 (23), 4728–4735.

[20] Hao, Q. L.; Kulikov, V.; et al. Sens. Actuators, B 2003, 94 (3), 352–357.

[21] Krondak, M.; Broncova, G.; et al. J. Solid State Electrochem. 2006, 10 (3), 185 191.

[22] Amrani, M.E.H.;Payne,P.A.;etal.Sens.Actuators,B1996,33(1–3),137–141.

[23] Ghita, M.; Gheorghe, M.; et al. In Proceedings of the 22nd International Conference on Microelectronics Serbia, 14–17 May 2000.

[24] Malliaras, G.; Friend, R. Phys. Today 2005, 58 (5), 53–58.

[25] VandeLeur, R.H.M.;vanderWaal,A.Synth.Met.1999,102(1–3),1330–1331.

[26] Blackwood, D.; Josowicz, M. J. Phys. Chem. 1991, 95 (1), 493–502.

[27] Topart, P.; Josowicz, M. J. Phys. Chem. 1992, 96 (19), 7824–7830.

[28] Charlesworth, J. M.; Partridge, A. C.; et al. J. Phys. Chem. 1993, 97 (20), 5418–5423.

[29] Liao, F.; Chen, C.; et al. Sens. Actuators, B 2005, 107 (2), 849–855.

[30] Kittlesen, G. P.; White, H. S.; et al. J. Am. Chem. Soc. 1984, 106 (24), 7389–7396.

[31] Andersson, P.; Berggren, D.; et al. Forest Ecol. Manage. 2002, 157 (1–

3), 39–53.

[32] Bredas, J. L.; Scott, J. C.; et al. Phys. Rev. B 1984, 30 (2), 1023–1025.

[33] Christie, S.; Scorsone, E.; et al. Sens. Actuators, B 2003, 90 (1–3), 163–169.

[34] Yuan, J. M.; El-Sherif, M. A. IEEE Sens. J. 2003, 3 (1), 5–12.

[35] Cao, W. Q.; Duan, Y. X. Sens. Actuators, B 2005, 110 (2), 252–259.

[36] Savvate'ev, V.; Chen-Esterlit, Z.; et al. Appl. Phys. Lett. 2002, 81 (24), 4652–4654.

[37] Vasilopoulou, M.; Georgiadou, D. G.; et al. Microelectron. Eng. 2009, 86 (4–6), 1511–1514.

[38] Yakuphanoglu, F.; Senkal, B. F. Synth. Met. 2009, 159 (3–4), 311–314.

[39] King, W. H. Anal. Chem. 1964, 36 (9), 1735.

[40] Wohltjen, H.; Dessy, R. Anal. Chem. 1979, 51 (9), 1458–1464.

[41] Milella, E.; Penza, M. Thin Solid Films 1998, 329, 694–697.

[42] Penza, M. Milella, E.; et al. IEEE Trans. Ultrason. Ferroelectr. Freq. Control 1998, 45 (5), 1125–1132.

[43] Chang, S. M.; Muramatsu, H.; et al. Mater. Sci. Eng., C 2000, 12 (1–2), 111–123.

[44] Sauerbrey, G. Z. Phys. 1959, 155 (2), 206–222.

[45] Kim, S. R.; Choi, S. A.; et al. Synth. Met. 1995, 71 (1–3), 2027–2028.

[46] Chen, Z. K.; Ng, S. C.; et al. Synth. Met. 1997, 87 (3), 201–204.

[47] Deng, Z. P.; Stone, D. C.; et al. Analyst 1997, 122 (10), 1129–1138.

[48] Syritski, V.; Reut, J.; et al. Synth. Met. 1999, 102 (1–3), 1326–1327.

[49] Newman, J. D.; Turner, A. P. F. Biosens. Bioelectron. 2005, 20 (12), 2435–2453.

[50] Clark, L. C., Jr.; Lyons, C. Ann. N.Y. Acad. Sci. 1962, 102, 29–45.

[51] Turner, A. P. F. Sens. Actuators 1989, 17 (3–4), 433–450.

[52] Cass, A. E. G.; Davis, G.; et al. Anal. Chem. 1984, 56 (4), 667–671.

[53] Vijayakumar, A. R.; Csoregi, E.; et al. Anal. Chim. Acta 1996, 327 (3), 223–234.

[54] Murray, R. W. Philos. Trans. R. Soc. Lond., A 1981, 302 (1468), 253–265.

[55] Foulds, N. C.; Lowe, C. R. J. Chem. Soc., Faraday Trans. 1986, 82, 1259–1264.

[56] Gregg, B. A.; Heller, A. J. Phys. Chem. 1991, 95 (15), 5976–5980.

[57] Huang, W. S.; Humphrey, B. D.; et al. J. Chem. Soc., Faraday Trans. 1986, 82, 2385.

[58] Yue, F.; Ngin, T. S.; et al. Sens. Actuators, B 1996, 32 (1), 33–39.

[59] Rahman, A.; Won, M. S.; et al. Anal. Chem. 2003, 75 (5), 1123–1129.

[60] Kumar, S. A.; Chen, S. M. Sens. Actuators, B 2007, 123 (2), 964–977.

[61] Guimard, N. K.; Gomez, N.; et al. Prog. Polym. Sci. 2007, 32, 876–921.

[62] Peng, H.; Zhang, L. J.; et al. Biomaterials 2009, 30 (11), 2132–2148.

[63] Korri-Youssoufi, H.; Garnier, F.; et al. J. Am. Chem. Soc. 1997, 119 (31), 7388–7389.

[64] Rodriguez, M. I.; Alocilja, E. C. IEEE Sens. J. 2005, 5 (4), 733–736.

[65] Mouffouk, F.; Higgins, S. J. Electrochem. Commun. 2006, 8 (2), 317–322.

[66] Riccardi, C. D. S.; Kranz, C.; et al. Anal. Chem. 2008, 80 (1), 237–245.

[67] Barton, A. C.; Collyer, S. D.; et al. Biosens. Bioelectron. 2004, 20 (2), 328–337.

[68] Law, K. A.; Higson, S. P. J. Biosens. Bioelectron. 2005, 20 (10), 1914–1924.

[69] Singh, S.; Solanki, P. R.; et al. Anal. Chim. Acta 2006, 568 (1–2), 126–132.

[70] Matharu, Z.; Arya, S. K.; et al. Anal. Chim. Acta 2009, 634 (2), 243–249.

[71] Dang, L. A.; Haccoun, J.; et al. Electrochim. Acta 2006, 51 (19), 3934–3943.

[72] Reisberg, S.; Piro, B.; et al. Bioelectrochemistry 2006, 69 (2), 172–179.

[73] Mouffouk, F.; Brown, S. J.; et al. J. Mater. Chem. 2005, 15 (11), 1186–1196.

[74] Nishizawa, M.; Matsue, T.; et al. Anal. Chem. 1992, 64 (21), 2642–2644.

[75] Lange, U.; Roznyatouskaya, N. V.; et al. Anal. Chim. Acta 2008, 614 (1), 1–26.

[76] McQuade, D. T.; Pullen, A. E.; et al. Chem. Rev. 2000, 100 (7), 2537–2574.

[77] Sadik, O. A.; Wallace, G. G. Anal. Chim. Acta 1993, 279 (2), 209–212.

[78] Gooding, J. J.; Wasiowych, C.; et al. Biosens. Bioelectron. 2004, 20 (2), 260–268.

[79] Tully, E.; Higson, S. P.; et al. Biosens. Bioelectron. 2008, 23 (6), 906–912.

[80] Dadarwal, R.; Namvar, A.; et al. Mater. Sci. Eng., C 2009, 29 (3), 761–765.

[81] Rai, P.; Jung, S.; et al. IEEE Sens. J. 2009, 9 (12), 1987–1995.

[82] Yan, F.; Mok, S. M.; et al. Biosens. Bioelectron. 2009, 24 (5), 1241–1245.

[83] Zhang, Q. T.; Subramanian, V. In IEEE International Electron Devices Meeting, 10– 12 December 2007; Vols. 1 and 2, pp 229–232, 1043.

[84] Bartic, C.; Campitelli, A.; et al. Appl. Phys. Lett. 2003, 82 (3), 475–477.

[85] Zhu, Z. T.; Mabeck, J. T.; et al. Chem. Commun. 2004, 13, 1556–1557.

[86] Bernards, D. A.; Macaya, D. J.; et al. J. Mater. Chem. 2008, 18 (1), 116–120.

[87] Shim, N. Y.; Bernards, D. A.; et al. Sensors 2009, 9 (12), 9896–9902.

[88] Yang, S. Y.; DeFranco, J. A.; et al. Lab Chip 2009, 9 (5), 704–708.

[89] Liu, J.; Agarwal, M.; et al. Sens. Actuators, B 2008, 135 (1), 195–199.

[90] Bernards, D. A.; Malliaras, G. G.; et al. Appl. Phys. Lett. 2006, 89 (5), 053505.

[91] Vockenroth, I. K.; Atanasova, P. P.; et al. Langmuir 2008, 24 (2), 496–502.

[92] Riul, A.; de Sousa, H. C.; et al. Sens. Actuators, B 2004, 98 (1), 77–82.

[93] Parra, V.; Arrieta, A. A.; et al. Sens. Actuators, B 2006, 115 (1), 54–61.

[94] Hoven, C. V.; Garcia, A.; et al. Adv. Mater. 2008, 20 (20), 3793–3810.

Chapter 2

2 Highly conformable conducting polymer electrodes

Electronic devices that interface with living tissue have become a necessity in clinics to improve diagnosis and treatments. Devices such as cardiac pacemakers and cochlear implants stimulate and monitor electrically active cells, restoring lost function and improving quality of life. On a more fundamental level, most breakthroughs in our understanding of the basic mechanisms of information processing in the brain have been obtained by means of recordings from implantable electrodes. [1–3] Materials science is playing a pivotal role in this field. For example, state-of-the-art implantable electrodes are microfabricated devices that contain high-density arrays of metal sites on a silicon shank (silicon probes). [4] Still, as neuroscience continues to advance and more options for electrical intervention become a reality for patients (ocular implants, deep-brain stimulation for epilepsy and Parkinson's disease), [5] there is a tremendous need for developing advanced materials solutions for the biotic/abiotic interface. One such example is the necessity to develop electrodes that can conform to the curvilinear shapes of organs (e.g., the surface of the brain or its sulci) and form high-quality electrical contacts. Such surface electrodes are needed for electrocorticography (ECoG), which is increasingly used for functional mapping of cognitive processes before certain types of brain surgery (e.g., tumors) or for diagnosis purposes (e.g., epilepsy). [6] Placed on the somatosensory cortex, surface electrode arrays are also being used in brain-machine interfaces, an assistive technology for people with severe motor disabilities. [7] In contrary to silicon probes that penetrate the brain and cause tissue damage, these arrays are placed on the surface of the brain and are hence less invasive.

Not surprisingly, there has been a lot of interest within the materials science community to develop conformable electrodes. As bending rigidity decreases with thickness, thin sheets of polymeric materials, including polyimide, [8,9] poly-dimethylsiloxane, [10,11] and parylene [12–14] are being used as substrates and insulation layers for the fabrication of such surface arrays, typically in conjunction with Au, Ir, or Pt electrodes. To ensure that these arrays are sufficiently self-supporting and can be handled during surgery, they are built to a total thickness exceeding 10 μm (and in some cases 100 μm), which, however, limits their conformability. A creative solution involving the use of bioresorbable substrates was recently reported by the Rogers and co-workers: [15] Ultra thin electrode arrays (which were not self-supporting on their own) were fabricated by sandwiching Au electrodes between two 1.2 μm thick layers of polyimide. They were transferred onto films of silk, which made handling possible and dissolved after flushing with saline.

In a parallel effort, conducting polymers have emerged as ideal electrode materials for interfacing with neurons and are being used to overcoat metal electrodes and improve the performance of silicon probes. [16–18] Conducting polymer electrodes were shown to reduce the foreign body response of the brain to the probe and to enable the recording of electrical activity for longer time intervals. Moreover, they were shown to lower the electrical impedance at the interface with tissue, improving the quality of recordings. [19] Although this is not understood in a quantitative manner, it is often attributed to a lwoer impedance at the biotic/abiotic interface, due to the ability of polymers to conduct ions. [16] Furthermore, conducting polymers have been used to release drugs such as neurotrophins, enabling combined electrical/biochemical stimulation. [18,20] Finally, conducting polymer electrodes were used to detect transmitter molecule release from single cells, [21] creating the tantalizing potential for combined electrical/biochemical recording at a single cell level.

Given the high demand for the development of biocompatible and conformable electrodes for *in vivo* applications and given the advantages provided by conducting polymers for neuronal interfacing, it is essential to develop general procedures for integrating conducting polymers with flexible substrates. This demand has remained largely unanswered. Actual solutions available rely almost exclusively on electrochemically grown conducting polymers on pre-patterned metal electrodes, [16] which dramatically limits the range of polymers that can be utilized. One exception involves a rather exotic patterning technique based on microfluidics and results in thick arrays with limited conformability. [22] Here, we provide a generic solution to this challenge and demonstrate highly conformable electrode arrays that consist of a 4 μm-thick parylene C film that contains photo- lithographically defined microelectrodes based on poly(3,4- ethylenedioxythiophene) doped with

poly(styrene sulfonate) (PEDOT:PSS). PEDOT:PSS is an obvious choice as electrode material, given its state-of-the-art conductivity, its biocompatibility, [23] its chemical stability, [18] and the fact that it is commercially available. Similarly obvious is the choice of parylene as a substrate and an insulator, given its combination of biocompatibility [24] and good mechanical (flexibility) and electrical (insulation) properties. We demonstrate the use of these electrode arrays for *in vivo* electrocorticography (ECoG) in rats, in which sharp-wave events mimicking epileptic spikes were successfully recorded. We also show that the arrays provide high spatial resolution and that PEDOT:PSS electrodes outperform Au ones during *in vivo* evaluation of devices of similar geometry.

2.1 Fabrication process

The fabrication process and the resulting layout of the con- ducting polymer electrodes are shown in Figure 1. The fabrication started by depositing a 2-μm-thick parylene film, which became the substrate of the array, on a quartz wafer. Au con- tact pads and interconnects were subsequently patterned using a standard lift-off process. The sample was then coated for a second time with a 2-μm-thick parylene film, which became the insulator of the array, and a window was opened over part of the Au film via photolithography and etching. The PEDOT:PSS film was deposited from solution, and the sample was coated for a third time with a sacrificial parylene film whose purpose was to protect the conducting polymer electrode from the sub- sequent processing steps. Final photolithography and etching steps defined the structure of the PEDOT:PSS electrodes. The fabrication ended with immersion in deionized water, which removed the parylene film overlying the PEDOT:PSS and exposed the electrodes. Finally, the arrays were peeled-off the quartz wafer before use. This process is fairly generic and relies on the better adhesion of the conducting polymer on the metal electrode than on the overlying parylene film. As the latter is hydrophobic, it is expected to work with most conducting polymers, which obtain some hydrophilic character due to their doping. It should be noted that, in separate tests, it was established that the deposition and removal of a parylene film from a PEDOT:PSS film did not affect the conductivity of the latter

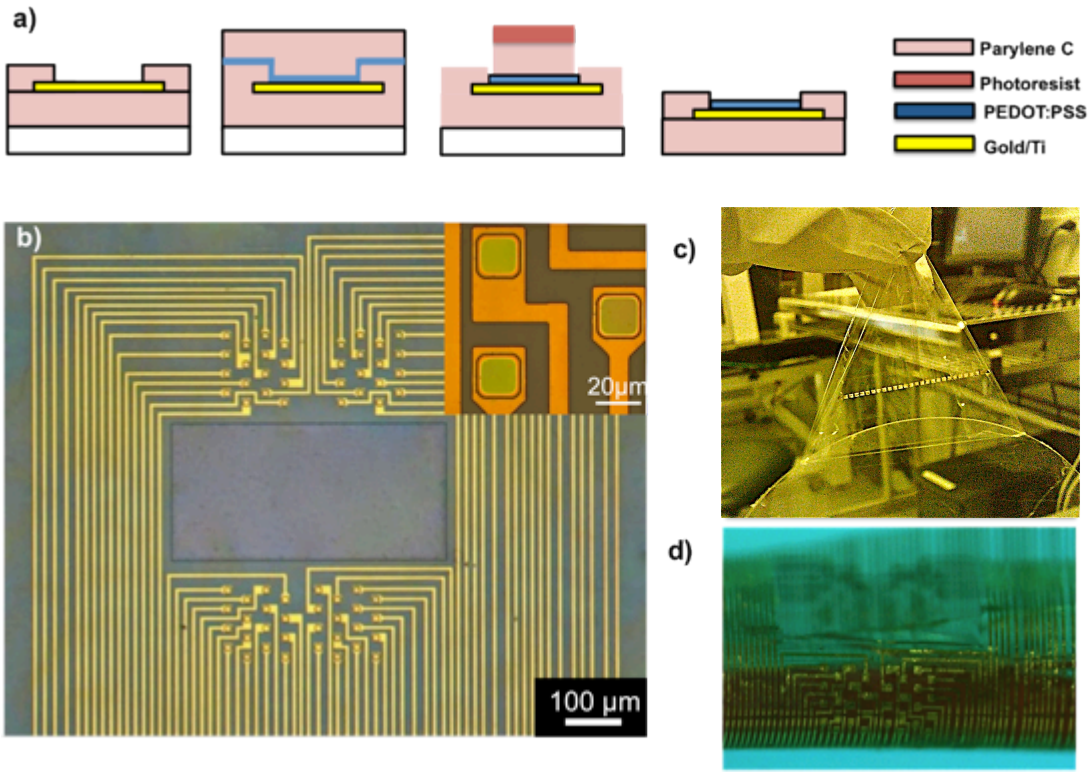

Figure 1. a) Schematic representation of the fabrication process indicating of an electrode (not to scale). b) Microscopy images of the array showing which a silicon probe was inserted and a detailed view of three electrodes. The electrode array is shown to support the weight of a quartz wafer (c), and to conform to a cylinder with a radius of 2mm.

The process described above yielded electrode arrays with a total thickness of 4 µm , with the Au interconnects and the PEDOT:PSS located at the neutral mechanical plane. The layout of an array is shown in Figure 1b. The arrays had a rectangular opening in the middle (through the parylene film), in order to allow the simultaneous insertion of a silicon probe (see below). Two sets of 32 electrodes each were placed above and below the opening. Each set consisted of two subsets of 16 electrodes each, placed on a hexagonal lattice, with individual electrodes having an area of 20 µm x 20 µm and a center-to-center distance of 60 µm. This particular design provides a fine surface map of the electrical activity of a brain region of interest, while at the same time it allows depth-recordings (2 mm) from a silicon probe to be performed. Despite their thinness, the electrode arrays had adequate mechanical strength to be self-supporting and to be manipulated by a surgeon. Figure 1c shows a partially peeled array (Au contact pads are visible) supporting not only its own weight, but also the weight of a 100 mm quartz wafer (1 mm thick). At the same time, the arrays were able to conform to surfaces with a small

radius of curvature. Figure 1d shows a microscopy image of an array conforming to a cylinder with a radius of 2.2 mm, a conformability which is adequate for most in vivo applications.

2.2 In vivo experiments

In order to validate the PEDOT:PSS array and show that it can record signals of biological origin, the following experiment was performed: An array was attached to a printed circuit board (with its recording end extending into free space), which provided connections to the recording electronics and helped place the array on the brain of an anesthetized rat. A small craniotomy was performed above the somatosensory cortex, the dura was removed, and the array was placed on the surface of the brain (Figure 2). At the same time, a silicon probe (Neuronexus) attached to a stereotaxic frame was implanted through the hole in the center of the array. The silicon probe had a single shank with 16 Ir electrodes (177 μm^2 area each) arranged in a linear configuration with a center-to-center distance of 100 μm. Simultaneous recordings from PEDOT:PSS electrodes placed on the surface of the brain and from Ir electrodes on the silicon probe implanted in the cortex are shown in Figure 2c. The recordings were carried out after the addition of 100 μM of bicuculline, a GABAA receptor antagonist that enables the genesis of sharp-wave events, which mimic epileptic spikes. [25] This typical activity is recorded by the silicon probe in the different cortical layers. As the recordings were taken after sufficient time was elapsed for the effects of bicuculline to diffuse in the cortical layers (20 min), a stronger activity is measured by the silicon probe at the deepest layers of the cortex. At the same time, the PEDOT:PSS electrodes were also able to record the same sharp-wave events as a depth/volume summation. The coincidence of the peaks recorded by the PEDOT:PSS electrodes and the silicon probe provides validation for the former and shows that the measured signals are indeed of biological origin. It should be noted that the polarity of the ECoG signal is inverted, due to the fact that the electrical dipoles that generate the bicuculline-triggered sharp-wave activity are located deep in the cortex. [26]

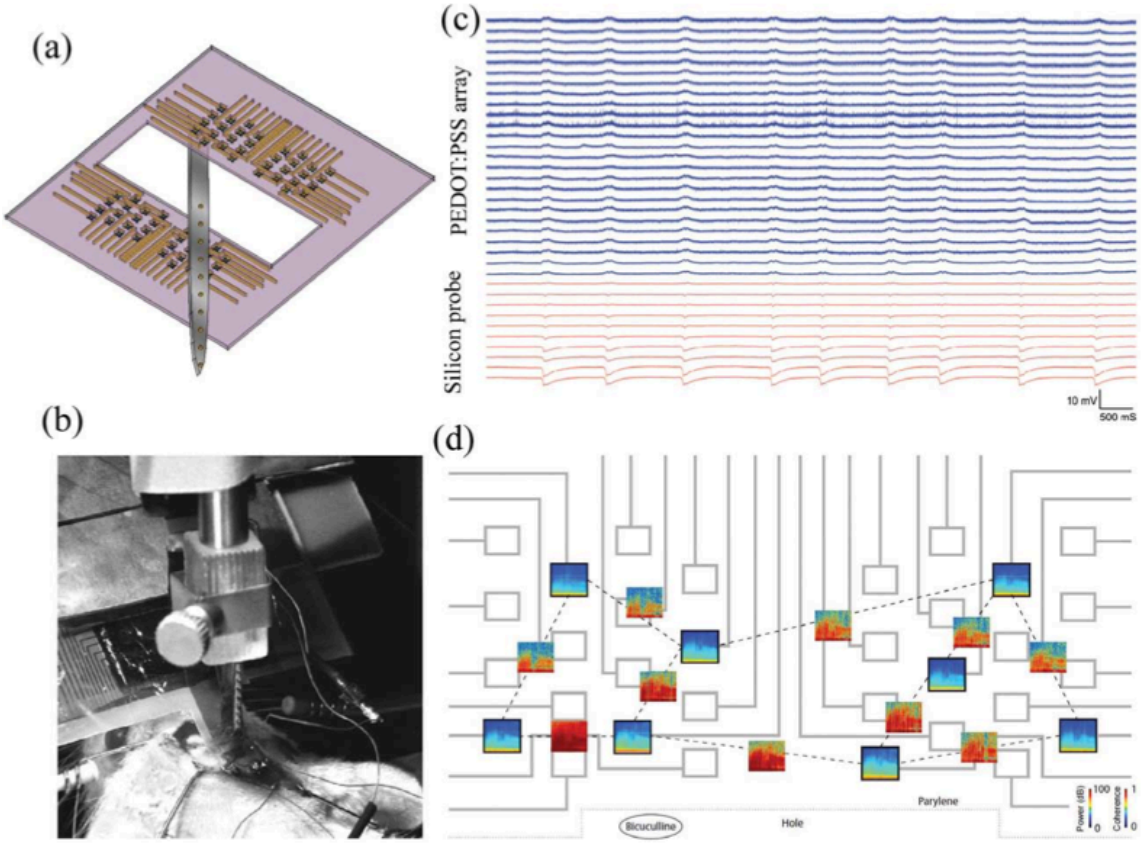

Figure 2. Schematic of the experiment used for the validation of the PEDOT:PSS array with a silicon probe viewed from inside the brain (a) and photograph showing the implantation (b). Recordings from 25 electrodes in the PEDOT:PSS array, and from 10 electrodes in the silicon probe, ordered from superficial to deeper in the cortex (c). d) Time-frequency (TF) analysis of the signals recorded by a few electrodes (black frames, X-axis: time, 10 min; y-axis: frequency, 0.1–50 Hz; color coding: power, dB) and their cross-spectrum coherences (open boxes, same axes as TF plots, color coding: coherence).

In order to assess the spatial resolution of the PEDOT:PSS array, we evaluated correlations in the signals recorded by selected electrodes, located at different distances from the position of bicuculline injection. A time–frequency (TF) analysis (0.1 to 50 Hz over 10 min) of signals recorded by these electrodes is shown in Figure 2d. Each TF plot shows a high power in the 1–2 Hz band and an elevated power in the 30 Hz, corresponding to the epileptiform sharp-wave activity triggered by the bicuculline. Also shown in Figure 2d are the computed cross-spectrum coherences between these electrodes. For the two electrodes close to the site of bicuculline injection (the ones at the bottom left of the Figure), similarities are seen in all the frequency spectra of the recorded signals. On the other hand, as the distance

between two electrodes increases, significant coherence (red color) is only seen in the 1–2 Hz and 30 Hz bands, while a low coherence (blue color) is observed in the rest of the spectrum. This indicates that, even if all the sites do record synchronously the sharp-wave events (as seen through the 1–2 and 30 Hz bands), each ECoG signal is specific to the particular location of the electrode, meaning that the spatial resolution of the array is of the order of the interelectrode spacing.

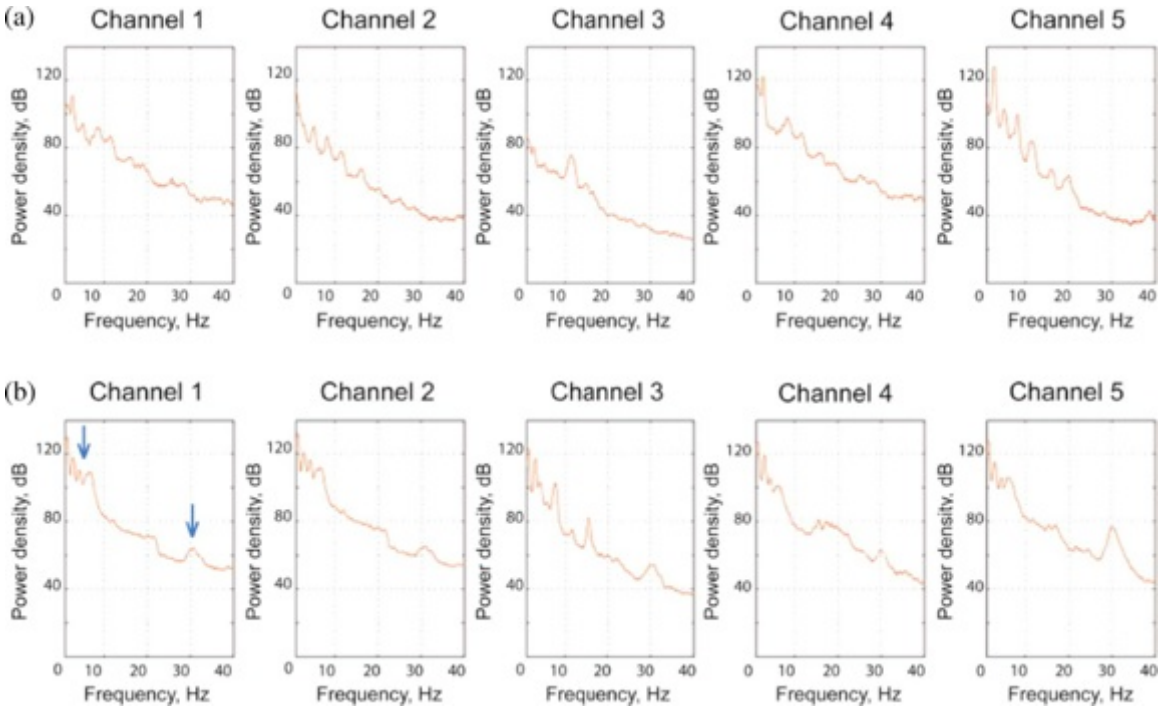

Figure 3. Power spectra of representative recordings with Au (a) and PEDOT:PSS (b) electrodes. The arrows indicate the 1–10 Hz and the 30 Hz (gamma) bands.

2.3 Discussion

As seen in Figure 1a, the addition of PEDOT:PSS electrodes adds to the complexity of fabrication. The question, therefore, arises as to how these electrodes compare to plain Au ones. To address this issue, arrays with similar geometry consisting of plain Au electrodes were fabricated by terminating the fabrication after the deposition and etching of the second parylene layer. An array with Au electrodes was placed on the brain of an anesthetized rat and recordings were per- formed for a period of 30 min, after which time an array with PEDOT: PSS electrodes was placed on the same spot and recorded for the same amount of time. Figure 3 shows the power

spectra of recordings from five representative channels from Au and from PEDOT:PSS electrodes. Both show the typical 1/f property of the ECoG spectrum. [26] The power spectra of the PEDOT:PSS electrodes, however, show a better definition of the 1–10 Hz and the 30 Hz (gamma) bands, which are indicated by arrows in the first panel of Figure 3b. These frequency bands, as shown in Figure 2d, are the dominant ones during bicuculline-triggered sharp-wave events. Thus, PEDOT:PSS electrodes record the electrophysiological signal with a higher accuracy, which highlights the importance of incorporating conducting polymers in a highly conformable electrode array format.

2.4 Conclusions

In conclusion, we developed a generic process for incorporating conducting polymer electrodes on highly conform- able substrates. Contrary to previously reported methods such as electrochemical growth off of patterned metal electrodes, the process described here involves the direct patterning of the polymer layer and thereby enables the use of "champion" materials such as PEDOT:PSS. Arrays of PEDOT:PSS electrodes were fabricated on parylene substrates, and their total thickness of 4 mm endowed them with high conformability. Their use in electrocorticography was demonstrated and validated against a silicon probe, and they were shown to outperform Au electrodes of similar geometry. In addition to their application in ECoG, highly conformable electrode arrays can find a host of other applications in Neuroscience. They can be folded on themselves, creating arrays with electrodes on both sides. Such arrays provide a means of recording ECoG signals inside sulci in the human brain, which will further diagnostic capabilities. Moreover, with the aid of an appropriate insertion shuttle, they can be implanted deep in the brain, where, owing to their high mechanical flexibility, they might be less invasive than traditional electrode arrays made from hard materials.

2.5 Experimental section

2.5.1 Array Fabrication

The fabrication process, outlined in Figure 1a, included the deposition and patterning of parylene, metal and PEDOT:PSS. These steps were performed as follows: Parylene C was deposited using a SCS Labcoater 2 to a thickness of 2 mm (at which thickness parylene films are pinhole-free). These films were patterned with the aid of a 4.6 mm thick layer of AZ9260 photoresist and reactive ion etching by an O2 plasma using an Oxford 80 plus. Metal pads and interconnects were patterned by a lift-off process. A bilayer photoresist, LOR 5A and S1813, was spin coated on the parylene film and exposed to UV light using a SUSS MBJ4 contact aligner, then developed using MF-26 developer. This was followed by the deposition of 5 nm of

titanium and 100 nm of gold using a metal evaporator. Lift-off was performed using 1165 stripper. For the preparation of the PEDOT:PSS films, 20 mL of aqueous dispersion (PH-500 from H.C. Stark) was mixed with 5 mL of ethylene glycol, 50 μl of dodecyl benzene sulfonic acid (DBSA), and 1 wt % of 3-glycidoxypropyltrimethoxysilane (GOPS, as a cross-linker), and the resulting dispersion was spin-coated at 650 rpm. The films were subsequently baked at 140 C for 1 h and were immersed in phosphate buffered saline (PBS) to remove any excess low molecular weight compounds.

2.5.2 *In Vivo* Evaluation

All the protocols have been approved by the Institutional Animal Care and Use Committee of INSERM. Male Wistar rats (Charles River, MA, weight of 400-500 g) were anesthetized with a ketamine/xylazine mixture [35 and 1 mg kg^{-1}, intramuscular (i.m.)]. Additional doses of ketamine/xylazine (7 and 0.3 mg kg^{-1}, i.m.) were given as needed. Other rats, used for the implantation of both a deep-brain probe and an ECoG, were anesthetized with urethane (1.5 g kg^{-1}, intraperitoneal) and ketamine/xylazine (80 and 2 mg kg^{-1}, i.m.). The animals were restrained and their skulls were immobilized in a stereotaxic apparatus. Their body temperature was monitored and kept constant with a heating pad. A 5 mm × 3 mm craniotomy was performed in the right hemisphere above the somatosensory cortex (centered at –3 mm in the anterio-posterior axis and –2 mm in the medio-ateral axis relative to Bregma). The dura matter was removed and the PEDOT:PSS electrode array was slowly lowered on the surface of the brain. Two miniature stainless steel screws were driven into the skull above the cerebellum and served as ground and reference electrodes respectively. The electrodes were connected to a HST headstage (Plexon), which was connected to a multi-channel Digital Lynx 10S system (Neuralynx). The neurophysiological signals were amplified (1000×), band pass-filtered (1 Hz–5 kHz) and acquired continuously at 32 kHz on the 64-channel Neuralynx system (16-bit resolution). To validate the PEDOT:PSS electrodes, an implantable probe (Neuronexus A1 x 16–3 mm–100–177, with a single, 3 mm long shank, and a linear array of 16 electrodes with 100 μm spacing and 177 μm^2 area/electrode) was inserted through the center of the PEDOT:PSS array in the cortex to reach a final depth of 2 mm. All analysis was performed using custom-written tools in MATLAB (Mathworks). The signal was firstly whitened to reduce the dyna leakage of low frequencies in the higher frequency bins during spectrum estimation. [27] Spectral analysis were performed using fast Fourier transform of the ECoG signal between 0.1 and 50 Hz and coherence was computed using direct multi-taper estimates. [27–28] Typically, window sizes of 2–4 s and three to five tapers were used.

References

[1] J. O'Keefe, *Exp. Neurol.* **1976,** *51,* 78.

[2] F. Sargolini, M. Fyhn, T. Hafting, B. L. McNaughton, M. P. Witter, M. B. Moser, E. I. Moser, *Science* **2006,** *312,* 758. H.

[3] Gelbard-Sagiv, R. Mukamel, M. Harel, R. Malach, I. Fried, *Science* **2008,** *322,* 96. K.

[4] D. Wise, A. M. Sodagar, Y. Yao, M. N. Gulari, G. E. Perlin, K. Najafi, *Proc. IEEE* **2008,** *96,* 1184.

[5] F. Fregni, A. Pascual-Leone, *Nat. Clin. Pract. Neurol.* **2007,** *3,* 383.

[6] A. Kuruvilla, R. Flink, *Seizure* **2003,** *12,* 577.

[7] G. Schalk, D. J. McFarland, T. Hinterberger, N. Birbaumer, J. R. Wolpaw, *IEEE Trans. Biomed. Eng.* **2004,** *51,* 1034.

[8] B. A. Hollenberg, C. D. Richards, R. Richards, D. F. Bahr, D. M. Rector, *J. Neurosci. Methods* **2006,** *153,* 147.

[9] B. Rubehn, C. Bosman, R. Oostenveld, P. Fries, T. Stieglitz, *J. Neural. Eng.* **2009,** *6,* 036003.

[10] K. W. Meacham, R. J. Giuly, L. Guo, S. Hochman, S. P. DeWeerth, *Biomed. Microdevices* **2008,** *10,* 259.

[11] Z. Yu, O. Graudejus, C. Tsay, S. P. Lacour, S. Wagner, B. Morrison, 3rd, *J. Neurotrauma* **2009,** *26,* 1135.

[12] D. C. Rodger, A. J. Fong, L. Wen, H. Ameri, A. K. Ahuja, C. Gutierrez, I. Lavrov, Z. Hui, P. R. Menon, E. Meng, J. W. Burdick, R. R. Roy, V. R. Edgerton, J. D. Weiland, M. S. Humayun, Y. C. Tai, *Sens. Actua- tors B* **2008,** *132,* 449.

[13] H. Toda, T. Suzuki, H. Sawahata, K. Majima, Y. Kamitani, I. Hasegawa, *NeuroImage* **2011,** *54,* 203.

[14] C. Metallo, R. D. White, B. A. Trimmer, *J. Neurosci. Meth.* **2011,** *195,* 176.

[15] D. H. Kim, J. Viventi, J. J. Amsden, J. L. Xiao, L. Vigeland, Y. S. Kim, J. A. Blanco, B. Panilaitis, E. S. Frechette, D. Contreras, D. L. Kaplan, F. G.

Omenetto, Y. G. Huang, K. C. Hwang, M. R. Zakin, B. Litt, J. A. Rogers, *Nat. Mater.* **2010,** *9,* 511.

[16] D.-H. Kim, S. Richardson-Burns, L. Povlich, M. R. Abidian,S. Spanninga, J. Hendricks, D. C. Martin, in *Indwelling Neural Implants: Strategies for Contending with the In-Vivo Environment,* (Ed: W. M. Reichert), CRC Press, Taylon and Francis, Boca Raton, FL **2008,** p. 165.

[17] G. G. Wallace, S. E. Moulton, G. M. Clark, *Science* **2009,** *324,* 185.

[18] M. Asplund, T. Nyberg, O. Inganas, *Polym. Chem.* **2010,** *1,* 1374.

[19] K. A. Ludwig, J. D. Uram, J. Y. Yang, D. C. Martin, D. R. Kipke, *J. Neural Eng.* **2006,** *3,* 59.

[20] D. T. Simon, S. Kurup, K. C. Larsson, R. Hori, K. Tybrandt, M. Goiny, E. W. H. Jager, M. Berggren, B. Canlon, A. Richter-Dahlfors, *Nat. Mater.* **2009,** *8,* 742.

[21] S. Y. Yang, B. N. Kim, A. A. Zakhidov, P. G. Taylor, J.-K. Lee, C. K. Ober, M. Lindau, G. G. Malliaras, *Adv. Mater.* **2011,** *23,* H184.

[22] A. Blau, A. Murr, S. Wolff, E. Sernagor, P. Medini, G. Iurilli, C. Ziegler, F. Benfenati, *Biomaterials* **2011,** *32,* 1778.

[23] M. Berggren, A. Richter-Dahlfors, *Adv. Mater.* **2007,** *19,* 3201.

[24] T. Y. Chang, V. G. Yadav, S. De Leo, A. Mohedas, B. Rajalingam, C. L. Chen, S. Selvarasah, M. R. Dokmeci, A. Khademhosseini, *Langmuir* **2007,** *23,* 11718.

[25] Y. Chagnac-Amitai, B. W. Connors, *J. Neurophysiol.* **1989,** *61,* 747.

[26] G. Buzsaki, R. D. Traub, T. A. Pedley, in *Current Practice of Clinical Electroencephalography,* 3rd ed. (Eds: J. S. Ebersole, T. A. Pedley), Lippincott, Williams and Wilkins, Philadelphia **2003,** p. 1.

[27] A. Sirota, S. Montgomery, S. Fujisawa, Y. Isomura, M. Zugaro, G. Buzsaki, *Neuron* **2008,** *60,* 683.

[28] P. P. Mitra, B. Pesaran, *Biophys. J.* **1999,** *76,* 691.

Chapter 3

3 High-speed and high-density organic electrochemical transistor

Interfacing transistors with aqueous electrolytes is of interest to the development of biosensors. Work on silicon- based ion-sensitive field-effect transistors, for example, has yielded biosensors for a variety of applications, ranging from the detection of metabolites like glucose to the monitoring of the activity of living cells. [1] In these devices, the gate dielectric (usually silicon oxide) separates and protects the silicon channel from the aqueous environment. A key advantage of transistors compared to other transducers lies in their miniaturization, which can yield high-density arrays that enable the simultaneous detection of multiple analytes. Advances in the field of organic electronics are making available an alter- native family of materials for field-effect transistors, based on conjugated small molecules and polymers. [2] The interfacing of these organic field-effect transistors (OFETs) with aqueous electrolytes is a rather recent endeavor. Examples include OFETs in which the organic semiconductor is separated from the electrolyte by an ultra-thin dielectric [3] (and which are, therefore, qualitatively similar to their silicon cousins mentioned above) as well as OFETs in which the organic semiconductor is in direct contact with water. [4,5] The latter are either

gated through a bottom gate, separated from the organic semiconductor by a dielectric,[4] or gated through a metal electrode immersed in water, that is, deionized in order to minimize ion penetration in the organic and maintain a field-effect mechanism of operation.[5]

Organic electrochemical transistors (OECTs), developed in 1984 by White et al., [6] provide an alternative to field-effect transistors. These devices utilize an electrolyte as an integral part of the device structure: In the usual configuration, they consist of a conducting polymer film (channel) brought in contact with an electrolyte. A gate electrode is immersed in the latter, while source and drain electrodes measure the cur- rent that flows through the channel (drain current, Id). The application of an appropriate bias at the gate (gate voltage, Vg) causes ions from the electrolyte to enter the polymer film and dedope it, thereby decreasing the drain current [6]. As such, OECTs act as ion-to-electron converters, [7] in which an ionic current in the electrolyte causes a change in the (electronic) drain current. Owing to the high conductivity of both the electrolyte and the channel, these devices operate at low voltages and are hence compatible with aqueous electrolytes, where voltages of the order of 1V can cause electrolysis. OECTs have been used in biosensors, for the detection of ions [8,9] and metabolites such as glucose and lactate. [10,11] The vast majority of OECTs developed today are based on poly(3,4-ethylenedioxythiophene) doped with poly(styrene sulfonate) (PEDOT:PSS), a commercially available polymer with high conductivity, which is also biocompatible. This latter fact enabled some very creative uses of these devices: Bolin et al.[12] cultured epithelial cells on the channel of a PEDOT:PSS OECT and was able to spatially control cell adhesion by adjusting the bias applied to the gate and the drain. Lin et al. [13] used an OECT as a sensor that monitors the attachment of cancer cells and fibroblasts, cultured directly on its PEDOT:PSS channel.

To take this work a step further, it is important to miniaturize OECTs and explore the impact of this process on their characteristics. An obvious target would be to reduce the channel of OECTs to cellular dimensions (1–10 mm), which would enable interfacing with single electrically active cells. [14] The fabrication of high-density array architectures is highly desirable in this case, as it increases the likelihood that, in a culture, a cell will be found directly on top of the channel of a transistor. These challenges have not been tackled to date and the limits of performance of OECTs have not been explored. Toward this goal, we developed a generic process for miniaturizing OECTs and developing high- density arrays using photolithography.

3.1 Fabrication process

As a proof-of principle, arrays consisting of 64 OECTs with channels lengths of 6 μm, capable of responding to a gate pulse with a time constant of 100 ms, are demonstrated.

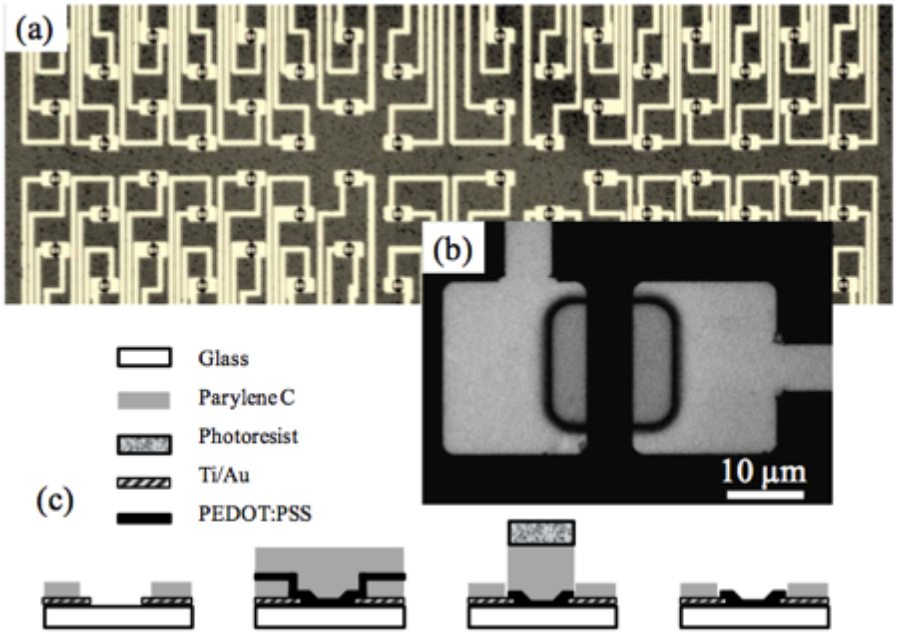

Fig. 1: The overall architecture of the OECT array (a), a micrograph of a single OECT (b), and the fabrication process (c).

The overall architecture of the transistor array is shown in Figure 1(a), with micrograph of a single OECT in Figure 1b and the fabrication process in Figure 1(c). The OECTs are arranged in a 85 μm center-to-center distance from each other, with each one of them having a PEDOT: PSS channel that is 6 μm long and 15 μm wide. Au was used to define source and drain electrodes and interconnects. The fabrication began with depositing an Au film anchored with Ti on a glass slide using a standard lift-off process. The sample was then coated with a 2 μm thick parylene C film, which ended up being the insulator layer. Parylene C is an obvious choice due to its good dielectric properties and its biocompatibility. The area where the PEDOT: PSS should be deposited are defined using a second lithography step followed by dry etching. The PEDOT: PSS film was then spin coated from dispersion (PH-500 from H.C. Starck) and annealed at 140° C for 60 min to yield a 80 nm thick film. To improve the conductivity of the resulting PEDOT: PSS films, 5ml of ethylene glycol and 50 μl of dodecyl benzene sulfonic acid (DBSA) were added per 20 ml of PEDOT:PSS dispersion. Additionally, 0.25 g of the crosslinker 3-glycidoxypropyltrimethoxysilane was added to the above dispersion to prohibit PEDOT:PSS dissolution. The samples were then coated with a sacrificial parylene C film which protected the conducting polymer

channel from the subsequent process steps. Final photolithography and etching steps defined the PEDOT: PSS regions on the sample. The fabrication ended with immersion in deionized water, which removed the sacrificial layer of parylene C film on top of the PEDOT: PSS patterned layer and subsequent thorough rinsing in deionized water.

3.2 Electrical characterization

Before testing, a reservoir made of polydimethylsiloxane (PDMS) was attached to the array and was used to contain phosphate buffered saline (PBS). The tip of a Pt wire with a diameter of 250 mm was immersed in the PBS and was used as a gate electrode. Out of 64 transistors fabricated on the same glass slide, 60 had a resistance value for the channel that varied less than 10% from the mean value, while the other 4 were open circuited due to incomplete Au lift-off. The mean channel resistance was 670 Ω, corresponding to a conductivity of 75 S/cm for the PEDOT:PSS film. This value is four times lower than that specified by the manufacturer for PH-500 (300 S/cm), and we found the difference to arise mainly due to the addition of the crosslinker and due to the final washing step (presumably due to the removal of low molecular weight dopants).

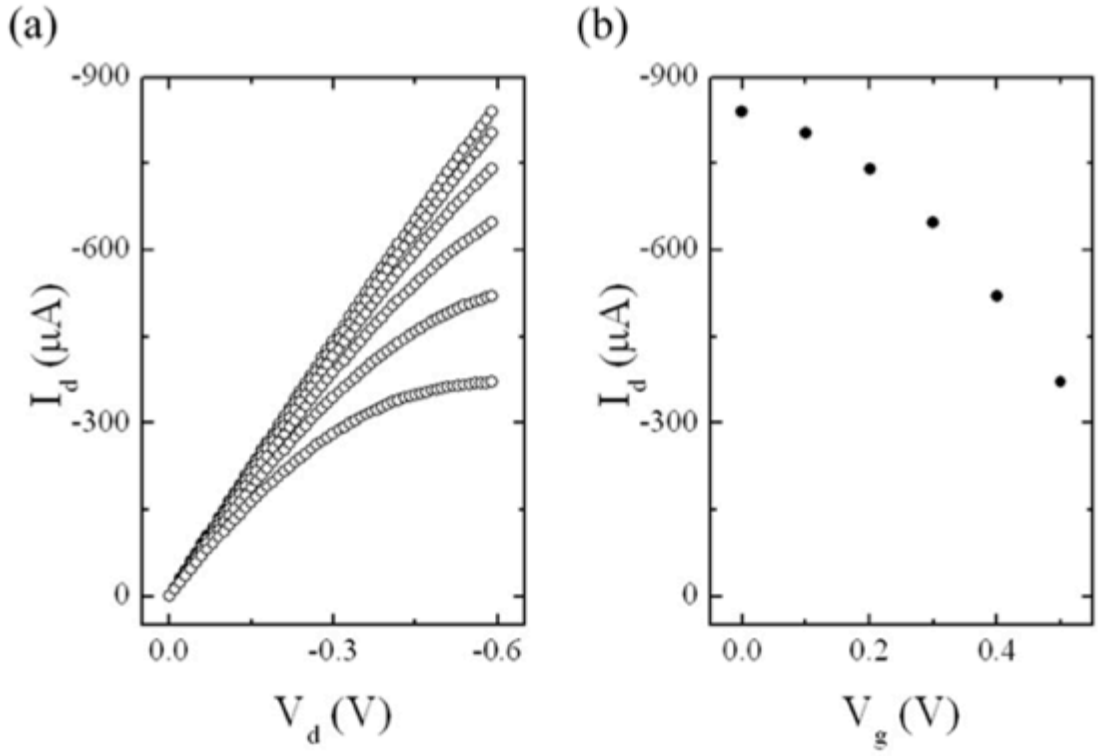

Fig. 2: Output characteristics for Vg varying from 0 V (top curve) to 0.5 V (bottom curve) (a), and transfer characteristics of an OECT for Vd= -0.5 V (b).

Figure 2a shows the output characteristics of an OECT in the third quadrant, with negative bias at the drain (Vd), and Vg varying from 0 V to 0.5 V. These characteristics show the typical low voltage operation which is the hallmark of OECTs, and are consistent with operation in the depletion regime, as described by Bernards and Malliaras. [6] The time delay between sourcing Vd and Vg and measurement time of Id was set to 150ms, which was found to be long enough for the drain current to reach steady-state. The gate current, also measured after the same delay, was 15 nA for Vd = -0.6 V and Vg = +0.5 V. The transfer characteristics are shown in Figure 2(b) for a drain voltage of -0.5 V.

PEDOT:PSS consists of a semiconducting polymer chain (PEDOT), which is degenerately doped p-type, with the anions on the PSS playing the role of acceptors. When a positive bias is applied on the gate, cations from the electrolyte enter the PEDOT:PSS film, compensate the anions on the PSS, and decrease hole density on the PEDOT, which is reflected in the decrease of the drain current seen in Figure 2b. This process is analogous to compensation doping in traditional semiconductors, e.g., when an n-type dopant is implanted in p-type silicon. It should be noted that more efficient gating (a more significant reduction of the drain current for the same value of gate volt- age) can be obtained by using a larger Pt electrode, [16] but the increased capacitance of the gate can degrade the time response of the transistor. Alternatively, a Ag/AgCl gate electrode can be used to yield more efficient gating, at the cost of a larger gate current [15].

OECTs integrate the ionic current in the electrolyte: The change in the drain current reflects the total number of ions from the electrolyte that were “implanted” in the channel. The higher the ionic flux in the electrolyte, the faster the drain current will reach its steady-state. As such, their response time depends on the gate current. [6]

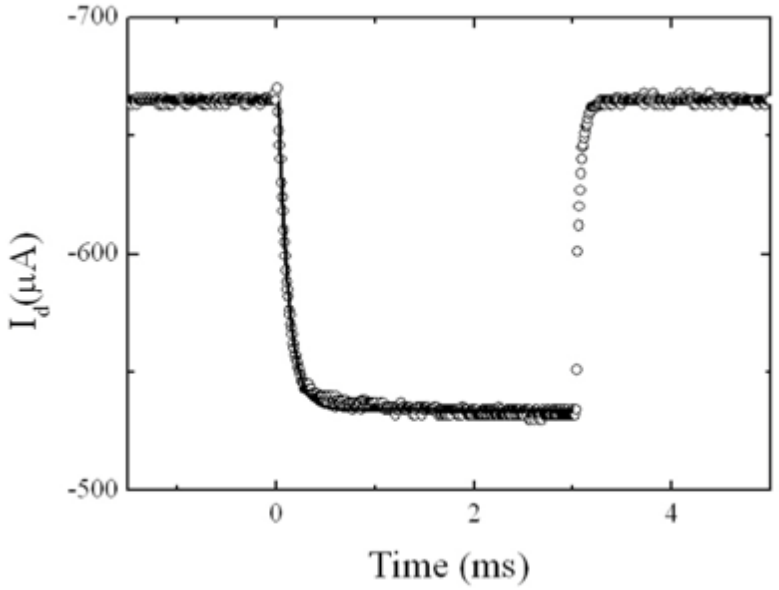

Fig. 3: Temporal response of the drain current of an OECT to a 0.4 V pulse applied at the gate (Vd= -0.5 V). The line is a fit to a single exponential decay with τ=101±1 μs.

In the organic transistor literature, transistor speed is quantified by measuring response to a gate bias pulse. Accordingly, Figure 3 shows the time response of the drain current of an OECT to a 0.4 V pulse applied at the gate. The bias at the drain was -0.5 V. The OECT was connected in series with a 100 Ω resistor, and the voltage drop across the latter (from which the drain current was calculated) was measured with an oscilloscope. The line is a fit with an exponential decay giving a time constant of 101 μs. This is the fastest response reported to an OECT, and it is a consequence of miniaturization of the OECT channel. It is fast enough to allow accurate recording of action potentials from neurons, which have a duration in the millisecond range It should be mentioned that when the values of drain and gate voltage were corrected for the presence of the series resistor, the values of drain current recorded during the transient experiment correspond well to the steady-state output characteristics of Figure 2a, therefore the transistor reaches steady-state within the duration of the gate pulse.

3.3 Conclusion

In conclusion, we presented a lithographic process that allows the fabrication of high-density organic electrochemical transistor arrays. The transistors were based on PEDOT:PSS, had a channel length of 6 μm, and used an aqueous electrolyte as integral part of their structure. Source and drain contacts and interconnects were insulated from the solution with the biocompatible material parylene C, making the arrays suitable for integration with living cells. Together with a low operating voltage and a response time of 100 μs, these features make OECTs excellent candidates for interfacing with single electrically active cells as well as for a variety of biosensing applications.

Reference:

[1] M. J. Schoning and A. Poghossian, Electroanal **18** (19-20), 1893-1900 (2006).

[2] G. Malliaras and R. Friend, Physics Today **58** (5), 53-58 (2005).

[3] M. Gollner, M. Huth and B. Nickel, Advanced Materials **22** (39), 4350-+ (2010).

[4] T. Someya, A. Dodabalapur, A. Gelperin, H. E. Katz and Z. Bao, Langmuir **18** (13), 5299-5302 (2002).

[4] M. E. Roberts, S. C. B. Mannsfeld, N. Queralto, C. Reese, J. Locklin, W. Knoll and Z. N. Bao, Proceedings of the National Academy of Sciences of the United States of America **105** (34), 12134-12139 (2008).

[5] H. S. White, G. P. Kittlesen and M. S. Wrighton, Journal of the American Chemical Society **106** (18), 5375-5377 (1984).

[6] D. A. Bernards and G. G. Malliaras, Adv. Funct. Mater. **17** (17), 3538-3544 (2007).

[7] D. Nilsson, T. Kugler, P. O. Svensson and M. Berggren, Sensors and Actuators B- Chemical **86** (2-3), 193-197 (2002).

[8] P. Lin, F. Yan and H. L. W. Chan, Acs Appl Mater Inter **2** (6), 1637-1641 (2010).

[9] D. A. Bernards, G. G. Malliaras, G. E. S. Toombes and S. M. Gruner, Appl Phys Lett **89** (5), - (2006).

[10] D. A. Bernards, D. J. Macaya, M. Nikolou, J. A. DeFranco, S. Takamatsu and G. G. Malliaras, Journal of Materials Chemistry **18** (1), 116-120 (2008).

[11] S. Y. Yang, J. A. DeFranco, Y. A. Sylvester, T. J. Gobert, D. J. Macaya, R. M. Owens and G. G. Malliaras, Lab on a Chip **9** (5), 704-708 (2009).

[12] M. H. Bolin, K. Svennersten, D. Nilsson, A. Sawatdee, E. W. H. Jager, A. Richter-Dahlfors and M. Berggren, Adv. Mater. **21** (43), 4379-+ (2009).

[13] P. Lin, F. Yan, J. J. Yu, H. L. W. Chan and M. Yang, Adv. Mater. **22** (33), 3655-+(2010).

[14] P. Fromherz, Progress in Convergence: Technologies for Human Wellbeing **1093,** 143-160 (2006).

[15] F. Cicoira, G. Tarabella, C. Santato, S. Y. Yang, S. Iannotta and G. G. Malliaras, Appl Phys Lett **97** (12) (2010).

Chapter 4

4 High Transconductance Organic Electrochemical Transistor

The interfacing electronics with the biological world is an emerging field that holds the key for the development of a wide variety of technologies such as medical diagnostics and bioelectronic implants. They will dominate the future of healthcare and help increase the span and quality of our lives [1]. Organic electronic materials offer a range of advantages for the biotic/abiotic interfacing, including better biological and mechanical compatibility with tissue than traditional "hard" electronic materials [2,3]. Furthermore, many organic electronic materials are mixed conductors, meaning that ions (in addition to electronic charge) can move efficiently in a film, at room temperature. Given the importance of ionic fluxes as the main vehicle of information transport in biological organisms, devices made of these materials enable a new means of communication with biology.

An example is the organic electrochemical transistors (OECT), developed in 1984 by White et al. [4] This device involves a direct contact between an organic electronic layer and an electrolyte. Ion transport across this interface changes the electronic properties of the organic layer, thereby providing a simple way to interface electrolytes with solid-state electronics. As such, OECTs have been used for the detection of metabolites such as glucose and lactate, and of DNA and antibodies, for measuring ion transport across bilayer membranes, and for controlling and assessing cell adhesion [5-10].

Given the wide range of applications of OECTs, it is important to explore, understand, and extend their limits of performance. Of particular importance is their efficacy in translating ionic into electronic signals, which has received

little attention up to now. In this communication we report a lithographically fabricated OECTs that show a very high transconductance, which, normalized for channel width, is in excess of 50 S/m. Moreover, these devices show constant gain up to a cut-off frequency of approximately 5 kHz.

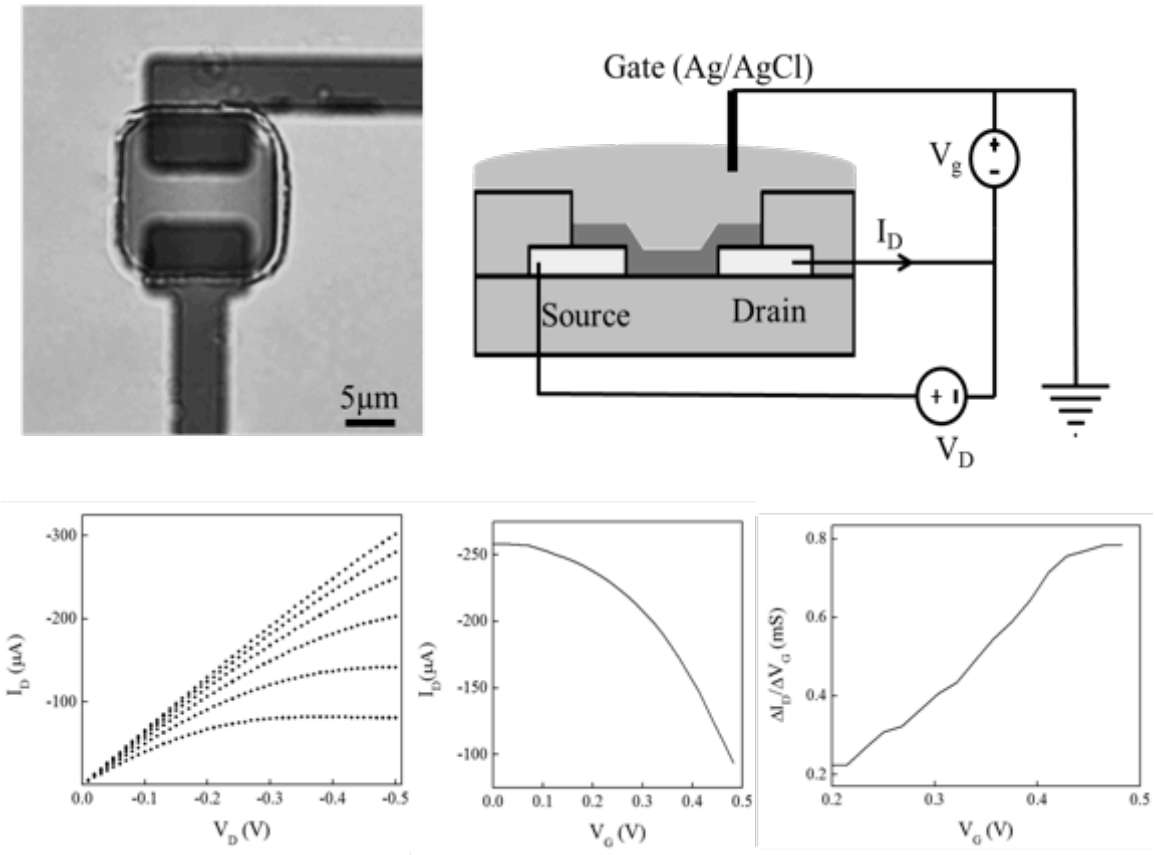

Figure 1. (a) Optical micrograph of the channel of the transistor, (b) wiring diagram, (c) output characteristics for V_g varying from 0 V (top curve) to +0.5 V (bottom curve), (d) transfer curve for V_d = -0.4 V, and, (e) transconductance for V_d = -0.4 V.

4.1 Electrical characterization

Figure 1a shows a micrograph of the channel of the OECT. It is fabricated on a glass substrate and has Au source and drain contacts, which define a channel with length and width of 6 µm and 15 µm, respectively. Its channel consists of the conducting polymer poly(3,4-ethylenedioxythiophene) doped with poly(styrene sulfonate) (PEDOT:PSS). A 2 µm thick parylene film insulates the contacts from the electrolyte solution. The transistor is driven in a common-source configuration (Figure 1b), with a grounded Ag/AgCl reference electrode as the gate and using Ringer's solution as the electrolyte. Figure 1c shows the output characteristics of an OECT in the third quadrant,

with negative bias at the drain (V_d), and for gate bias (V_g) varying from 0V to +0.5 V. These characteristics show the typical low voltage operation which is the hallmark of OECTs. The time delay between sourcing V_d and V_g and measuring the drain current (I_d) was set to 100 ms, which was found to be long enough for the drain current to reach steady-state. The gate current, also measured after the same delay, was 15 nA for V_d= -0.4 V and V_g= +0.5 V.

The transistor's transfer characteristics are shown in Figure 1d for V_d=-0.4 V. PEDOT:PSS consists of a semiconducting polymer chain (PEDOT), which is degenerately doped *p*-type, with the anions on the PSS playing the role of acceptors. When a positive bias is applied on the gate, cations from the electrolyte enter the PEDOT:PSS film, compensate the anions on the PSS, and decrease hole density on the PEDOT, which is reflected in the decrease of the drain current seen in Figure 1d. As a result, the transconductance increases with V_g and reaches 800 μS at V_g=0.5 V (Figure 1e). Normalized per channel width, this value (53 S/m) is three orders of magnitude larger than that of organic thin film transistors (OTFTs) utilizing solid dielectrics [11-13], and two orders of magnitude larger than that of OTFTs utilizing high-capacitance gel electrolytes to gate the transistor [14-16].

4.2 Frequency response

In order to measure the frequency dependence of the OECT transconductance, a low amplitude ($50mV_{peak-peak}$) oscillation was added on the gate bias. The small signal transconductance of the transistor was determined by the amplitude ratio between the drain current oscillations and the corresponding input sine wave. Figure 2 demonstrates the frequency response of the transconductance for V_d=-0.4 V at different gate voltages. The cutoff frequency of the transistor (at which the transconductance drops by 3 dB from its plateau value) is 5 kHz at V_g=0.5 V.

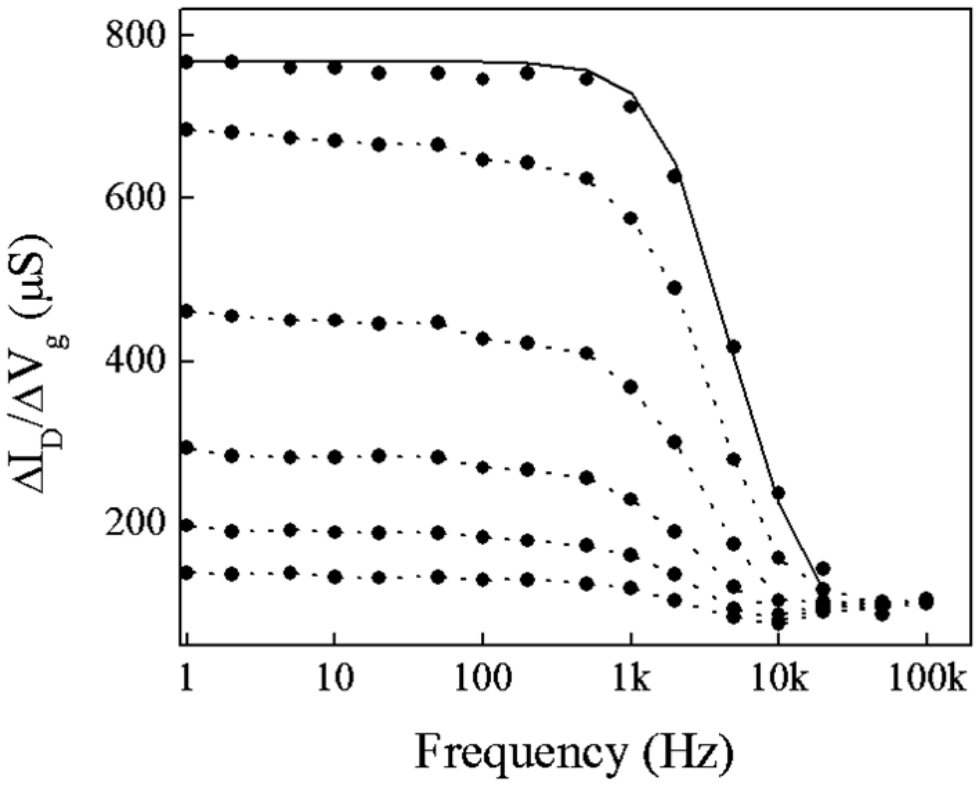

Figure 2. Frequency response of the transconductance for different gate voltages +0.5V (top curve) to 0 V (bottom curve). The solid line is a fit to the small signal response of the transistor.

4.3 Analytical modeling of transconductance

Bernards *et al.,* [17] developed a model to explain the steady-state and transient behavior of OECTs. According to this model, the drain current density in the Ohmic region is given by equation 1. For devices operating at saturation, spatial voltage profiles cannot be analytically be determined in this regime of device operation.

$$J_d(t) \approx q\mu p(t)\frac{V_d}{L} + qfL\frac{dp(t)}{dt}, \quad (1)$$

Where q is the electron charge, μ is the hole mobility, L is channel length, f is a proportionality constant that accounts for the spatial non-uniformity of the de-doping process and $p(t)$ is the charge carrier density at a given time t. The above equation reflects that two effects determine the transient behavior of OECTs, the injection of cations from the electrolyte into the organic film (first term at the right hand side of Eq. 1) and the removal of holes at the source electrode (second term). The hole density is given by:

$$p(t) = p_0\left(1 - \frac{Q(t)}{qp_0\upsilon}\right), \tag{2}$$

Where p_0 is the intrinsic hole density in the PEDOT:PSS film, υ is the volume of the film, and Q is the total charge of cations injected into the film from the electrolyte. A resistor and capacitor in series can represent the electrolyte/polymer interface: The resistor describes the conductivity of the interface and depends on its ionic strength. The capacitor accounts for polarization at the electrolyte/polymer and gate electrode-electrolyte interfaces. This circuit is named the ionic circuit of the OECT. In the case of Ag/AgCl gate electrode the latter can be neglected. Therefore, the time dependence of the cation injection can be expressed as:

$$Q(t) = Q_0 + \tilde{Q} = CV_{g0} + C\tilde{V}_g\frac{1}{1+i\omega RC} \tag{3}$$

Where $\tilde{Q}$and $\tilde{V}_g$ are the small signal phasor representations of cationic charge and gate voltage, and ω is the angular frequency. Combining Equations 1 through 3 results in a drain current:

$$I_d(t) \approx \underbrace{GV_d - G\frac{CV_{g0}}{qp_0\upsilon}V_d}_{I_{d0}} \underbrace{-G\frac{C\tilde{V}_g\frac{1}{1+i\omega RC}}{qp_0\upsilon}V_d + fC\tilde{V}_g\frac{i\omega}{1+i\omega RC}}_{\widetilde{I_d}}, \tag{4}$$

Where I_{d0} and $\widetilde{I_d}$ are the steady-state and small signal components of the drain current, respectively, and G is the conductance of the channel. From Equation 4 it is possible to directly derive the transconductance of the OECT:

$$g_m = \frac{d\widetilde{I_d}}{d\widetilde{V_g}} \approx -\frac{GCV_d}{qp_0\upsilon(1+i\omega RC)} + fC\frac{i\omega}{1+i\omega RC} \tag{5}$$

This term, which represents the change in drain current due to cation injection into the PEDOT:PSS film, is dominant at lower frequencies ($\omega \to 0$). The second term, which represents hole extraction at the source electrode, is dominant at high frequencies ($\omega \to +\infty$). The absolute value of the transconductance is:

$$|g_m| \approx \sqrt{\frac{(\frac{GCV_d}{qp_0\upsilon})^2 + (fC\omega)^2}{1+(\omega RC)^2}} \tag{6}$$

The line in Figure 2 is a fit to Equation 6, yielding RC= 95 μs. It represents the time that ions take to penetrate into the polymer film and dedope the film.

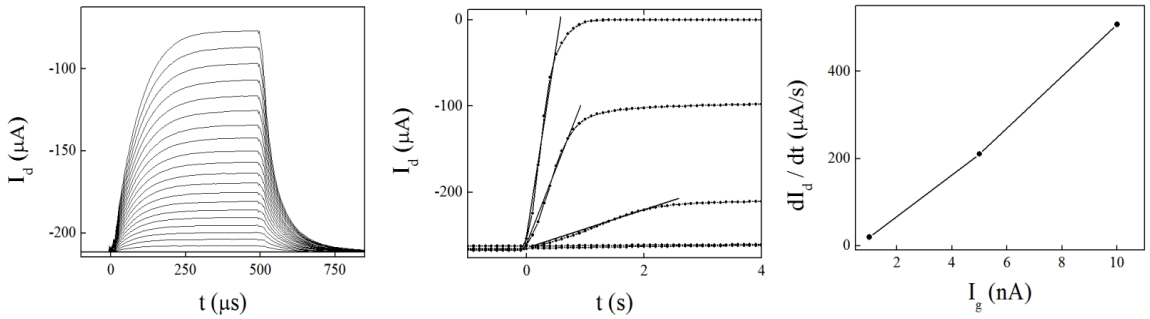

Figure 3. (a) Temporal response of drain current for V_g varying from 0.5 V (top curve) to 0 V (bottom curve), (b) temporal response of drain current for gate current varying from 500pA (bottom curve) to 5nA (top curve), and, (c) first derivative of drain current with time as a function of gate current.

In order to understand what limits the bandwidth of the OECT we quantified the drain current response to gate voltage and current pulses. Figure 3a shows the temporal response of the drain current upon gate voltage pulses (0-0.5 V) with duration of 500 μs. The monotonic decay observed in the drain current indicates, according to Bernards *et al.,* [17] that the transient response of the transistor is dominated by the RC time constant of the ionic circuit. The line in Figure 3a is a fit to an exponential decay, yielding a time constant of 95 ± 1 μs. This time constant is consistent with the maximum frequency of oscillation (f_{max}= 10 kHz) of the transistor as shown in figure 2.

Further insights can be obtained by driving the transistor with gate current pulses. In this case the kinetics of the ionic circuit is fixed, which enables the extraction of the hole mobility in the PEDOT:PSS channel. Figure 3b shows the response of the drain current to constant gate current (applied at t=0 s). The response time is shown to depend on the gate current, with higher ionic fluxes in the electrolyte forcing the drain current to reach its steady-state faster. According to Bernards *et al.,*[17] the slope of these curves is inversely proportional to the "time-of-flight" of the holes across the channel. Figure 3c shows that this relationship is obeyed in micron-scale OECTs, and the fit yields a hole mobility of 3.4×10^{-2} cm^2V^{-1} s^{-1}. This value is consistent with reported values in the literature [18]. It should be noted that the extracted hole mobility corresponds to a time-of-flight across the channel that is 18 μs at Vd=-0.4 V. This value is an order of magnitude faster than the ionic time constant of the device, confirming that the ionic circuit dominates the transistor temporal response.

The transconductance at below cut-off frequency based on equation 6 can be derived

$$\lim_{\omega \to 0} \ |g_m| \approx \frac{\mu \cdot C}{L^2} V_d \approx \mu c_d \frac{W}{L} V_d \qquad (7)$$

Where C_d is the electrolyte/polymer capacitance per unit area (c_d=C_d.A). Please not that the dependency of the transconductance on gate voltage is embedded in interface capacitance ($C_d = \frac{Q}{V_G}$). Increasing the channel thickness (T) will increase the transconductance but it comes with the price of longer ionic time constant ($\tau_i = RC$) and slower cut-off frequency. Moreover, equation 7 is consistent with the transconductance of the FET at linear regime (the capacitance represents the gate insulator capacitance) [19]. Therefore the same design rules (high $\frac{W}{L}$) and high mobility can improve the transconductance.

One potential application of OECTs is to interface with electrically active cells and living tissues to measure electrophysiological signals. Usually such signals are recorded using electrodes that measure the nearby electric field fluctuations. However, the electrode/electrolyte impedance varies by frequency and limits the quality and linearity of the recordings. Alternatively, silicon based Ion-Sensitive-Field-Effect-Transistor (ISFET) are used to provided a better interface owing the local amplification of the signal at the interface [20]. The OECT has 2 orders of magnitude higher transconductance compare to ISFET used for neural interface and biosensing applications [21,22]. Moreover, the OECT provides constant amplification rate for different signals at electrophysiological frequencies. As such, OECTs are ideal candidates for establishing abiotic/biotic electrical communication.

4.4 Conclusion

In conclusion, we presented microfabricated organic electrochemical transistors based on the conducting polymer PEDOT:PSS. The transconductance per channel width exceeded 50 S/m, and was independent of frequency up to a cut-off frequency of 5 kHz. The temporal response was found to be limited by the RC constant of the gate/electrolyte/channel circuit rather than by the hole mobility in the channel. The standard model for OECTs provided a good description of the data and gave predictions on how to navigate the trade-off between transconductance and cut-off frequency. Based on these results, PEDOT:PSS OECTs emerge as promising candidates for applications in electrophysiology.

4.5 Experimental

4.5.1 Device Fabrication

The fabrication process included the deposition and patterning of parylene, metal and PEDOT:PSS. These steps were performed as follows: parylene C was deposited using a SCS Labcoater 2 to a thickness of 2 μm (at which thickness parylene films are pinhole-free). These films were patterned with the aid of a 4.6 μm thick layer of AZ9260 photoresist and reactive ion etching by an O2 plasma using an Oxford 80 plus. Metal pads and interconnects were patterned by a lift-off process. A bilayer photoresist, LOR 5A and S1813, was spin coated on the parylene film and exposed to UV light using a SUSS MBJ4 contact aligner, then developed using MF-26 developer. This was followed by the deposition of 5 nm of titanium and 100 nm of gold using a metal evaporator. Lift-off was performed using 1165 stripper. For the preparation of the PEDOT:PSS films, 20 mL of aqueous dispersion (PH-1000 from H.C. Stark) was mixed with 5mL of ethylene glycol, 50ìL of dodecyl benzene sulfonic acid (DBSA), and 1 wt% of 3-glycidoxypropyltrimethoxysilane (GOPS, as a cross-linker), and the resulting dispersion was spin-coated at 650 rpm. The films were subsequently baked at 140 C for 1 hour and were immersed in deionized water to remove any excess low molecular weight compounds.

4.5.2 Electrolyte

A Ringer's solution (150mM NaCl, 3mM KCl, 2mM $CaCl_2$, 1mM $MgCl_2$ and 10 HEPES, adjusted to pH to 7.2 with NaOH) used as the electrolyte to provide physiological concentration

4.5.3 Measurement setup

The transistor was wired in a common source configuration while the grounded reference electrode served as gate. An Ag/AgCl wire (Warner Instruments) was used as the gate electrode. The terminals were biased and the drain current was registered using two NPI-VA10 transimpedance amplifiers and customized LabView software.

Reference

[1] I. Willner and E. Katz, *Bioelectronics: From Theory to Applications* (Wiley-VCH, 2005), p. 476.

[2] R.M. Owens and G.G. Malliaras, 35, 449-456 (2010).

[3] M. Berggren and A. Richter-Dahlfors, Advanced Materials 19, 3201-3213 (2007).

[4] H.S. White, G.P. Kittlesen, and M.S. Wrighton, Journal of American Society of Chemistry, 5375-5377 (1984).

[5] D. Khodagholy, V.F. Curto, K.J. Fraser, M. Gurfinkel, R. Byrne, D. Diamond, G. G. Malliaras, F. Benito-Lopez, and R.M. Owens, Journal of Materials Chemistry, 4440-4443 (2012).

[6] D.A. Bernards, D.J. Macaya, M. Nikolou, J.A. DeFranco, S. Takamatsu, and G.G. Malliaras, Journal of Materials Chemistry 18, 116-120 (2008).

[7] P. Lin, X. Luo, I.-M. Hsing, and F. Yan, Advanced Materials (Deerfield Beach, Fla.) 23, 4035-40 (2011).

[8] D. A. Bernards, G.G. Malliaras, G.E.S. Toombes, and S.M. Gruner, Applied Physics Letters 89, 053505 (2006).

[9] P. Lin, F. Yan, J. Yu, H.L.W. Chan, and M. Yang, Advanced Materials 22, 3655-60 (2010).

[10] M.H. Bolin, K. Svennersten, D. Nilsson, A. Sawatdee, E.W.H. Jager, A. Richter-Dahlfors, and M. Berggren, Advanced Materials 21, 4379-4382 (2009).

[11] H. Klauk, U. Zschieschang, and M. Halik, Journal of Applied Physics 102, 074514 (2007).

[12] T. Yokota, T. Sekitani, Y. Kato, K. Kuribara, U. Zschieschang, H. Klauk, T. Yamamoto, K. Takimiya, H. Kuwabara, M. Ikeda, and T. Someya, MRS Communications 1, 3-6 (2011).

[13] F. Ante, D. Kälblein, U. Zschieschang, T.W. Canzler, A. Werner, K. Takimiya, M. Ikeda, T. Sekitani, T. Someya, and H. Klauk, Small (Weinheim an Der Bergstrasse, Germany) 7, 1186-91 (2011).

[14] D. Braga, N.C. Erickson, M.J. Renn, R.J. Holmes, and C.D. Frisbie, Advanced Functional Materials 22, 1623–1631 (2012).

[15] J.H. Cho, J. Lee, Y. Xia, B. Kim, Y. He, M.J. Renn, T.P. Lodge, and C.D. Frisbie, Nature Materials 7, 900-6 (2008).

[16] M.J. Panzer and C.D. Frisbie, Journal of the American Chemical Society 129, 6599-607 (2007).

[17] D. A. Bernards and G. G. Malliaras, Advanced Functional Materials 17, 3538-3544 (2007).

[18] Y. Li and Y. Zou, Advanced Materials 20, 2952-2958 (2008).

[19] S.M. Sze and K.K. Ng, *Physics of Semiconductor Devices* (Wiley, 2007), p. 815.

[20] P. Fromherz, A. Offenhausser, T. Vetter, and J. Weis, Science 252, 1290-1293 (1991).

[21] F. Felderer and P. Fromherz, Applied Physics A 104, 1-6 (2011).

[22] K.-M. Chang, C.-T. Chang, and K.-M. Chan, Sensors (Basel, Switzerland) 10, 6115-27 (2010).

Chapter 5

5 *In vivo* recordings of brain activity using organic transistors

Most breakthroughs in our understanding of the basic mechanisms of information processing in the brain have been obtained by means of recordings from electrodes implanted into, or placed on the surface of the brain. Such recordings allowed the discovery of place cells, grid cells, mirror neurons [1-3], and more. They also provided an insight into the organization of the brain4, and showed that oscillations constitute the hallmark of brain activity. These oscillations are divided into different frequency bands, from ultraslow to ultrafast, including delta (0.5-3 Hz), theta (4-12 Hz), gamma (40-80 Hz), ripples (100-200 Hz), and sleep spindles (>500 ms long 10-14 Hz oscillations) [4,5]. Specific oscillations are also recorded in pathological contexts such as spike and wave discharges (SWD) between 7 and 11 Hz in experimental models of absence epilepsy. For other types of epilepsies the epileptogenic regions may be determined by assessing the presence of interictal spikes and/or very fast ripples (>200 Hz) [6].

State-of-the-art recordings are currently performed with microfabricated arrays of metal electrodes (silicon probes, Utah arrays and tetrodes [7]), which capture the local field potentials (LFPs) generated by the spatio-temporal summation of current sources and sinks (caused by the flux of ions through ion channels localized in the cell membrane) in a given brain volume [4]. Such probes are also being used in the clinic to improve diagnosis and treatments. For example, stereoelectroencephalography (sEEG) and

electrocorticography (ECoG) probes are used to localize epileptogenic zones and to provide functional mapping of the brain before surgery [8-12]. Although ECoG probes are easier to use than sEEG probes, recordings performed on the brain surface pick up a highly integrated, global signal, which corresponds to the summation of different signals generated at different depths. Hence, ECoG probes are not able to accurately detect activities generated by smaller cell assemblies, except those generated right below an electrode. In addition to clinical applications, microfabricated probes are also likely to play a key role in the design of future brain-machine interfaces [13,14]. However, major technological advances are still needed: the probes must be fully biocompatible (to enable long-term recordings), small/thin (to decrease invasiveness), highly conformable (to comply with the complex 3D architecture of the brain), and most importantly, must provide an increased SNR through a built-in pre-amplification/processing system.

Neurons and brain networks generate small electric potentials, which are difficult to extract from noise when recorded with classical electrodes made of metals such as Ir, Pt and Au. Advances in microelectronics have given rise to the electrolyte/oxide/silicon field-effect transistor (FET), a more sophisticated device that has been used to measure *in vitro* signals from cell cultures and tissues slices [15-18]. In these devices, the transmembrane current from a neuron in the electrolyte polarizes the gate dielectric and leads to a change in the conductance of the underlying silicon channel. The use of transistors rather than simple electrodes provides the potential of increased SNR due to local amplification endowed by the transistor, and of massive integration which is possible through the use of matrix addressing technology developed for flat panel displays [15-18]. These advances, however, have so far been limited to *in vitro* recordings, mostly due to the poor biocompatibility of the oxide layer of the FETs. Although silicon FETs have recently been integrated into *in vivo* probes as a means of enabling simultaneous addressing of hundreds of electrodes [19], the recordings were carried out by classical electrodes, while the transistors themselves were carefully encapsulated to avoid direct contact with the brain.

An alternative transistor architecture, termed the organic electrochemical transistor (OECT), was developed in the '80s [20]. In contrast to FETs, where an oxide separates the channel from the electrolyte and prohibits any ion transport between these two layers, the channel of OECTs is in direct contact with an electrolyte. As a result, the channel/electrolyte interface constitutes an integral part of the operation mechanism of OECTs. State-of-the-art OECTs are based on the conducting polymer poly(3,4-ethylenedioxythiophene) doped with poly(styrene sulfonate) (PEDOT:PSS) [21]. This material is a heavily doped *p-type* organic semiconductor, in which holes on the PEDOT chains (the semiconductor) are compensated by sulfonate anions on the PSS (the dopant) [22]. The application of a positive

bias on a gate electrode immersed in the electrolyte causes cation injection into the PEDOT:PSS film. These cations compensate the sulfonate anions and dedope the PEDOT, thereby decreasing the drain current [23]. PEDOT:PSS OECTs work, therefore, in the depletion mode. Accumulation mode OECTs, based on intrinsic organic semiconductors, have also been reported, but they typically show higher operation voltages [24]. Since OECTs capture ion fluxes [25,26], they constitute the optimal solution to measure electrophysiological signals – fluctuations of the electric field (field potentials), generated by the movement of ions [27]. OECTs offer additional advantages that make them attractive candidates for neural interfacing, including cytocompatibility and straightforward integration with mechanically flexible (hence conformable) substrates [17,18]

Here we demonstrate the first *in vivo* use of a transistor to record brain activity. We fabricated highly conformable arrays of OECTs and used them to carry out ECoG on the somatosensory cortex of rats. Simultaneous recordings from penetrating and surface electrodes were used to validate the transistor recordings in two animal models. Compared to surface electrodes, OECTs showed a superior SNR due to local amplification. They also revealed a richer electrophysiological signal, similar to that obtained with penetrating electrodes.

5.1 Structure of the transistor arrays

We fabricated ECoG probes that contained organic electrochemical transistors as well as electrodes made from PEDOT:PSS. Micrographs of an ECoG probe and the layouts of a transistor and an electrode are shown in Figure 1. A 2 μm thick parylene film was used as the substrate, onto which Au and PEDOT:PSS films were photolithographically patterned. Au served as source and drain electrodes, electrode pads and interconnect lines, while PEDOT:PSS was used for the transistor channel and the surface electrodes. A second 2 μm thick parylene film, appropriately patterned to allow access to the channel and to the electrodes, was deposited on top and used as the insulator (Figures 1c and d). The total thickness of the arrays was approx. 4 μm, resulting in probes that were highly conformable yet had enough mechanical strength to be self-supporting and allow manipulation during surgery. Each probe contained 17 transistors with a channel length of 6 μm and a channel width of 15 μm, and 8 electrodes with dimensions of 12×12 μm^2. The Au structures were completely covered with PEDOT:PSS or parylene, and were not exposed to the electrolyte. Parylene is an FDA-approved polymer used in implantable devices such as pacemakers, while PEDOT-based electrodes have been extensively used as recording electrodes *in vivo* [28], and have been shown to outperform traditional metal electrodes in

chronic experiments [29]. Therefore, the arrays exposed biocompatible-only materials to the electrolyte. A through hole at the center of the array allowed the insertion of a silicon probe. At the other end of the probe, pads compatible with a zero insertion force (ZIF) connector allowed easy interfacing to electronics for recording, as shown in the insert of Figure 1a.

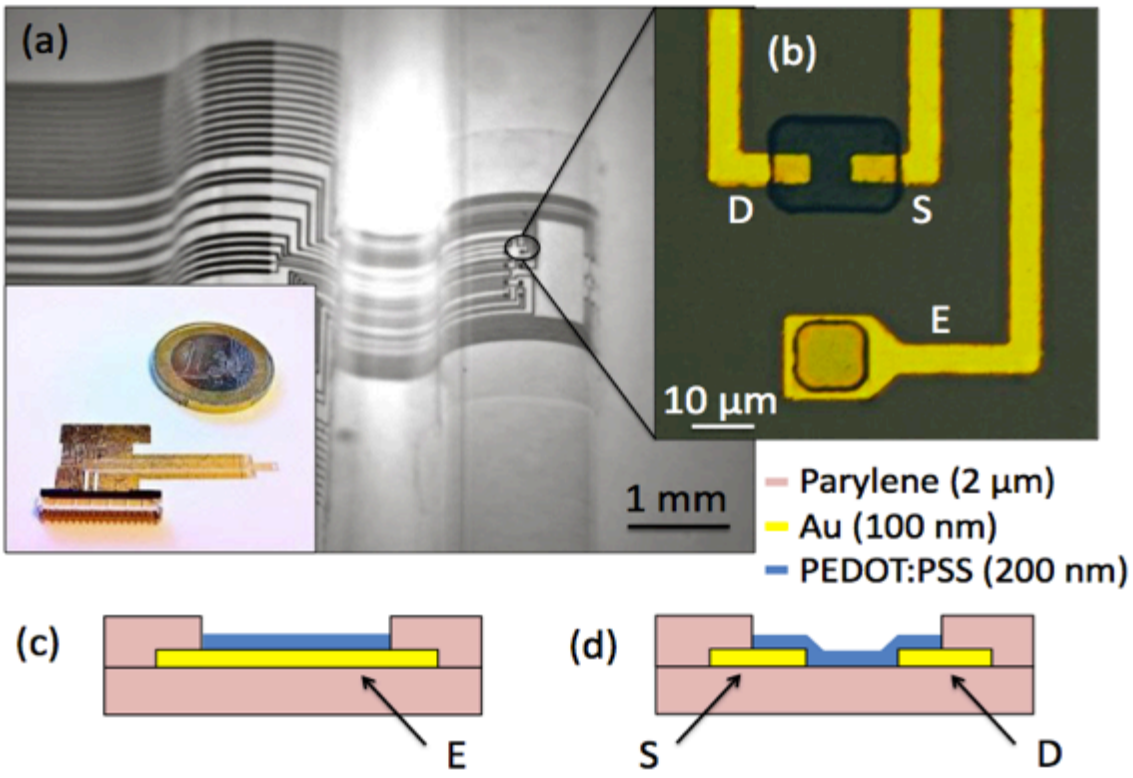

Figure 1: Optical micrographs of the ECoG probe conforming onto a curvilinear surface (a), and of the channel of a transistor and a surface electrode (b), in which the Au films that act as source (S), drain (D), and electrode pad (E) are identified. The inset in (a) shows the whole probe. The transistor/electrode arrays are on the right hand-side of this image, while the external connections, onto which a ZIF connector is attached, are on the left hand-side. Layouts of the surface electrode and of the transistor channel are shown in (c) and (d), respectively (not to scale).

5.2 *In vitro* characterization

The transistors were characterized *in vitro* using Ringer's solution as the electrolyte and a stainless steel gate electrode. Their output characteristics, shown in Figure 2a for a drain voltage (VD) between 0 and -0.4 V and a gate voltage (VG) between 0 and 0.5 V, are typical for operation in the depletion regime [23]. Upon the application of a positive gate voltage, cations from the

electrolyte enter the polymer film and dedope it, decreasing the drain current (ID). Due to the absence of a gate oxide and due to the high conductivity of PEDOT:PSS, the transistors show a low operation voltage which permits operation in aqueous environments. The corresponding transfer curve for VD=-0.4 V, shown in Figure 2b, exhibits a slope that increases with gate voltage. This is reflected in a transconductance that increases with VG up to 0.42 V, where it reaches a maximum of 900 μS. Normalized for channel width, this value (60 S/m) is two orders of magnitude larger than that of planar silicon-based FETs used in *in vitro* neural interfaces [16] and three orders of magnitude larger than that of typical organic FETs [30], which reflects the efficient gating of the polymer channel due to direct contact with the electrolyte. The transconductance was constant up to 1 kHz (Appendix B Figure 1), which is above the fastest oscillations recorded in the brain [31]. It should be noted that the steady-state gate current was less than 10 nA for VD=-0.4 V and VG=0.5 V.

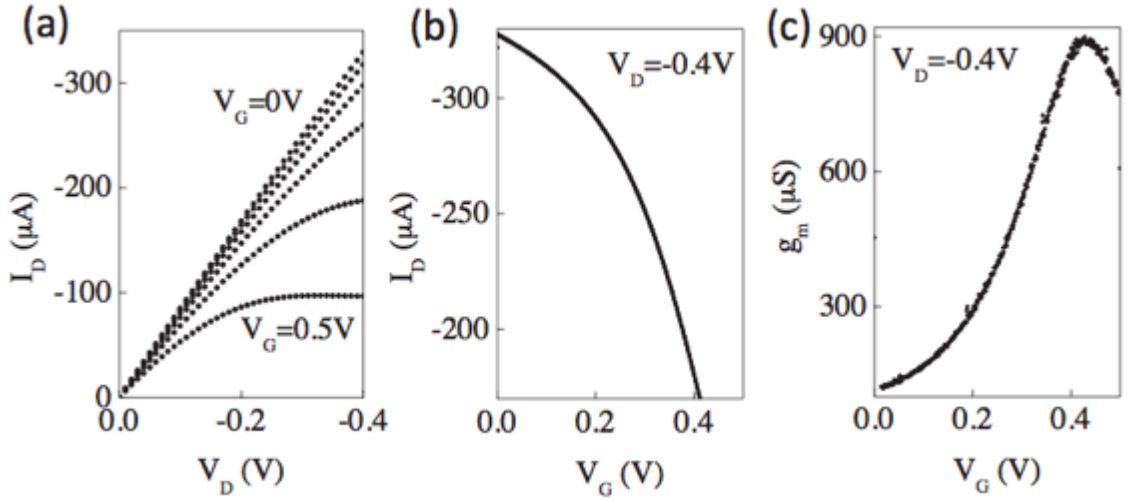

Figure 2: *In vitro* output characteristics (a) for VG=0 V to 0.5 V (with a step of 0.1 V) of a PEDOT:PSS transistor in Ringer's solution and with a stainless steel gate electrode. Transfer curve (b), and resulting transconductance at VD=-0.4 V (c).

5.3 *In vivo* characterization

Since the first application of OECT-based ECoGs is likely to be for epilepsy diagnosis and cortical mapping, we first characterized the *in vivo* performance of the transistors in an experimental model of epileptiform activity in rats. Animals were deeply anesthetized and a craniotomy was performed. The ECoG probe was placed on the somatosensory cortex and a silicon probe displaying a linear array of Ir electrodes was implanted through

the hole in the center of the ECoG probe (Figure 3a). The transistor was wired in a common source configuration (Figure 3b), with the grounded screw used as the gate electrode. We used VD=-0.4 V and VG=0.3 V. Bicuculline, a GABAA receptor antagonist, was perfused on the surface of the brain. Blockade of GABAergic inhibition invariably leads to the genesis of spikes that resemble interictal spikes [32]. Representative recordings from an OECT, a PEDOT:PSS surface electrode, and the penetrating electrodes of the silicon probe are shown in Figure 3c. The temporal coincidence of the peaks in the data indicates that the transistor records the same information as the electrodes. The background activity signal is shown at the same scale for the three recording devices, demonstrating the far superior SNR of the transistor.

The SNR was calculated by taking the highest peak during a period of epileptiform activity and the standard deviation (STD) of the background during a period of low biological activity. For the OECT recordings, these values were 1.5 μA and 9.5 nA, respectively, yielding an SNR of 44 dB, while the PEDOT:PSS surface electrode yielded an SNR of 24.2 dB (4.3 mV peak, 0.26 mV STD background). Although the OECT and the surface electrode were next to one another, and thus picked up the same activity in terms of fluxes of charges on the surface of the brain, the transistor recorded with a much higher SNR. The biological origin of this signal was confirmed by performing current source density (CSD) analysis on the silicon probe recordings (Figure 3d). The latter reveals the presence of the source and sink (hence the dipole) generating the epileptiform spike. It should be noted that all recordings were band-pass filtered between 0.1 and 200 Hz (see methods) in order to minimize the influence of the acquisition system on the SNR. Although this does not completely eliminate the influence of the acquisition system, it still demonstrates the superior gain provided by the local amplification of the signal by the transistor.

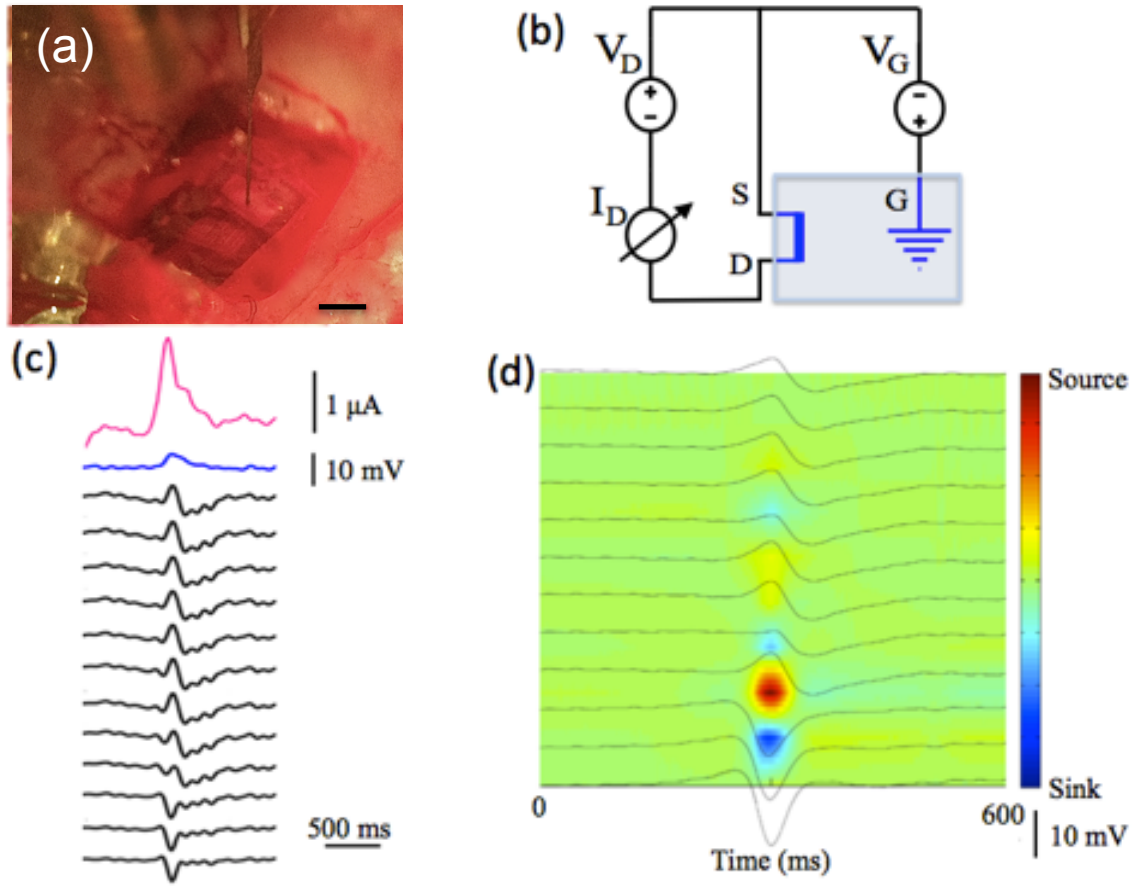

Figure 3: Optical micrograph of the ECoG probe placed over the somatosensory cortex of a Wistar rat (a), the scale bar is 1mm (b), with the blue box indicating the brain of the animal. (c) Recording of a bicuculline induced epileptiform spike from a transistor (pink), a PEDOT:PSS surface electrode (blue), and 12 of the 16 Ir penetrating electrodes (black) in a Wistar rat. The transistor was biased with VD = -0.4 V and VG = 0.3 V, and the scale of 10 mV is for both surface and penetrating electrodes. (d) Current source density map of a bicuculline-induced epileptiform spike showing a strong sink and source around the reversal of the event, in the deeper electrodes in the somatosensory cortex.

In the above experiments, the evaluation of the OECT performance was obtained by triggering epileptiform activity with bicuculline. In a second set of experiments, we used a more relevant experimental model, the Genetic Absence Epilepsy Rat from Strasbourg (GAERS) [33]. This model has been validated in terms of isomorphism, homology and pharmacological predictability to be reminiscent of typical absence epilepsy, a form of generalized non-convulsive epilepsy. GAERS rats show spontaneous large amplitude SWDs at a frequency between 7 and 11 Hz, associated with behavioral arrest and slight perioral automatisms. Despite the fact that deep

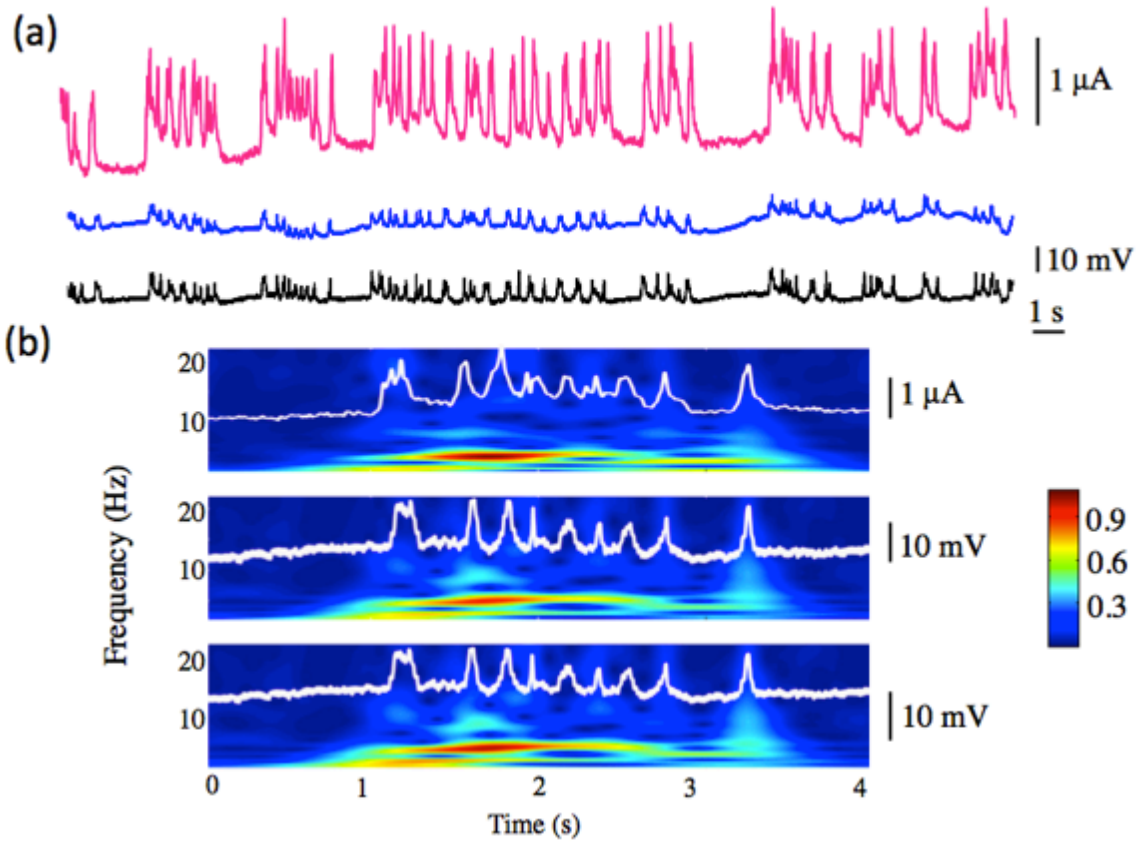

Figure 4: (a) Recordings in a GAERS rat from an OECT (pink), a PEDOT:PSS surface electrode (blue) and Ir penetrating electrodes (black). The transistor was biased with VD = -0.4 V and VG = 0.3 V, and the scale of 10 mV is for both surface and penetrating electrode. Note the superior SNR of the OECT as compared to the surface electrode. (b) Time-frequency analysis of epileptiform activity during a short period, OECT (top), a PEDOT:PSS surface electrode (middle), Ir penetrating electrode (bottom). The color bar represents the normalized power intensity.

anesthesia alters the expression of SWDs in GAERS rats, pathological epileptiform activity could be recorded (Figure 4a) from the OECT, the PEDOT:PSS surface electrode, and from Ir penetrating electrodes of a silicon probe implanted in the first three superficial layers of the somatosensory cortex. The transistor is shown again to outperform the surface electrode: the SNR for the OECT was 52.7 dB (1.3 µA peak, 3 nA STD background), and 30.2 dB (13 mV peak, 0.4 mV STD background) for the PEDOT:PSS surface electrode. For the sake of completeness, the SNR for the Ir penetrating electrode was 32.0 dB (10 mV peak, 0.3 mV STD background), though the different location of the probe (depth versus surface recording) does not permit a direct comparison.

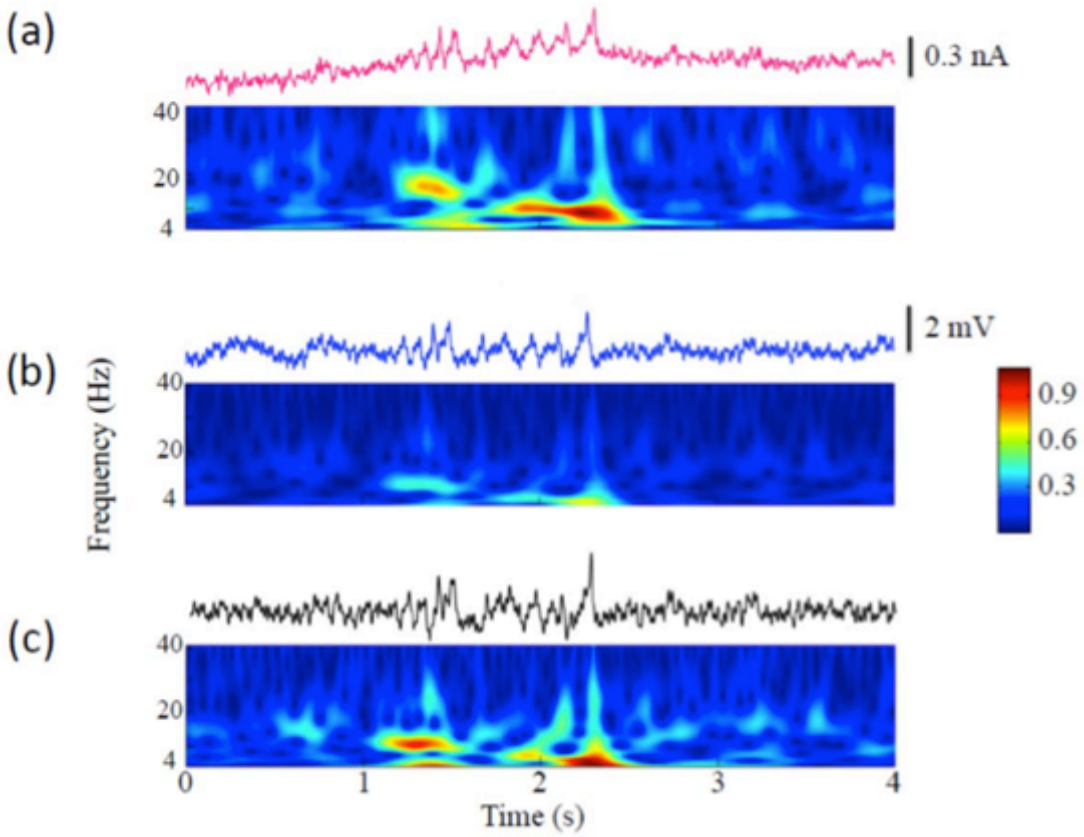

Figure 5: Recordings of oscillations in the spindle frequency range from an OECT (top), a PEDOT:PSS surface electrode (middle), and an Ir penetrating electrode (bottom), shown together with their corresponding Time-Frequency analysis plots (normalized TF energy), scaled to their minimum/maximum values. These oscillations, which have a lower amplitude than SWD, are picked up equally well by the OECT and the depth electrode, but are not well-resolved by the PEDOT:PSS surface electrode.

The time-frequency analysis of epileptiform activity during a short period (figure 4b), revealed the presence of typical oscillations in the 5-10 Hz band (Figure 4b). Moreover, for better illustration of the SNR improvement, the corresponding time traces were normalized according to the peaks of the activity. Electrodes and OECTs alike detected the same signal, in keeping with the fact that SWDs are generalized discharges, which sum up to give rise to a strong signal on the surface. The situation was, however, remarkably different during recordings in between epileptiform activities, where oscillations in the frequency range of spindle activity were observed. Spindle oscillations are a typical physiological activity occurring during early sleep stages [34]. They represent a lower amplitude activity as compared to

SWDs and are characterized by a 8-14 Hz oscillatory component. The signal represented in Figure 5 displays similarities in terms of frequency range and low amplitude with spindles (even if it cannot be considered as a spindle *per se* due the depth of anesthesia). Time-frequency analysis of recordings showed that the OECT and the Ir penetrating electrode were able to pick up these low-amplitude signals, while the PEDOT:PSS surface electrode showed poor resolution (Figure 5). The SNR was 22.3 dB for the OECT (300 nA peak, 23 nA STD background), 13.5 dB for the surface electrode (3.5 mV peak, 0.74 mV STD background), and 18.2 dB for the penetrating electrode (3 mV peak, 0.37 mV STD background), with the caveat that the latter recorded in a different location. It should be noted that the depth of anesthesia used here prevented us from assessing the presence of faster oscillations (such as gamma oscillations) in this case.

5.4 Discussion

In both conducting polymer electrodes [28] and OECTs [23], ion fluxes go in and out of the polymer film in response to the LFP at the interface with the electrolyte. The temporal coincidence between OECT and electrode recordings confirms this similarity in the nature of the response of the two recording devices. The key difference between transistors and electrodes, however, lies in the inherent amplification of the former. OECTs convert a small gate current into a much larger change in the drain current [23,26] and as such they act as amplifiers. The ion fluxes across the electrolyte/channel that are induced by the LFP become part of the gate current, and their transduction leverages the inherent amplification of the OECT. The applied gate bias is the 'handle" that controls this amplification by helping access a high transconductance region of the transfer curve. Electrode recordings, on the other hand, are pre-amplified outside the head of the animal, and the leads and connections pick up noise, which is amplified as well, decreasing the SNR.

In general, a higher SNR translates into a shorter overall recording time to obtain the same information. For example, when recording evoked potentials, it is necessary to average many individual signals. It also means that new, previously unobserved features can be recorded. Electrodes placed on the surface of the brain record the local field potentials associated with the summation of the electrical activity of neural networks, which can be located very far from the recording site. In contrast, penetrating electrodes provide more local, and thus more precise, information on the activity of small populations of neurons. We have previously reported that PEDOT:PSS ECoG electrodes show a better SNR than classical Au electrodes placed on the surface of the brain [35]. However, PEDOT:PSS electrodes showed less definition as compared to both OECTs and depth electrodes. The use of OECTs for *in vivo* recordings thus constitutes a major breakthrough, as they

are likely to record small and more local activities. This is particularly important in the field of epilepsy, where identifying zones generating high frequency oscillations or micro-seizures is key for diagnosis6, [36] OECTs can also provide detailed information on local information processing when functional mapping of brain regions is performed in the operating room before surgery. The biocompatibility of OECTs and their highly conformable nature make them particularly suited for these applications.

Small penetrating electrodes are used to capture single unit recordings, which represent the activity of a single neuron located in the vicinity of the electrode [7]. This raises the question of whether an OECT placed on a penetrating probe will be able to record single unit activity, and what new information, if any, will be revealed by the higher SNR. These experiments are currently ongoing. Finally, OECTs can help answer basic questions in neuroscience about the coupling between electrical activity and metabolism. In order to function, the brain needs energy in the form of glucose, which is carried in the blood. A dysfunction in this supply system results in pathological activities. Hypometabolism, for example, is one signature of epileptic regions [37]. The question of how the brain makes use of glucose in different contexts has never been addressed precisely, because it requires the simultaneous recording of neuronal activity and glucose level at the single neuron scale. PEDOT:PSS OECTs coupled with the redox enzyme glucose oxidase have been shown to make simple yet sensitive glucose sensors [38]. Their integration with electrodes that probe electrophysiology is rather straightforward. Such multi-modal probes would, for the first time, record electrophysiology and metabolism with high spatial resolution. The impact of such probes would be considerable and widespread, in basic physiology, pathology, and even in the clinic to interpret metabolic imaging.

5.5 Experimental

5.5.1 Fabrication and characterization

The fabrication and *in vivo* validation of PEDOT:PSS electrodes [35], and the patterning of PEDOT:PSS OECTs [39] were discussed in previous publications. Here we used an adapted fabrication process that involved the deposition and patterning of parylene, Au and PEDOT:PSS films as follows: Parylene C was deposited using a SCS Labcoater 2 to a thickness of 2 μm (at which thickness parylene films are pinhole-free). These films were patterned with the aid of a 4.6 μm thick layer of AZ9260 (MicroChemicals) photoresist and reactive ion etching by an O2 plasma (160 W, 50 sccm O2, 15 minutes) using an Oxford 80 plus. Metal pads and interconnects were patterned by a lift-off process. A photoresist, S1813 (Shipley), was spin-coated on the parylene film at 3500 rpm, baked at 110° C for 60 s, exposed to UV light (150 mJ/cm2) using a SUSS MJB4 contact aligner, and then developed using MF-26 developer. This was followed by the deposition of 5 nm of titanium and 100 nm of gold using a metal evaporator (Alliance Concept EVA450). Lift-off was performed using 1165 stripper. For the preparation of the PEDOT:PSS films, 20 mL of aqueous dispersion (PH-1000 from H.C. Stark) was mixed with 5 mL of ethylene glycol, 50 μL of dodecyl benzene sulfonic acid (DBSA), and 1 wt% of 3-glycidoxypropyltrimethoxysilane (GOPS, as a cross-linker), and the resulting dispersion was spin-coated at 650 rpm. The films were subsequently baked at 140° C for 1 hour and were immersed in deionized water to remove any excess low molecular weight compounds. The transistors were characterized *in vitro* using Ringer's solution (150 mM sodium, 3 mM potassium, 2 mM calcium, 1 mM magnesium and 10 HEPES/NaOH to adjust the pH to 7.2) as the electrolyte. A stainless steel screw was immersed in the electrolyte and used as the gate electrode. This was the same type of screw that was used as a gate electrode in the *in vivo* experiments (see below). A Keithley 2612A dual SourceMeter was used to bias the transistor and record the drain and gate currents. The time delay between sourcing voltages and measuring currents was 100 ms, which was found to be long enough for reaching steady-state.

5.5.2 *In vivo* evaluation

All protocols have been approved by the Institutional Animal Care and Use Committee of INSERM. Four ECoG probes were tested, two with Wistar rats and two with Genetic Absence Epilepsy Rats from Strasbourg (GAERS) rats. The Wistar rats were obtained from Charles River, MA, and the GAERS rats were obtained from Antoine Depaulis (Grenoble- Institut des Neurosciences, Grenoble, France). Upon receipt, they were maintained under controlled environmental conditions (23° C' 12 hour light/dark cycle). The GAERS rats

(females, weight of 188 and 196 g, respectively) were initially anesthetized with 5% isoflurane (Forene, Abbott France) in 0.5 l/min O2 and maintained under anesthesia with 2% isoflurane. In order to record faster oscillations, the depth of the anesthesia was decreased by reducing the amount of isoflurane to 1.5%. The Wistar rats (males, weight of 505 and 551 g, respectively) were anesthetized with a ketamine/xylazine mixture (35 and 1 mg/kg, i.m.). Additional doses of ketamine/xylazine (7 and 0.3 mg/kg, i.m) were given as needed. For surgery, the head of the rat was immobilized in a stereotaxic apparatus. The body temperature was monitored and kept constant with a heating pad. Two miniature stainless steel screws were driven into the skull above the cerebellum and served as ground and reference electrodes, respectively. A 5×3 mm2 craniotomy was performed in the right hemisphere above the somatosensory cortex (centered at –4 mm in the anterio-posterior axis and –2 mm in the medio-lateral axis, relative to Bregma). The dura matter was removed and the ECoG array was slowly lowered on the surface of the brain. The surface of the cortex was regularly rinsed with a 0.12M phosphate buffer (33.76 g NaH2PO4-H2O, 7.72 g NaOH in 1 l bi-distilled H2O, pH = 7.4). The ECoG probe was accessed *via* a Molex ZIF connector with flat flexible cable (FFC) to flexible printed circuitry (FPC) configuration. 40 µl of a 100 µM bicuculline solution (Sigma-Aldrich) was deposited with a micropipette onto the brain surface of the Wistar rats after the dura matter was removed. The recordings (figure 3c) were taken after sufficient time (20 min) for the effects of bicuculline to diffuse through the cortical layers. In the Wistar rats, an implantable probe (Neuronexus A1×16–3 mm 100–177, with a single, 3 mm long shank containing a linear array of 16 electrodes of 177 µm2 area each, spaced at 100 µm from each other) was inserted through the center of the ECoG in the cortex to reach a final depth of 2 mm. In the GAERS rats, an implantable probe with small pitch between the electrodes (Neuronexus A1×8–3 mm 50–177, with a single, 3 mm long shank containing a linear array of 8 electrodes of 177 µm2 area each, spaced at 50 µm from each other) was inserted through the center of the ECoG array in the cortex to reach a final depth of 1 mm. The penetrating probes were connected to a multi-channel Digital Lynx 10S system (Neuralynx) *via* a 1× HST headstage (Plexon). The signals were amplified (×1,000), band-pass filtered (0.1 Hz–5 kHz), and acquired continuously at 32 kHz on the 64-channel Neuralynx system (16-bit resolution). Signals from the ECoG PEDOT:PSS electrodes were also acquired by the same amplifier and under the same conditions. A Keithley 2612A dual SourceMeter was used to bias the transistor and record the drain and gate currents continuously at 0.3 kHz. Post-acquisition treatment: All recordings (from electrodes and OECTs alike) were digitally filtered with a 0.1-200 Hz band-pass filter in order to minimize the contribution of the frequency response of the two different acquisition systems used and enable a more fair comparison between OECT and electrode recordings. The recordings were also digitally filtered with a 50 Hz

notch filter to remove line noise. The calculation of the SNR was based on recordings filtered in this manner. The data were analyzed using MATLAB (MathWorks). A Gabor wavelet time-frequency analysis was used to determine the frequency content of local field potentials. CSD analysis of the simultaneously field potentials recorded with the penetrating probe was used to eliminate volume conduction and localize synaptic currents during epileptic discharges. CSD was computed as the second spatial derivative of the recorded raw LFPs (average of 44 events centered on the trough of the epileptic spikes on the deeper electrode of the penetrating probe). The 44 averaged signals superimposed to the CSD were digitally filtered with a 50 Hz notch filter.

References

[1] O'Keefe, J. Place units in the hippocampus of the freely moving rat. *Exp Neurol* **51,** 78-109 (1976).

[2] Sargolini, F. et al. Conjunctive representation of position, direction, and velocity in entorhinal cortex. *Science* **312,** 758-62 (2006).

[3] Solstad, T., Boccara, C.N., Kropff, E., Moser, M.B. & Moser, E.I. Representation of geometric borders in the entorhinal cortex. *Science* **322,** 1865-8 (2008).

[4] Buzsáki, G. Rhythms of the brain (Oxford University Press, Oxford ; New York, 2006).

[5] Herrmann, C.S., Frund, I. & Lenz, D. Human gamma-band activity: a review on cognitive and behavioral correlates and network models. *Neurosci Biobehav Rev* **34,** 981-92 (2010).

[6] Blanco, J.A. et al. Unsupervised classification of high-frequency oscillations in human neocortical epilepsy and control patients. *J Neurophysiol* **104,** 2900-12 (2010).

[7] Kipke, D.R. et al. Advanced neurotechnologies for chronic neural interfaces: new horizons and clinical opportunities. *J Neurosci* **28,** 11830-8 (2008).

[8] McGonigal, A. et al. Stereoelectroencephalography in presurgical assessment of MRI-negative epilepsy. *Brain* **130,** 3169-83 (2007).

[9] Jasper, H.H., Arfel-Capdeville, G. & Rasmussen, T. Evaluation of EEG and cortical electrographic studies for prognosis of seizures following surgical excision of epileptogenic lesions. *Epilepsia* **2,** 130-7 (1961).

[10] Crone, N.E. Functional mapping with ECoG spectral analysis. *Adv Neurol* **84,** 343-51 (2000).

[11] Canolty, R.T. et al. High gamma power is phase-locked to theta oscillations in human neocortex. *Science* **313,** 1626-8 (2006).

[12] Bancaud, J. et al. Functional stereotaxic exploration (SEEG) of epilepsy. *Electroencephalogr Clin Neurophysiol* **28,** 85-6 (1970).

[13] Pfurtscheller, G., Graimann, B., Huggins, J.E. & Levine, S.P. Brain-computer communication based on the dynamics of brain oscillations. *Suppl Clin Neurophysiol* **57,** 583-91 (2004).

[14] Waldert, S. et al. A review on directional information in neural signals for brain-machine interfaces. *J Physiol Paris* **103,** 244-54 (2009).

[15] Fromherz, P. Joining microelectronics and microionics: Nerve cells and brain tissue on semiconductor chips. *Solid-State Electronics* **52,** 1364-1373 (2008).

[16] Hutzler, M. & Fromherz, P. Silicon chip with capacitors and transistors for interfacing organotypic brain slice of rat hippocampus. *European Journal of Neuroscience* **19,** 2231-2238 (2004).

[17] Qing, Q. et al. Nanowire transistor arrays for mapping neural circuits in acute brain slices. *Proceedings of the National Academy of Sciences* **107,** 1882-1887 (2010).

[18] Timko, B.P. et al. Electrical Recording from Hearts with Flexible Nanowire Device Arrays. *Nano Letters* **9,** 914-918 (2009).

[19] Viventi, J. et al. Flexible, foldable, actively multiplexed, high-density electrode array for mapping brain activity in vivo. *Nat Neurosci* **14,** 1599-605 (2011).

[20] Kittlesen, G.P., White, H.S. & Wrighton, M.S. Chemical Derivatization of Microelectrode Arrays by Oxidation of Pyrrole and N-Methylpyrrole - Fabrication of Molecule-Based Electronic Devices. *Journal of the American Chemical Society* **106,** 7389-7396 (1984).

[21] Owens, R.M. & Malliaras, G.G. Organic electronics at the interface with biology. *Mrs Bulletin* **35,** 449-456 (2010).

[22] Elschner, A., Kirchmeyer, S., Lövenich, W., Merker, U. & Reuter, K. in PEDOT, Principles and Applications of an Intrinsically Conductive Polymer 113-166 (CRC Press, 2010).

[23] Bernards, D.A. & Malliaras, G.G. Steady-state and transient behavior of organic electrochemical transistors. *Advanced Functional Materials* **17,** 3538-3544 (2007).

[24] Cho, J.H. et al. Printable ion-gel gate dielectrics for low-voltage polymer thin-film transistors on plastic. *Nat Mater* **7,** 900-906 (2008).

[25] Nilsson, D., Kugler, T., Svensson, P.O. & Berggren, M. An all-organic sensor-transistor based on a novel electrochemical transducer concept printed electrochemical sensors on paper. *Sensors and Actuators B-Chemical* **86,** 193-197 (2002).

[26] Bernards, D.A., Malliaras, G.G., Toombes, G.E.S. & Gruner, S.M. Gating of an organic transistor through a bilayer lipid membrane with ion channels. *Applied Physics Letters* **89,** - (2006).

[27] Buzsáki, G., Anastassiou, C.A. & Koch, C. The origin of extracellular fields and currents — EEG, ECoG, LFP and spikes. *Nat Rev Neurosci* **13,** 407-420 (2012).

[28] Kim, D.-H. et al. in Indwelling Neural Implants: Strategies for Contending with the In-Vivo Environment (ed. Reichert, W.M.) 165-207 (CRC Press, Taylon and Francis, Boca Raton, FL, 2008).

[29] Ludwig, K.A., Uram, J.D., Yang, J.Y., Martin, D.C. & Kipke, D.R. Chronic neural recordings using silicon microelectrode arrays electrochemically deposited with a poly(3,4- ethylenedioxythiophene) (PEDOT) film. *Journal of Neural Engineering* **3,** 59-70 (2006).

[30] Klauk, H., Zschieschang, U. & Halik, M. Low-voltage organic thin-film transistors with large transconductance. *Journal of Applied Physics* **102,** 074514 (2007).

[31] Buzsáki, G. & Draguhn, A. Neuronal Oscillations in Cortical Networks. *Science* **304,** 1926-1929 (2004).

[32] Chagnac-Amitai, Y. & Connors, B.W. Horizontal spread of synchronized activity in neocortex and its control by GABA-mediated inhibition. *J Neurophysiol* **61,** 747-58 (1989).

[33] Danober, L., Deransart, C., Depaulis, A., Vergnes, M. & Marescaux, C. Pathophysiological mechanisms of genetic absence epilepsy in the rat. *Prog Neurobiol* **55,** 27-57 (1998).

[34] Steriade, M. Sleep, epilepsy and thalamic reticular inhibitory neurons. *Trends Neurosci* **28,** 317- 24 (2005).

[35] Khodagholy, D. et al. Highly Conformable Conducting Polymer Electrodes for In Vivo Recordings. *Advanced Materials* **23,** H268-+ (2011).

[36] Stead, M. et al. Microseizures and the spatiotemporal scales of human partial epilepsy. *Brain* **133,** 2789-97 (2010).

[37] Duncan, J.S. Imaging and epilepsy. *Brain* **120 (Pt 2),** 339-77 (1997).

[38] Bernards, D.A. et al. Enzymatic sensing with organic electrochemical transistors. *Journal of Materials Chemistry* **18,** 116-120 (2008).

[39] Khodagholy, D. et al. High speed and high density organic electrochemical transistor arrays. *Applied Physics Letters* **99** (2011).

Chapter 6

6 Organic Electrochemical Transistor incorporating an ionogel as a solid state electrolyte for lactate sensing

The detection of lactate (deprotonated form of lactic acid) in blood provides a biochemical indicator of anaerobic metabolism in patients with circulatory failure. [1] In addition to its presence in blood, lactate can be found in sweat (concentration range between 9 and 23 mM), reflecting, in an indirect way, eccrine gland metabolism. [2] It is well known that lactate concentration increases during physical exercise, making it a useful parameter to monitor wellness, physical fitness and the effects of exercise. [3] Detection in sweat offers a less invasive and dynamic way of measuring lactate concentration, particularly during exercise. Current methods of detection of lactate include fiber optics, [4] conducting polyaniline films, [5] carbon nanotubes, [6] screen printed Prussian blue electrodes, [7] and biosensors based on electro-chemi-luminescent detection. [8] Commercial lactate sensors are also available, [9] based on standard electrochemical methods. One example is the lactate SCOUT (Senslab), which, however, samples from blood, making real-time detection impractical. Therefore, the possibility of a fast, reliable, robust, miniaturized and cheap way of measuring lactate concentration in physiological fluids will open the way to lactate biosensors for health and sport applications. Flexibility plays an important role, here also, as biosensors for lactate sensing in sweat are in demand as wearable sensors, integrate for example on textiles.

Conducting polymers are interesting biosensing materials owing to their low-cost, mechanical flexibility, and ionic conductivity. Such materials have been

exploited in the field of organic electronics to fabricate biosensors. One such device is the organic electrochemical transistor (OECT). OECTs have been utilized in a variety of biosensing applications such as the detection of metabolites, [10,11] ions, [12,13] neurotransmitters, [14] cells, [15] antibodies16 and DNA. [17] The OECT was first described by White et al. in 1984. [18] In general, OECTs are three terminal devices containing source and drain electrodes that measure the current across the conducting polymer (the transistor channel) and a gate electrode. The channel and the gate electrode are in ionic contact via an electrolyte. The working mechanism of the OECT relies on changing the doping state of the conducting polymer channel by application of a positive potential at the gate electrode. Such potential forces cations from the electrolyte to penetrate into the channel and decreases the number of charge carriers (holes), consequently decreasing the channel current. [19] The vast majority of OECTs are based on poly(3,4-ethylenedioxythiophene) doped with poly(styrene sulfonate) (PEDOT:PSS), a commercially available polymer with high conductivity, which is also biocompatible. [20]

6.1 Room temperature ionic liquids (RTLIs)

Room Temperature Ionic Liquids (RTILs) are low temperature molten salts that are entirely composed of cations and anions. Due to their unique properties such as large electrochemical stability window, high conductivity and thermal stability, ionic liquids have received increasing attention from the scientific community for applications in green chemistry [21] and electrochemistry, [22] among others. For instance, RTILs provide an attractive alternative to conventional organic solvents to solubilize and stabilize biomolecules such as enzymes and proteins. [21] There are three main strategies to solubilize biomolecules in RTILs: firstly by direct dispersion, secondly, through surface protein modification by PEGylation (covalent attachment of polyethylene glycol polymer chains to the protein) and thirdly by creating a hydrated RTIL. [22] The last method seems to be the most suitable for biosensors, because the addition of small amounts of water to ionic liquids strongly influences the protein solubility while retaining the properties of the selected ionic liquid. Fujita et al. [23] have demonstrated that certain proteins are, in fact, soluble, stable and remain active for up to 18 months in RTILs.

We have previously integrated an OECT with a RTIL to make a glucose sensor, in which the glucose oxidase enzyme was dispersed in the ionic liquid. [24] In this paper we report the development of a simple, yet robust biosensor that measures lactic acid, an important metabolite involved in several biological mechanisms. The novelty rests with the use of an ionogel which enables the development of a fully solid state yet flexible sensor, suitable for

analysis of lactate in sweat. Ionogels are solid or gel- like polymeric materials that endow room temperature ionic liquids (RTILs) with structure and dimensional stability. Le Bideau et al. [25] summarized this new class of hybrid materials, in which the properties of the IL are hybridized with those of various components, which may be organic (low molecular weight gelator, (bio)polymer), inorganic (e.g. carbon nanotubes, silica, etc.) or hybrid organic–inorganic (e.g. polymer and inorganic fillers). These materials are thought to inherit all of the desirable RTIL properties whilst maintaining a gel-like structure. Here, we present the first step towards achieving a fast, flexible, miniaturized and cheap way of measuring lactate concentration in sweat through development of a biosensor based on an OECT that uses an ionogel as a solid-state electrolyte both to immobilize the enzyme and to serve as a supporting electrolyte.

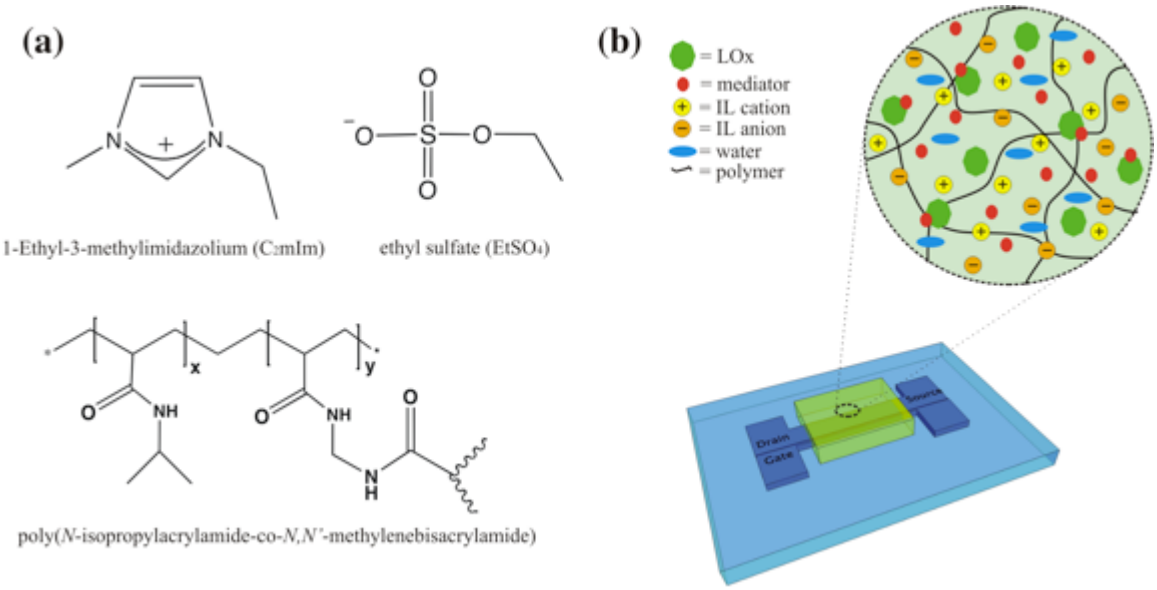

Figure 1: (a) Ionogel components and (b) a schematic representation of the OECT device with ionogel / enzyme mixture.

6.2 Fabrication and preparation

The OECT fabrication started with the deposition of a 2 µm thick sacrificial parylene C layer on a glass wafer. This parylene layer was subsequently patterned with a standard lithography followed by a dry etch using O2 plasma, defining a contact mask for the PEDOT:PSS channel and gate electrode. A 200 nm thick PEDOT: PSS film was then spin-coated from dispersion (PH-500 from H. C. Stark) and annealed at 140° C for 60 min. To improve the PEDOT:PSS conductivity, 5 ml of ethylene glycol and 50 ml of dodecyl benzene sulfonic acid (DBSA) were added per 20 ml of PEDOT:PSS dispersion. Additionally, 0.25 g of the cross-linker 3-

glycidoxypropyltrimethoxysilane (GOPS) was added to the above dispersion to render the PEDOT:PSS film insoluble. 35 Finally the parylene layer was peeled off mechanically to reveal the PEDOT:PSS channel and the gate electrode. A similar process was followed to make transistors on parylene: the glass wafer was coated with a 2 μm thick parylene film (which would become the OECT support), and was treated with a detergent in order to enable the peel-off of the sacrificial parylene layer. The ionogel consists of two monomeric units: N-iso- propylacrylamide (NIPAAm) and N,N0 -methylene-bis(acryl- amide) (MBAAm) in the molar ratio of 100 : 2, respectively (the chemical structure is shown in Figure 1a). 1-Ethyl-3- methylimidazolium ethyl-sulfate ionic liquid, [C_2mIm][$EtSO_4$] (Sigma Aldrich, used as received), was chosen because of its miscibility with water, thus avoiding mixing problems with the phosphate buffer solution (PBS) containing the analyte. The reaction mixture was prepared firstly by dissolving a ferrocene mediator [bis(n-5-cyclopentandienyl) iron] (Fc, 10 mM) (Sigma Aldrich) in the IL and subsequently mixing the NIPAAm monomer, the crosslinker MBAAm and the photo-initiator dimethoxyphenylacetophenone DMPA in 0.8 ml of [C_2mIm] [EtSO4]. A significant advantage was found in the solubility of the Fc in the ionic liquid, as Fc shows very poor solubility in aqueous solutions such as PBS. Although it is possible that Fc may not be suitable as a mediator in a wearable device due to toxicity concerns, this may be addressed by ensuring that it is covalently bound to the ionogel and thus will not leach out. Alternative redox mediators also exist and have been used for example for subcutaneous glucose sensors which are FDA approved. [26] The mixture was then sonicated at 45° C for 10 minutes and a clear and monophasic solution was obtained. Additionally, stock solutions of 100 mM LOx (Sigma Aldrich) and 1 M lactic acid (Sigma Aldrich) were prepared, both in PBS.

By mixing the RTIL mixture and the PBS solution containing the LOx enzyme with a ratio of 4 : 1 (17% w/w of water) a clear liquid was obtained. The hydrated IL completely dissolved the protein and no precipitation was observed. 20 ml of the final solution was placed at the center of the device where a poly- dimethylsiloxane (PDMS) well of a diameter of 8 mm was previously attached to avoid solution leakage after drop casting. Then, the monomers were photo-polymerized within the ionic liquid matrix using a UV irradiation source (three LED arrays at wavelength 365 nm, UV light intensity ≈ 330 mW cm^2) for 1 minute. It should be noted that UV exposure time was kept short to avoid denaturation of the protein.

Figure 1b shows the layout of the planar OECT, consisting of two parallel stripes of PEDOT: PSS, with widths of 100 μm and 1 mm, serving as the gate electrode and channel of the OECT, respectively (it has been shown that for enzymatic sensing the area of the channel must be larger than the gate electrode [27]). The hydrated ionogel which contains the LOx enzyme, and

the Fc mediator (schematic representation Figure 1b), covers parts of the channel and the gate of the OECT, as defined by the well.

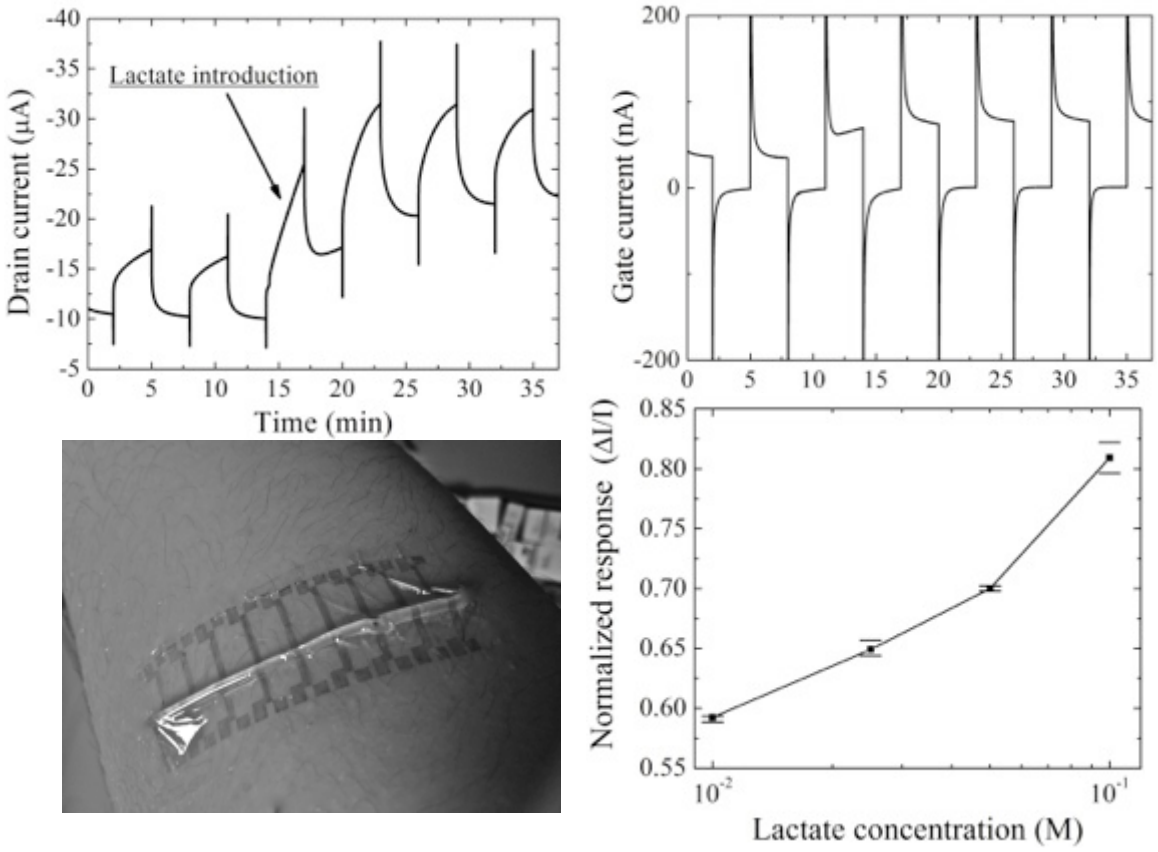

Figure 2: (a) Drain current vs. Time with addition of 25 mM lactate indicated by arrow (b) Corresponding Gate current vs. Time (c) Normalized response of the OECT vs. lactate concentration (d) Conformal OECT with gel shown on forearm.

6.3 Results and discussion

Measurements were carried out by applying -0.3 V potential across the channel while triggering the gate electrode at 0.4 V by 3 min long square pulses. Figure 2a shows the modulation of the drain current before (t < 15 min) and after the introduction of 20 ml of a PBS solution with the desired lactate concentration. The introduction of the analyte is shown to lead to an increase in the modulation of the drain current, consistent with the mode of operation of OECT-based enzymatic sensors.[10] Figure 3a depicts the series of reactions that take place upon introduction of the lactate. As lactic acid is oxidized to pyruvate, lactate oxidase is reduced and cycles back by the Fc/Ferricenium ion (Fc+) couple, which carries electrons to the gate electrode. This leads to a decrease in the potential across the gate/electrolyte interface and a concomitant increase of the potential at the channel/electrolyte interface. As a result, more cations from the solution enter and dedope the channel (Figure 3b) and the modulation of the drain current in response to a voltage pulse at the gate increases.

The modulation in the drain current is much larger than the gate current due to the inherent amplification characteristics of the OECT. This is demonstrated in Figure 2b, where approximately 100 nA of current at the gate results in 11 mA modulation at the drain current. Figure 2c shows the normalized response of the transistor (DI/I) as a function of lactate concentration in the range 10 - 100 mM. The response of the transistor is defined as the difference in the modulation level of the drain channel during application of a gate voltage in the absence and presence of the analyte. The data shown represent the average of three measurements, and the error bars represent the standard deviation from the mean. The time required for the sensor to reach steady-state after addition of analyte is approximately 10 minutes. This is most likely due to the time it takes for the analyte to diffuse to the enzyme through the gel and may thus be improved by increasing the enzyme concentration, decreasing the gel thickness, etc. The data clearly show the detection of lactate in the relevant physiological range, covering the relevant range of lactate present in sweat, and suggesting the potential application of this device in the field of sport science as well as in healthcare. It should be noted that the sensor would also be compatible with the detection of lactate in blood (normal physiological range 0.3 - 1.3 mM, up to 25 mM during exercise). [28]

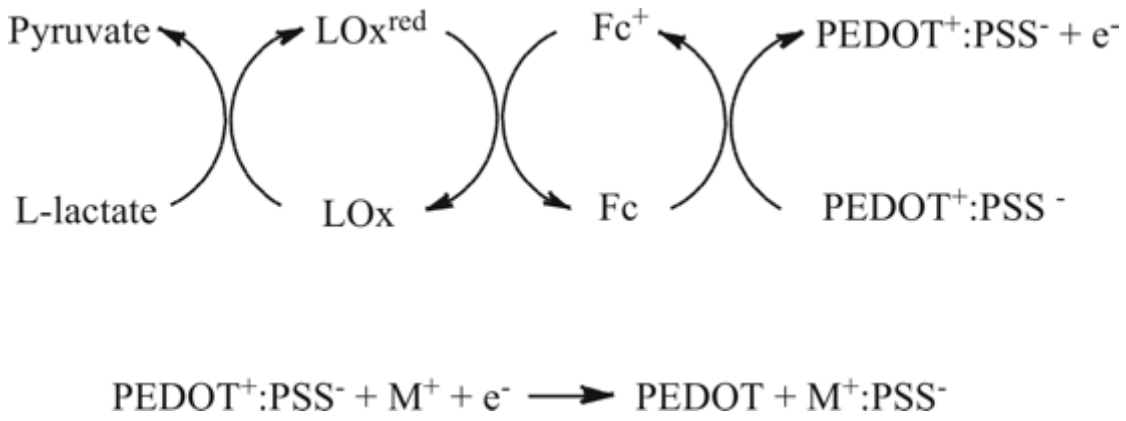

Figure 3: Reactions at the gate electrode (a) and at the channel (b) of the OECT

Physiological testing is an important tool for athletes and coaches to check the athlete's health and develop individualized training strategies. While laboratory testing may be increasingly widespread, there is a great demand for wearable sensors to be used in the field. [29] Today's wearable technologies are based on physical sensors, such as electrocardiograph (ECG) electrodes, thermistors and accelerometers. [30] These sensors respond to physical changes in their environment e.g. heat, movement and light. Wearable chemo-sensors, in contrast, have the potential to measure many more variables relating to the individual's well-being and safety. The integration of chemical sensors (such as lactate) into a textile substrate is a challenging task, as a chemical reaction must happen for these devices to generate a signal and the sensors must be robust, non-invasive, low-power and straightforward to use. The OECT sensor presented here is a step forward towards such devices. Figure 2d shows a prototype of an array of these sensors (deposited on parylene) in a conformal configuration on a human forearm, demonstrating their wear- ability. The integration of this prototype with a wireless working platform, previously demonstrated for sweat analysis for non- invasive real time measurements, is currently ongoing [29].

6.4 Conclusions

In summary, we demonstrate the detection of lactate in a relevant physiological range using an OECT sensor with an ionogel solid- state electrolyte. The significance of this work for sensing applications lies in the configuration of the sensor; we show for the first time a solid-state electrolyte on a flexible transistor-based biosensor. This has implications for the wearability of the sensor and the storage of the sensor due to the enhanced stability of the enzyme in the ionogel. We envision the use of this sensor as a wearable bandage-type sensor, which can be worn during exercise or health monitoring, allowing sweat to diffuse into the sensor with consequent detection of the lactate analyte. This could also have application for the detection of other sweat components such as pH.

References:

1. M. H. Weil and A. A. Afifi, *Circulation*, 1970, **41**, 989-1001.

2. J. M. Green, R. C. Pritchett, T. R. Crews, J. R. McLester, Jr. and D. C. Tucker, *Eur J Appl Physiol*, 2004, **91**, 1-6.

3. L. V. Billat, *Sports Med*, 1996, **22**, 157-175.

4. X. J. Liu and W. H. Tan, *Mikrochim Acta*, 1999, **131**, 129-135.

5. A. Chaubey, K. K. Pande, V. S. Singh and B. D. Malhotra, *Anal. Chim. Acta*, 2000, **407**, 97-103.

6. J. Weber, A. Kumar, A. Kumar and S. Bhansali, *Sensors and Actuators B-Chemical*, 2006, **117**, 308-313.

7. E. I. Yashina, A. V. Borisova, E. E. Karyakina, O. I. Shchegolikhina, M. Y. Vagin, D. A. Sakharov, A. G. Tonevitsky and A. A. Karyakin, *Anal Chem*, 2010, **82**, 1601-1604.

8. X. Cai, J. L. Yan, H. H. Chu, M. S. Wu and Y. F. Tu, *Sensors and Actuators B-Chemical*, 2010, **143**, 655-659.

9. Y. Wang, H. Xu, J. M. Zhang and G. Li, *Sensors-Basel*, 2008, **8**, 2043-2081.

10. D. A. Bernards, D. J. Macaya, M. Nikolou, J. A. DeFranco, S. Takamatsu and G. G. Malliaras, *Journal of Materials Chemistry*, 2008, **18**, 116-120.

11. S. Y. Yang, J. A. DeFranco, Y. A. Sylvester, T. J. Gobert, D. J. Macaya, R. M. Owens and G. G. Malliaras, *Lab on a Chip*, 2009, **9**, 704-708.

12. D. A. Bernards, G. G. Malliaras, G. E. S. Toombes and S. M. Gruner, *Appl Phys Lett*, 2006, **89**, -.

13. P. Lin, F. Yan and H. L. W. Chan, *Acs Appl Mater Inter*, 2010, **2**, 1637-1641.

14. S. Y. Yang, B. N. Kim, A. A. Zakhidov, P. G. Taylor, J. K. Lee, C. K. Ober, M. Lindau and G. G. Malliaras, *Adv. Mater.*, 2011, **23**, H184-H188.

15. P. Lin, F. Yan, J. J. Yu, H. L. W. Chan and M. Yang, *Adv. Mater.*, 2010, **22**, 3655-+.

16. D.-J. Kim, N.-E. Lee, J.-S. Park, I.-J. Park, J.-G. Kim and H. J. Cho, *Biosensors and Bioelectronics*, 2010, **25**, 2477-2482.

17. P. Lin, X. Luo, I. M. Hsing and F. Yan, *Adv. Mater.*, 2011, **23**, 4035-4040.

18. H. S. White, G. P. Kittlesen and M. S. Wrighton, *J. Am. Chem. Soc.*, 1984, **106**, 5375-5377.

19. D. A. Bernards and G. G. Malliaras, *Adv. Funct. Mater.*, 2007, **17**, 3538-3544.

20. R. M. Owens and G. G. Malliaras, *Mrs Bull*, 2010, **35**, 449-456.

21. M. J. Earle and K. R. Seddon, *Pure Appl Chem*, 2000, **72**, 1391-1398.

22. M. Armand, F. Endres, D. R. MacFarlane, H. Ohno and B. Scrosati, *Nature Materials*, 2009, **8**, 621-629.

23. K. Fujita, D. R. MacFarlane, M. Forsyth, M. Yoshizawa-Fujita, K. Murata, N. Nakamura and H. Ohno, *Biomacromolecules*, 2007, **8**, 2080-2086.

24. S. Y. Yang, F. Cicoira, R. Byrne, F. Benito-Lopez, D. Diamond, R. M. Owens and G. G. Malliaras, *Chem Commun (Camb)*, 2010, **46**, 7972-7974.

25. J. Le Bideau, L. Viau and A. Vioux, *Chem Soc Rev*, 2011, **40**, 907-925.

26. A. Heller and B. Feldman, *Chem Rev*, 2008, **108**, 2482-2505.

27. G. Tarabella, C. Santato, S. Y. Yang, S. Iannotta, G. G. Malliaras and F. Cicoira, *Appl Phys Lett*, 2010, **97**.

28. B. Phypers and J. T. Pierce, *Continuing Education in Anaesthesia, Critical Care & Pain*, 2006, **6**, 128-132.

29. S. Coyle, F. Benito-Lopez, R. Byrne and D. Diamond, in *In Wearable and Autonomous Biomedical Devices and Systems, Issues and Characterisation*, eds. A. Lay-Ekuakille and S. C. Mukhopadhyay, Springer, 2011, pp. 177-193.

30. F. Axisa, P. M. Schmitt, C. Gehin, G. Delhomme, E. McAdams and A. Dittmar, *IEEE Transactions on Information Technology in Biomedicine*, 2005, **9**, 325-336.

Chapter 7

7 Conclusion

The work presented in this thesis contributes to the overarching goal of developing an improved abiotic/biotic interface. The majority of the work focuses on advancing the interface between the brain and electronics using conducting polymers as the active interfacing material. The "soft" nature of conducting polymers offers better mechanical compatibility with tissue than traditional electronic materials. More importantly, their ability to conduct ions in addition to electrons and holes opens up a new communication channel with biology. Furthermore, the work includes the development of biocompatible (to enable long-term recordings from brain), small/thin (to decrease invasiveness), highly conformable electronics (to comply with the complex 3D architecture of the brain), and most importantly, enhanced quality of brain activities recordings.

Chapter 2 presented a microfabricated highly conformable polymeric ECoG probe. In contrast to previously reported techniques such as electrochemical coating of patterned metal electrodes, the process involves the direct patterning of the polymer layer and thereby enables the use of "champion" materials such as PEDOT:PSS. The total thickness of the probe was 4 μm which made the probe highly conformability. Their use in electrocorticography was demonstrated and validated against a silicon probe and were shown to outperform Au electrodes of similar geometry owing the better impedance match between conducting polymers and brain. In Chapter 3 the organic electrochemical transistor (OECT) was presented. OECTs capture ion fluxes, and constitute the optimal solution to measure electrophysiological signals. The channel of the device is in direct contact with an electrolyte. As a result, the channel/electrolyte interface is considered an integral part of the transistor. The presented lithographic process enables fabrication of high-speed and high-density OECT arrays. Owing to its well

defined and micron-scale geometry the temporal response of the OECT is 100 μs, much faster than action potentials (~1ms). It utilizes parylene C, a biocompatible material, as the insulating material that make the arrays suitable for integration with living cells. Chapter 4 investigated on the OECT optimization. An analytical model was used to derive the frequency response and transconductance of the transistor. The model provided a good fit to the experimental data and yields predictions for navigating the trade-off between transconductance and cut-off frequency. The temporal response of the drain current was found to be limited by the RC constant of the gate/electrolyte/channel circuit rather than by the hole mobility in the channel. Based on the models, an OECT with transconductance per channel width exceeding 50 S/m, (3 orders of magnitude higher than OFETs and 2 orders of magnitude higher than silicon based ISFETs) was fabricated.

The first *in vivo* use of a transistor to record brain activity is introduced in chapter 5. The transistors were fabricated on a parylene C support and used to carry out ECoG on the somatosensory cortex of rats. Compared to conventional electrodes, OECTs showed a superior SNR due to local amplification, right at the interface with the brain. They also revealed a richer electrophysiological signal, similar to that obtained with penetrating electrodes that could not be observed by traditional surface electrodes.

Finally, Chapter 6 demonstrated integration of solid-state electrolytes with OECTs for biosensing applications. The OECT incorporated an ionogel for detection of lactate in a relevant physiological range. This had implications for the wearability of the sensor and the storage of the sensor due to the enhanced stability of the enzyme in the ionogel.

7.1 Outlook

There is a tremendous need for developing advanced materials technologies for interfacing with brain and record neural activities. This is particularly important in the study of epilepsy, where identifying zones generating high frequency oscillations or micro-seizures is key for diagnosis. Deep-brain electrodes are used to capture single unit recordings, which represent the activity of a single neuron located in the vicinity of the electrode. This raises the question of whether an OECT placed on a penetrating probe will be able to record single unit activity, and what new information, will be revealed.

OECTs can be used to record neural actives *in vitro*, too. It is possible to culture electrically active cells on top of an OECTs array and study the effect of drugs by means of recording the electrical activities of the cells. Even further, a single neuron response can be measured by performing patch-

clamp experiment on a neuron cultured on top of an OECT. The drain current of the device projects the ionic flux across the membrane, directly, as oppose to electric filed variations in case of field effect transistors.

OECTs can help answer basic questions in neuroscience about the coupling between electrical activity and metabolism. In order to function, the brain needs energy in the form of glucose, which is carried in the blood. A dysfunction in this supply system results in pathological activities. The question of how the brain makes use of glucose in different contexts has never been addressed precisely, because it requires the simultaneous recording of neuronal activity and glucose level at the single neuron scale. Such multi-modal probes would record electrophysiology and metabolism with high spatial resolution. The impact of such probes would be considerable and widespread, in basic physiology, pathology, and even in the clinic to interpret metabolic imaging.

Appendix A

8 Publications

This thesis is based on the following publications (in whole or in part):

- **Chapter 1:**

  D. Khodagholy, G. G. Malliaras, R. M. Owens, "*Polymer-based sensors", in Comprehensive Polymer Science, chapter 8, 2nd Edition*, K. Matyjaszewski, M. Möller, Eds. ,Elsevier BV, Amsterdam, Netherlands, (2012), in press.

- **Chapter 2:**

  D. Khodagholy, T. Doublet, M. Gurfinkel, P. Quilichini, E. Ismailova, P. Leleux, T. Herve, S. Sanaur, C. Bernard, and G.G. Malliaras, "*Highly conformable conducting polymer electrodes for in vivo recordings*", Adv. Mater. 36, H268 (2011).

- **Chapter 3:**

  D. Khodagholy, M. Gurfinkel, E. Stavrinidou, P. Leleux, T. Herve, S. Sanaur, and G.G. Malliaras, "*High speed and high density organic electrochemical transistor arrays*", Appl. Phys. Lett. 99, 163304 (2011).

- **Chapter 4:**

  D. Khodagholy, J. Rivnay, M. Gurfinkel, L. H. Jimison, M. Sessolo, E. Stavrinidou, P. Leleux, E. Ismailova, T. Herve, S. Sanaur, and G. G. Malliaras, "High transconductance Organic electrochemical transistor", Adv. Mater, submitted.

- **Chapter 5:**

  D. Khodagholy, T. Doublet, M. Gurfinkel, P. Leleux, P. Quilichini, A. Ghestem, E. Ismailova, T. Herve, S. Sanaur, C. Bernard and G. G. Malliaras, "*In vivo recordings of brain activity using organic transistors*", Nature comm., under review.

- **Chapter 6:**

  D. Khodagholy, V.F. Curto, K. J. Fraser, M. Gurfinkel, R. Byrne, D. Diamond, G. G. Malliaras, F. Benito-Lopez, and R. M. Owens, "*Organic electrochemical transistor incorporating an ionogel as solid state electrolyte for lactate sensing*", J. Mater. Chem., 22, 4440-4443, DOI: 10.1039/C2JM15716K (2012).

Appendix B

10 *Supplementary information of In vivo* recordings of brain activity using organic transistors

10.1 Gain as a function of frequency

In order to measure the frequency dependence of the OECT transconductance, a low amplitude (50 $mV_{peak\text{-}peak}$) oscillation was added on the gate bias of 0.5 V. The small signal transconductance of the transistor was determined by the amplitude ratio between the drain current oscillations and the corresponding input sine wave, as shown in Figure S1. The cutoff frequency (at which the transconductance drops by 3 dB from its plateau value) is approx. 5 kHz.

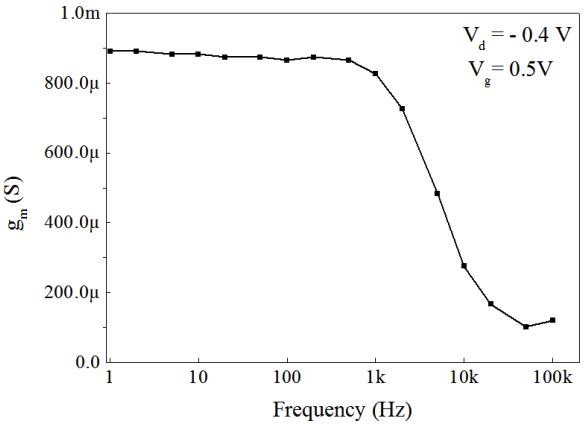

Figure S1: Frequency dependence of transconductance.

10.2 Device statistics

Figure S2 shows yield data on 32 OECTs fabricated on the same wafer. The yield was 100% (all devices worked as transistors). A Gaussian fit gave a mean drain current was 325.8 μA (V_d=-0.4 V, V_g=0 V), with a standard deviation of 61.5 μA.

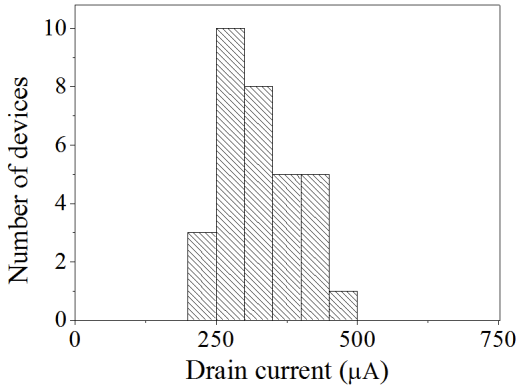

Figure S2: Histogram of drain current of 32 OECTs fabricated on the same wafer.

10.3 Device stability

The stability of PEDOT:PSS OECTs was accessed *in vitro* (thanks are due to Dr. Leslie Jimison for supplying the data). The OECT was immersed in DMEM complete cell culture media (Dulbecco) and placed inside an incubator (37° C). The modulation in the drain current ($\Delta I_d/I_d$) upon application of V_d=-0.3 V and V_g=0.2 V was measured every week. In between the measurements the transistor was left unbiased. The data are shown in Figure S3.

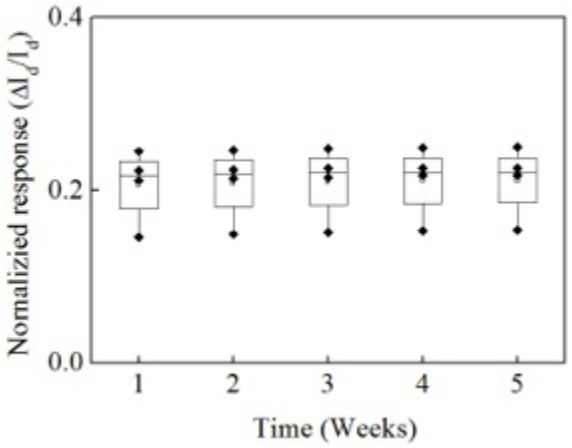

Figure S3: Results of an OECT stability test over 5 weeks.

A second test was performed in which an OECT with phosphate buffered saline as the electrolyte was subject to repeated gate voltage pulses with an amplitude of 0.3 V, a duration of 10 s, and a duty cycle of 50% (V_d=-0.3 V). The results are shown in Fig. S4.

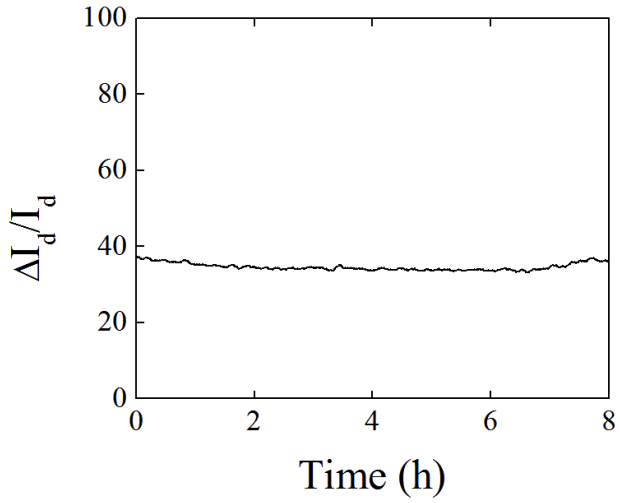

Figure S4: Results of an OECT stability test over 8 hours.

10.4 Background levels of the recordings

The PEDOT:PSS surface electrode recording in Fig. 3c was filtered at 0.1 – 200 Hz (plus a 50 Hz notch) and we obtain a background level of 0.26 mV. When we digitally filter this recording with a 1-50 Hz bandpass filter, we obtain a background level of 0.2 mV. The electrode recordings in Fig. 4a were filtered at 0.1 – 200 Hz (plus a 50 Hz notch) and we obtain background levels of 0.4 mV and 0.3 mV for the surface electrode and for the penetrating electrode, respectively. When we digitally filter the recordings with a 1-50 Hz bandpass filter, we obtain background levels of 0.2 mV and 0.1 mV for the surface electrode and for the penetrating electrode, respectively.

10.5 Signal-to-noise ratio (SNR) from the power spectrum

SNR is the ratio between the average power of the peaks of the signals and the average power of the background signals. These power values were calculated by integrating the power spectral density (PSD) of the signal. Note that the PSDs of the background activities are extracted by filtering out the corresponding frequency bands of relevant physiological signals – SWDs (5-10 Hz) and spindles' frequency band (7-14 Hz) oscillations – from the bandwidth of the measurements (0.1-200 Hz and notched at 50 Hz).

	Peak amplitude			Background $\int$ **SD (BW =0.1-200 Hz notched at 50Hz)**		
	OECT (μA)	**PEDOT:PSS (mV)**	**Ir (mV)**	**OECT (nA/√f)**	**PEDOT:PSS (μV/√f)**	**Ir (μV/√f)**
5-10 Hz	**1.3**	**13**	**12**	**0.2**	**21**	**28**
7-14 Hz	**0.3**	**3.5**	**3**	**1.6**	**260**	**52**